

UNCLASSIFIED

AD NUMBER

AD801873

LIMITATION CHANGES

TO:

Approved for public release; distribution is unlimited.

FROM:

Distribution authorized to U.S. Gov't. agencies and their contractors; Critical Technology; NOV 1966. Other requests shall be referred to Space Systems Division, Attn: SSBDD, AFB, Los Angeles, CA. This document contains export-controlled technical data.

AUTHORITY

AEDC ltr, 12 Oct 1972

THIS PAGE IS UNCLASSIFIED

AEDC-TR-66-202

**ARCHIVE COPY
DO NOT LOAN**

Cy1

**WIND TUNNEL INVESTIGATION TO DETERMINE STATIC
STABILITY AND PRESSURE DISTRIBUTION CHARACTERISTICS
OF SMALL-SCALE MODELS OF THE TITAN III/MOL LAUNCH
CONFIGURATION AT MACH NUMBERS FROM 0.60 TO 3.10**



**C. D. Riddle, T. O. Shadow, and J. A. Black
ARO, Inc.**

November 1966

This document is subject to special export controls and each transmittal to foreign governments or foreign nationals may be made only with prior approval of Space Systems Division (SSBD), Los Angeles, Calif.

*This document has been approved for public release
and its distribution is unlimited.*

per AF letter, 12 Oct. 72, William D. Cole

**PROPULSION WIND TUNNEL FACILITY
ARNOLD ENGINEERING DEVELOPMENT CENTER
AIR FORCE SYSTEMS COMMAND
ARNOLD AIR FORCE STATION, TENNESSEE**

AEDC TECHNICAL LIBRARY



647E TE000 0210 5
5 3769

PROPERTY OF U. S. AIR FORCE
AEDC LIBRARY
AF 40(600)1200

NOTICES

When U. S. Government drawings specifications, or other data are used for any purpose other than a definitely related Government procurement operation, the Government thereby incurs no responsibility nor any obligation whatsoever, and the fact that the Government may have formulated, furnished, or in any way supplied the said drawings, specifications, or other data, is not to be regarded by implication or otherwise, or in any manner licensing the holder or any other person or corporation, or conveying any rights or permission to manufacture, use, or sell any patented invention that may in any way be related thereto

Qualified users may obtain copies of this report from the Defense Documentation Center.

References to named commercial products in this report are not to be considered in any sense as an endorsement of the product by the United States Air Force or the Government.

WIND TUNNEL INVESTIGATION TO DETERMINE STATIC
STABILITY AND PRESSURE DISTRIBUTION CHARACTERISTICS
OF SMALL-SCALE MODELS OF THE TITAN III/MOL LAUNCH
CONFIGURATION AT MACH NUMBERS FROM 0.60 TO 3.10

C. D. Riddle, T. O. Shadow, and J. A. Black
ARO, Inc.

This document has been approved for public release
its distribution is unlimited. *per AF letter 12 Oct. 72*

~~This document is subject to special export controls
and each transmittal to foreign governments or foreign
nationals may be made only with prior approval of
Space Systems Division (SSBDD), Los Angeles, Calif.~~

William D. Cole

FOREWORD

The work reported herein was done at the request of the Space Systems Division (SSD), Air Force Systems Command (AFSC), for the Aerospace Division of the Martin-Marietta Corporation under Systems 624A and 632A.

The test results presented were obtained by ARO, Inc. (a subsidiary of Sverdrup & Parcel and Associates, Inc.), contract operator of the Arnold Engineering Development Center (AEDC), AFSC, Arnold Air Force Station, Tennessee, under Contract AF40(600)-1200. The test was conducted under ARO Project No. PT0655 from June 1 to July 7, 1966. The manuscript was submitted for publication on September 16, 1966.

Information in this report is embargoed under the Department of State International Traffic in Arms Regulations. This report may be released to foreign governments by departments or agencies of the U. S. Government subject to approval of SSD (SSBDD), Los Angeles, California, as Controlling Office or higher authority within the Department of the Air Force. Private individuals or firms require a Department of State export license.

This technical report has been reviewed and is approved.

Richard W. Bradley
Lt Col, USAF
AF Representative, PWT
Directorate of Test

Leonard T. Glaser
Colonel, USAF
Director of Test

ABSTRACT

Models of the Titan III/Manned Orbiting Laboratory (MOL) launch vehicle were tested in Tunnels 16T and 16S of the Propulsion Wind Tunnel Facility at Mach numbers from 0.60 to 3.10 to determine pressure and acoustical characteristics for structural design confirmation and to obtain force balance data for flight control and trajectory analysis. A calibration cone was also tested to evaluate tunnel background noise in the Titan III/MOL acoustical data. Force data were obtained by using four internal balances to sense separate aerodynamic loads on the composite model and on the MOL, MOL-Gemini, and solid rocket motors (SRM) sections. Modification of the SRM noses to a less blunt configuration resulted in a reduction of composite and SRM axial load and tended to position the composite longitudinal neutral point at a more forward location. Lateral neutral point for the composite model exhibited a maximum travel of 2.6 core diameters for the 0.60 to 3.10 Mach number range whereas the longitudinal neutral-point travel was 1.0 diameters. The acoustical results are not presented in this report.

CONTENTS

	<u>Page</u>
ABSTRACT	iii
NOMENCLATURE	xi
I. INTRODUCTION	1
II. APPARATUS	
2.1 Test Facilities	1
2.2 Model Geometry.	1
2.3 Instrumentation	2
III. TEST DESCRIPTION	
3.1 Procedure	3
3.2 Precision of Measurements.	3
IV. RESULTS	
4.1 Force Phase	4
4.2 Pressure Phase.	6
4.3 Flow Visualization.	7
V. SUMMARY OF RESULTS.	7

ILLUSTRATIONS

Figure

1. Sketch of Titan III/MOL Installation in Tunnel 16S.	9
2. Photograph of Titan III/MOL Pressure Model Installed in Tunnel 16S	10
3. Sketch of Titan III/MOL Installation in Tunnel 16T	11
4. Photograph of Titan III/MOL Force Model Installed in Tunnel 16T.	12
5. Titan III/MOL Geometry.	13
6. Details of Modified and Basic Gemini Configurations	14
7. Sketch of Force Model Showing Balance and Cavity Pressure Locations	15
8. Sketch of Pressure Model Showing Locations of Pressure Orifices and Microphones	16
9. Orientation of Forces and Moments	17
10. Variation of Reynolds Number with Mach Number.	18
11. Variation of Pitching-Moment Coefficient with Angle of Attack for the Gemini Section.	19

<u>Figure</u>	<u>Page</u>
12. Variation of Normal-Force Coefficient with Angle of Attack for the Gemini Section	20
13. Variation of Yawing-Moment Coefficient with Sideslip Angle for the Gemini Section	21
14. Variation of Side-Force Coefficient with Sideslip Angle for the Gemini Section	22
15. Variation of Forebody Axial-Force Coefficient with Angle of Attack for the Gemini Section, $\beta = 0$	
a. Mach Numbers 0.60 through 1.30	23
b. Mach Numbers 1.40 through 3.10	24
16. Variation of Base Axial-Force Coefficient with Angle of Attack for the Gemini Section, $\beta = 0$	
a. Mach Numbers 0.60 through 1.30	25
b. Mach Numbers 1.40 through 3.10	26
17. Variation of Forebody Axial-Force Coefficient with Mach Number for the Gemini Section	27
18. Variation of Base Axial-Force Coefficient with Mach Number for the Gemini Section	27
19. Variation of Pitching-Moment Coefficient with Angle of Attack for the MOL-Gemini Section in the Presence of SRM Configurations 1 and 2.	28
20. Variation of Normal-Force Coefficient with Angle of Attack for the MOL-Gemini Section in the Presence of SRM Configurations 1 and 2.	29
21. Variation of Yawing-Moment Coefficient with Sideslip Angle for the MOL-Gemini Section in the Presence of SRM Configurations 1 and 2.	30
22. Variation of Side-Force Coefficient with Sideslip Angle for the MOL-Gemini Section in the Presence of SRM Configurations 1 and 2	31
23. Variation of Forebody Axial-Force Coefficient with Angle of Attack for the MOL-Gemini Section in the Presence of SRM Configuration 1, $\beta = 0$	
a. Mach Numbers 0.60 through 1.30	32
b. Mach Numbers 1.40 through 3.10	33

<u>Figure</u>	<u>Page</u>
24. Variation of Base Axial-Force Coefficient with Angle of Attack for the MOL-Gemini Section in the Presence of SRM Configuration 1, $\beta = 0$	
a. Mach Numbers 0.60 through 1.30	34
b. Mach Numbers 1.40 through 3.10	35
25. Variation of Forebody Axial-Force Coefficient with Mach Number for the MOL-Gemini Section in the Presence of SRM Configurations 1 and 2.	36
26. Variation of Base Axial-Force Coefficient with Mach Number for the MOL-Gemini Section in the Presence of SRM Configurations 1 and 2	36
27. Variation of Pitching-Moment Coefficient with Angle of Attack for Configurations 1 and 2 of the Composite Model	37
28. Variation of Normal-Force Coefficient with Angle of Attack for Configurations 1 and 2 of the Composite Model	38
29. Variation of Yawing-Moment Coefficient with Sideslip Angle for Configurations 1 and 2 of the Composite Model	39
30. Variation of Side-Force Coefficient with Sideslip Angle for Configurations 1 and 2 of the Composite Model	40
31. Variation of Pitching-Moment Curve Slope with Mach Number for Configurations 1 and 2 of the Composite Model	41
32. Variation of Yawing-Moment Curve Slope with Mach Number for Configurations 1 and 2 of the Composite Model	41
33. Variation of Neutral-Point Location with Mach Number for Configurations 1 and 2 of the Composite Model	
a. Longitudinal Neutral Point	42
b. Lateral Neutral Point	42
34. Variation of Forebody Axial-Force Coefficient with Angle of Attack for Configurations 1 and 2 of the Composite Model, $\beta = 0$	
a. Mach Numbers 0.60 through 1.30	43
b. Mach Numbers 1.40 through 3.10	44

<u>Figure</u>	<u>Page</u>
35. Variation of Base Axial-Force Coefficient with Angle of Attack for Configurations 1 and 2 of the Composite Model, $\beta = 0$	
a. Mach Numbers 0.60 through 1.30	45
b. Mach Numbers 1.40 through 3.10	46
36. Variation of Forebody Axial-Force Coefficient with Mach Number for Configurations 1 and 2 of the Composite Model	47
37. Variation of Base Axial-Force Coefficient with Mach Number for Configurations 1 and 2 of the Composite Model	47
38. Variation of SRM Pitching-Moment Coefficient with Angle of Attack for Configurations 1 and 2	
a. Mach Numbers 0.60 through 0.90	48
b. Mach Numbers 1.00 through 1.20	49
c. Mach Numbers 1.30 through 1.80	50
d. Mach Numbers 2.00 through 2.60	51
e. Mach Numbers 2.80 and 3.10	52
39. Variation of SRM Normal-Force Coefficient with Angle of Attack for Configurations 1 and 2	
a. Mach Numbers 0.60 through 1.40	53
b. Mach Numbers 1.80 through 3.10	54
40. Variation of SRM Yawing-Moment Coefficient with Sideslip Angle for Configurations 1 and 2	
a. Mach Numbers 0.60 through 1.20	55
b. Mach Numbers 1.30 through 2.60	56
c. Mach Number 2.80	57
41. Variation of SRM Side-Force Coefficient with Sideslip Angle for Configurations 1 and 2	
a. Mach Numbers 0.60 through 1.20	58
b. Mach Numbers 1.30 through 2.60	59
c. Mach Numbers 2.80 and 3.10	60
42. Variation of SRM Forebody Axial-Force Coefficient with Angle of Attack for Configurations 1 and 2, $\beta = 0$	
a. Mach Numbers 0.60 through 1.30	61
b. Mach Numbers 1.40 through 3.10	62

<u>Figure</u>	<u>Page</u>
43. Variation of SRM Forebody Axial-Force Coefficient with Sideslip Angle for Configurations 1 and 2, $\alpha = 0$	
a. Mach Numbers 0.60 through 1.30	63
b. Mach Numbers 1.40 through 3.10	64
44. Variation of SRM Base Axial-Force Coefficient with Angle of Attack for Configurations 1 and 2, $\beta = 0$	
a. Mach Numbers 0.60 through 1.30	65
b. Mach Numbers 1.40 through 3.10	66
45. Variation of SRM Base Axial-Force Coefficient with Sideslip Angle for Configurations 1 and 2, $\alpha = 0$	
a. Mach Numbers 0.60 through 1.30	67
b. Mach Numbers 1.40 through 3.10	68
46. Variation of SRM Forebody Axial-Force Coefficient with Mach Number for Configurations 1 and 2	69
47. Variation of SRM Base Axial-Force Coefficient with Mach Number for Configurations 1 and 2	69
48. Variation of Centerbody Surface Pressure Coefficient with Model Station for Orifices Oriented at 0 and 180 deg for Configuration 1, $\beta = 0$	
a. Mach Numbers 0.60 and 0.70	70
b. Mach Number 0.80	71
c. Mach Number 0.85	72
d. Mach Number 0.90	73
e. Mach Number 0.95	74
f. Mach Number 1.00	75
g. Mach Number 1.10	76
h. Mach Number 1.20	77
i. Mach Number 1.30	78
j. Mach Number 1.40	79
k. Mach Number 1.80	80
l. Mach Numbers 2.00 and 2.20	81
m. Mach Numbers 2.60 and 2.80	82
n. Mach Number 3.00	83
49. Variation of Centerbody Surface Pressure Coefficient with Model Station for Orifices Oriented at 0 and 180 deg for Configuration 3, $\beta = 0$	
a. Mach Number 0.70	84
b. Mach Number 0.80	85
c. Mach Number 0.90	86
d. Mach Number 1.00	87

<u>Figure</u>	<u>Page</u>
49. Continued	
e. Mach Number 1.10	88
f. Mach Number 1.20	89
g. Mach Number 1.30	90
h. Mach Number 1.40	91
50. Variation of Surface Pressure Coefficient with Model Station for Orifices Oriented at 90 deg for Configuration 1, $\alpha = 0$	
a. Mach Numbers 0.60 through 0.80	92
b. Mach Numbers 0.85 and 0.90	93
c. Mach Numbers 0.95 and 1.00	94
d. Mach Numbers 1.10 and 1.20	95
e. Mach Numbers 1.30 through 1.80	96
f. Mach Numbers 2.00 through 3.00	97
51. Variation of Surface Pressure Coefficient with Model Station for Orifices Oriented at 90 deg for Configuration 3, $\alpha = 0$	
a. Mach Numbers 0.70 and 0.80	98
b. Mach Numbers 0.90 and 1.00	99
c. Mach Numbers 1.10 and 1.20	100
d. Mach Numbers 1.30 and 1.40	101
52. Schlieren Photographs of the SRM Noses for Configuration 1 at $\alpha = 0$ deg	
a. Mach Numbers 0.60 through 0.85	102
b. Mach Numbers 0.90 through 1.00	103
c. Mach Numbers 1.10 through 1.30	104
53. Schlieren Photographs of the SRM Noses for Configuration 2 at $\alpha = 0$ deg	
a. Mach Numbers 0.60 through 0.90	105
b. Mach Numbers 1.00 through 1.20	106
c. Mach Numbers 1.30 and 1.40	107

TABLE

I. Coefficient Uncertainties	108
--	-----

NOMENCLATURE

C_A	Total axial-force coefficient, $\frac{\text{measured axial force}}{q_\infty S}$
$C_{A, b}$	Base axial-force coefficient, $\sum_i \left(\frac{p_{\infty} - p_{b_i}}{q_\infty} \right) \frac{S_i}{S}$
$C_{A, F}$	Forebody axial-force coefficient, $C_A - C_{A, b}$
C_m	Pitching-moment coefficient (see Fig. 10 for moment reference locations), $\frac{\text{measured pitching moment}}{q_\infty SD}$
$C_{m\alpha}$	Pitching-moment curve slope, rate of change of pitching-moment coefficient with angle of attack ($dC_m/d\alpha$) evaluated at $\alpha = 0$ deg, per degree
C_N	Normal-force coefficient, $\frac{\text{measured normal force}}{q_\infty S}$
C_n	Yawing-moment coefficient, $\frac{\text{measured yawing moment}}{q_\infty SD}$
$C_{n\beta}$	Yawing-moment curve slope, rate of change of yawing-moment coefficient with sideslip angle ($dC_n/d\beta$) evaluated at $\beta = 0$ deg, per degree
C_p	Pressure coefficient, $\frac{p_L - p_\infty}{q_\infty}$
C_Y	Side-force coefficient, $\frac{\text{measured side force}}{q_\infty S}$
D	Core diameter (reference diameter), 0.535 ft
M_∞	Free-stream Mach number
p_{b_i}	Average base pressure for the i th section, psf
p_L	Static pressure measured on the pressure model, psf
p_∞	Free-stream static pressure, psf
q_∞	Free-stream dynamic pressure, psf
Re/ft	Reynolds number per foot, V_∞/ν_∞
S	Core cross-sectional area (reference area), 0.225 ft ²
S_i	Effective base area of the i th section, ft ²

V_{∞}	Free-stream velocity, ft/sec
x	Distance of pressure model orifices from model nose, ft
$x_{np\alpha}$	Longitudinal neutral-point location measured in reference diameters from the moment reference point (see Fig. 8), dC_m/dC_n at $\alpha = 0$ deg, positive forward
$x_{np\beta}$	Lateral neutral-point location measured in reference diameters from the moment reference point (see Fig. 8), dC_n/dC_y at $\beta = 0$ deg, positive forward
α	Model angle of attack with respect to the tunnel centerline, deg
β	Model sideslip angle with respect to the tunnel centerline, deg
ν_{∞}	Kinematic viscosity of the free stream, ft ² /sec
θ	Roll orientation of surface pressure orifices (see Fig. 9), deg

SUBSCRIPTS

1	Gemini section
2	MOL-Gemini section
3	Composite model
4	SRM

CONFIGURATIONS

1	Basic Titan III/MOL launch configuration
2	Titan III/MOL launch configuration with 20-deg SRM noses
3	Titan III/MOL launch configuration with modified Gemini shape

SECTION I INTRODUCTION

Models of the Titan III/Manned Orbiting Laboratory (MOL) launch vehicle were tested in the supersonic (16S) and transonic (16T) circuits of the Propulsion Wind Tunnel Facility (PWT) to obtain surface pressure and acoustical data for structural design confirmation and to obtain force balance data for flight control and trajectory analysis. A calibration cone was also tested to determine tunnel background noise in acoustical data obtained for the Titan III/MOL pressure model. The pressure model and calibration cone were investigated at Mach numbers from 0.60 to 3.00 and the force model was tested at Mach numbers from 0.60 to 3.10.

SECTION II APPARATUS

2.1 TEST FACILITIES

Tunnel 16T is a continuous flow, closed-circuit wind tunnel capable of operation from a stagnation pressure level of 40 to 4000 psf. The test section is 16 ft square by 40 ft long and is lined with perforated plates to allow continuous operation with minimum wall interference through the Mach number range from 0.5 to 1.6.

Tunnel 16S is a continuous flow, closed-circuit wind tunnel capable of operation between Mach numbers 1.7 and 3.2 at stagnation pressures from 100 to 2000 psf. The test section is 16 ft square by 40 ft long.

Details and photographs of the test sections showing model location and support strut arrangement are presented in Figs. 1 through 4. A more extensive description of each tunnel is given in the Test Facilities Handbook.¹

2.2 MODEL GEOMETRY

The Titan III/MOL launch vehicle combines a Titan III 120-in. -diam core and two 120-in. -diam, 7-segment strap-on solid rocket motors (SRM's) with the Manned Orbiting Laboratory (MOL). The MOL consists

¹Test Facilities Handbook (5th Edition). "Propulsion Wind Tunnel Facility, Vol. 3." Arnold Engineering Development Center, July 1963.

of a 120-in. -diam cylinder and is mounted aft of a Gemini spacecraft. Separate, geometrically identical 0.0535-scale force and pressure models of the basic launch vehicle were tested in each tunnel. Model details are presented in Fig. 5.

One additional configuration each of the force and pressure models was tested in tunnel 16T. The second force configuration was used to study the effect of SRM nose shape on composite vehicle axial force and consisted of the basic model with modified SRM nose geometry. The modified SRM noses are detailed in Fig. 5. The additional pressure configuration was the basic model with a modified Gemini shape. Details of the modified Gemini are shown in Fig. 6. The basic force and pressure models are subsequently referred to as configuration 1; the force model with modified SRM noses and the pressure model with the modified Gemini shape are identified as configurations 2 and 3, respectively.

2.3 INSTRUMENTATION

Four internal strain-gage balances, located as sketched in Fig. 7, were used to measure aerodynamic loads on the force model. The model centerbody was separated by gaps at the Gemini-MOL and MOL-core interfaces (Fig. 7), such that balances 1 and 2 sensed loads only on the Gemini and Gemini plus MOL, respectively. The composite vehicle loads were sensed by balance number 3; balance number 4 was used to measure loads on the left SRM. A total of 17 base and cavity pressure orifices (Fig. 7) were used to measure base pressures on the force model.

The pressure model was instrumented with 32 flush-mounted microphones and 361 surface pressure orifices for respective measurements of fluctuating and steady-state pressures. Microphone and orifice locations are shown in Fig. 8.

All microphone outputs were recorded on magnetic tape. The steady-state pressure orifices were connected to transducers. The outputs of the transducers and balances were recorded by means of the PWT data processing system described in the Test Facilities Handbook.

SECTION III TEST DESCRIPTION

3.1 PROCEDURE

Angles of attack (α) and sideslip (β) were obtained by pitching and rolling the sting to pre-calculated angles corresponding to the scheduled α - β combinations. The orientation of moments and forces and the moment reference locations for the force model are shown in Fig. 9.

Data for the force and pressure models were recorded by holding Mach number constant while α and β were varied from -11 to 11 deg. Mach number for the force model was varied from 0.60 to 1.40 in tunnel 16T and from 1.80 to 3.10 in tunnel 16S. The pressure model was tested at Mach numbers from 0.60 to 1.40 in tunnel 16T and from 1.80 to 3.00 in tunnel 16S.

Reynolds number variations for the various installations are shown in Fig. 10.

3.2 PRECISION OF MEASUREMENTS

The estimated precision of measurements is as follows:

Angle of attack or sideslip	± 0.10 deg
Mach number 0.60 to 1.10	± 0.003
1.20 to 1.40	± 0.010
1.80 to 3.10	± 0.020
Dynamic pressure $M_\infty \leq 1.40$	± 4 psf
$M_\infty > 1.40$	± 3 psf

The coefficient uncertainties are shown in Table I. These uncertainties were determined by a statistical method based on a 95-percent confidence level and a normal error distribution. The uncertainties quoted for Mach number relate to the variation of Mach number in the vicinity of the test article. The uncertainty in setting Mach number varied from ± 0.003 to ± 0.010 with increasing Mach number.

SECTION IV RESULTS

4.1 FORCE PHASE

Data from the force phase are presented sequentially for the Gemini, MOL-Gemini, composite, and left SRM sections. Subscripts 1 through 4 (see Nomenclature) are used to identify coefficients plotted for the four sections. Where applicable, data from configurations 1 and 2 are compared to determine the effects of SRM nose shape. Configuration 2 was tested in tunnel 16T only, limiting data comparisons to Mach numbers from 0.60 to 1.40.

4.1.1 Gemini

The Gemini aerodynamic results were essentially identical for configurations 1 and 2; data are therefore presented for configuration 1 only. Pitching-moment coefficient, C_m , and normal-force coefficient, C_N , are plotted as functions of angle of attack, α , for angles of sideslip, β , of 0, -4, and -8 deg in Figs. 11 and 12. The variations of yawing-moment coefficient, C_n , and side-force coefficient, C_y , with β for $\alpha = 0, 4, \text{ and } 8$ deg are shown in Figs. 13 and 14. Since the Gemini is basically a body of revolution, predictable similarities between C_y and C_N and between C_n and C_m are indicated.

Forebody axial-force coefficient, $C_{A,F}$, and base axial-force coefficient, $C_{A,b}$, for the Gemini are presented as functions of α in Figs. 15 and 16. There were no significant variations except at Mach number 0.80, where both $C_{A,F}$ and $C_{A,b}$ varied erratically with α . Repeat values of $C_{A,F}$ and $C_{A,b}$ obtained for the Gemini during configuration 2 testing are also presented at Mach number 0.80 and corroborate the erratic variations. Variations of $C_{A,F}$ and $C_{A,b}$ with Mach number at $\alpha, \beta = 0$ are shown in Figs. 17 and 18. Maximum values of $C_{A,F}$ were exhibited at Mach numbers 1.30 and 1.40; $C_{A,b}$ reached a maximum value at Mach number 0.80.

4.1.2 MOL-Gemini

The variations of C_m and C_N with α for $\beta = 0, -4, \text{ and } -8$ deg are presented for the MOL-Gemini section in the presence of SRM configurations 1 and 2 in Figs. 19 and 20. Similar variations of C_n and C_y with β for $\alpha = 0, 4, \text{ and } 8$ deg are shown in Figs. 21 and 22. The modification of the SRM noses from configuration 1 to configuration 2 effected a slight decrease in the absolute magnitude of C_y . The magnitudes of C_N

were similar from Mach numbers 0.60 to 1.00, but configuration 2 exhibited slightly larger absolute magnitudes from Mach numbers 1.10 to 1.40.

Trends of $C_{A,F}$ and $C_{A,b}$ with α are shown for configuration 1 in Figs. 23 and 24. Variations of $C_{A,F}$ and $C_{A,b}$ with Mach number for α , $\beta = 0$, comparing configurations 1 and 2, are given in Figs. 25 and 26. The magnitudes of the MOL-Gemini $C_{A,F}$ for the two configurations are in close agreement, with maximum values indicated at Mach numbers 1.30 and 1.40. The negative values of $C_{A,b}$ resulted from the location of the MOL-core interface gap (see Fig. 7) in a high pressure region between the core and noses of the SRM's. Figure 26 shows consistently more negative values of $C_{A,b}$ for configuration 1, indicating higher core surface pressures at the MOL-core gap for the blunter SRM nose.

4.1.3 Composite Model

The variations of C_m and C_N with α and C_n and C_Y with β for configurations 1 and 2 are presented in Figs. 27 through 30. Trends of the pitching-moment curve slope, $C_{m\alpha}$, and the yawing-moment curve slope, $C_{n\beta}$, with Mach number are shown in Figs. 31 and 32. Configuration 1 exhibited slightly more negative values of $C_{m\alpha}$, but the two configurations displayed similar trends and magnitudes of $C_{n\beta}$. Longitudinal and lateral neutral-point locations, $x_{np\alpha}$ and $x_{np\beta}$, are shown as functions of Mach number in Fig. 33. Configuration 1 exhibited a more rearward $x_{np\alpha}$ for Mach numbers from 0.60 to 1.20; differences in $x_{np\beta}$ for the two configurations were not consistent. The $x_{np\alpha}$ for configuration 1 was most forward at Mach number 0.60 and was most rearward at Mach number 3.10. The most forward and rearward $x_{np\beta}$ values for configuration 1 occurred at respective Mach numbers 0.90 and 2.60. The $x_{np\beta}$ for configuration 1 was more sensitive to Mach number change than was $x_{np\alpha}$; Fig. 33 shows maximum travels of 2.6 diameters for $x_{np\beta}$ and only 1.0 diameters for $x_{np\alpha}$.

Variations of $C_{A,F}$ and $C_{A,b}$ with α are presented for both configurations in Figs. 34 and 35. Figures 36 and 37 show variations of $C_{A,F}$ and $C_{A,b}$ with Mach number at α , $\beta = 0$. Configuration 2 exhibited significantly lower values of $C_{A,F}$ at the comparison Mach numbers from 0.60 to 1.40. For configuration 1, $C_{A,F}$ increased with increasing Mach number to a maximum value at Mach number 1.30, and decreased as Mach number was increased from 1.30 to 3.10. Configuration 2 exhibited slightly larger values of $C_{A,b}$ for Mach numbers 0.60 to 1.20. A maximum value of $C_{A,b}$ was observed for configuration 1 at Mach number 1.10.

4.1.4 SRM

As mentioned previously (Section 2.3) aerodynamic loads were measured on the left SRM. It should be noted that, as β is varied from positive to negative values, the left SRM moves from leeward to windward sides of the core, i. e., becomes more directly exposed to the free-stream flow.

Trends of C_m with α for $\beta = -8, -4, 0, 4,$ and 8 deg are shown for the two SRM configurations in Fig. 38. Not surprisingly, $C_{m\alpha}$ values become increasingly negative as the sideslip angle varies from positive to negative. The value of C_m at $\alpha, \beta = 0$ is slightly positive at Mach numbers from 0.60 to 2.20. This occurrence is attributed at least in part to the location of the thrust vector control rocket (TVC, see Fig. 5) along the bottom, aft portion of the left SRM. A high pressure region between the core and TVC and a low pressure region aft of the TVC shoulder along the bottom side are likely and would contribute a positive pitching moment at $\alpha, \beta = 0$.

Variations of C_N with α are presented in Fig. 39. In agreement with the effect of β on $C_{m\alpha}$, the most positive $C_{N\alpha}$ value for configuration 1 occurs at $\beta = -8$ deg and $C_{N\alpha}$ becomes less positive as β is increased from -8 to 8 deg.

Lateral coefficients C_n and C_Y are shown as functions of β for the two configurations at $\alpha = 0, 4,$ and 8 deg in Figs. 40 and 41. As α was increased from 0 to 8 deg, C_n became more positive and C_Y became more negative.

Variations of $C_{A,F}$ with α and β are compared for the two SRM configurations in Figs. 42 and 43. Figures 44 and 45 show variations of $C_{A,b}$ with α and β . A variation of β to more positive values tended to decrease the $C_{A,F}$ magnitude and caused the magnitude of $C_{A,b}$ to increase. Variations of $C_{A,F}$ and $C_{A,b}$ with Mach number at $\alpha, \beta = 0$ deg are presented in Figs. 46 and 47. The second SRM configuration exhibited smaller values of $C_{A,F}$ at the Mach numbers at which comparisons were made. The basic SRM configuration displayed a maximum $C_{A,F}$ at Mach number 1.20 and a maximum $C_{A,b}$ at Mach numbers from 1.10 to 1.20.

4.2 PRESSURE PHASE

Surface pressure data along the model centerbody were obtained for the basic launch vehicle (configuration 1) at Mach numbers from 0.60 to

3.00 and for the basic model with modified Gemini payload geometry (configuration 3) at Mach numbers from 0.60 to 1.40. Details of the modified Gemini shape are described in Fig. 6. Pressure coefficient, C_p , is presented as a function of model station, x/D , for longitudinal orifice row orientations, θ , of 0, 90, and 180 deg. The orifice row locations are shown in Fig. 8.

Variations of C_p with x/D for $\theta = 0$ and 180 deg and for $\beta = 0$ are presented at $\alpha = 0, -6,$ and -11 deg for configuration 1 in Fig. 48 and for configuration 3 in Fig. 49. For $\theta = 90$ deg, C_p is presented as a function of x/D for $\alpha = 0$ at $\beta = 0, 11,$ and -11 deg in Figs. 50 and 51 for configurations 1 and 3, respectively.

4.3 FLOW VISUALIZATION

Schlieren photographs of flow characteristics surrounding the launch vehicle were obtained at Mach numbers from 0.60 to 1.40. Flow photographs of the SRM noses at $\beta = 0, 4,$ and 6 deg for $\alpha = 0$ deg are presented for configurations 1 and 2 in Figs. 52 and 53, respectively.

SECTION V SUMMARY OF RESULTS

The data results are summarized as follows:

1. Maximum values of $C_{A, F}$ occurred at Mach numbers 1.30 and 1.40 for the Gemini and MOL-Gemini sections. Basic configurations of the composite model and the SRM section exhibited maximum $C_{A, F}$ at Mach numbers 1.30 and 1.20, respectively. Modification of the SRM noses to a less blunt configuration effected a reduction of $C_{A, F}$ for the SRM section and the composite model.
2. The most forward $x_{np\alpha}$ for the basic model occurred at Mach number 0.60 and the most rearward $x_{np\alpha}$ was at Mach number 3.10. The $x_{np\beta}$ was positioned most forward at Mach number 0.90 and was most rearward at Mach number 2.60. The configuration with modified SRM noses exhibited a more forward $x_{np\alpha}$ at Mach numbers from 0.60 to 1.20. The $x_{np\beta}$ for the basic model was more variant with Mach number than was $x_{np\alpha}$; $x_{np\beta}$ displayed a maximum travel of 2.6 diameters compared to 1.0 diameters for $x_{np\alpha}$.

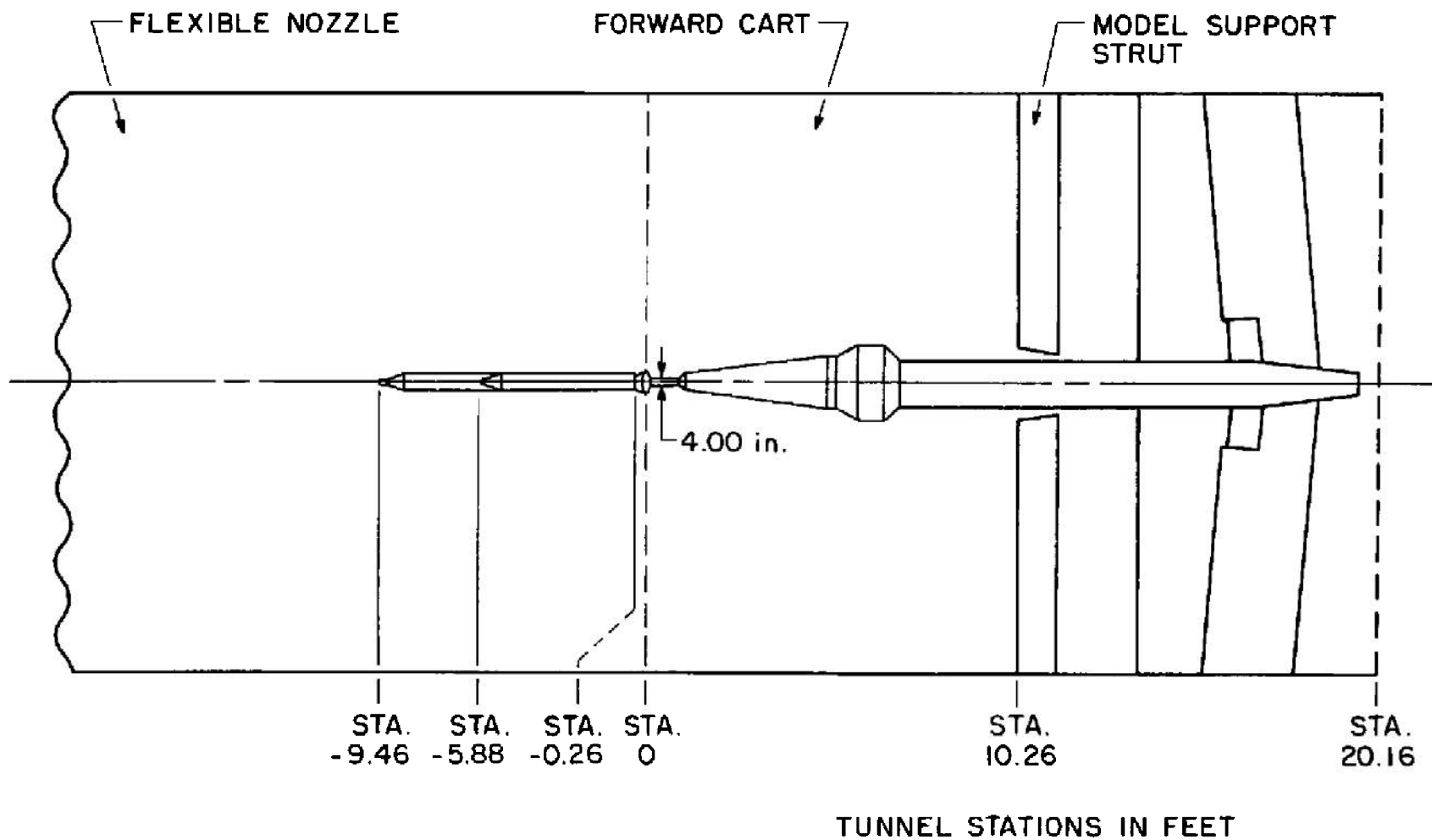
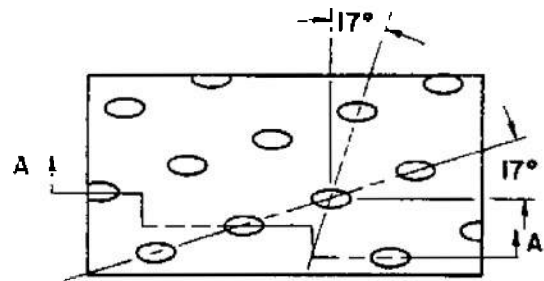


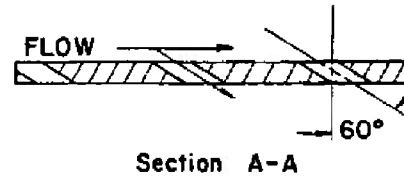
Fig. 1 Sketch of Titan III/MQL Installation in Tunnel 165



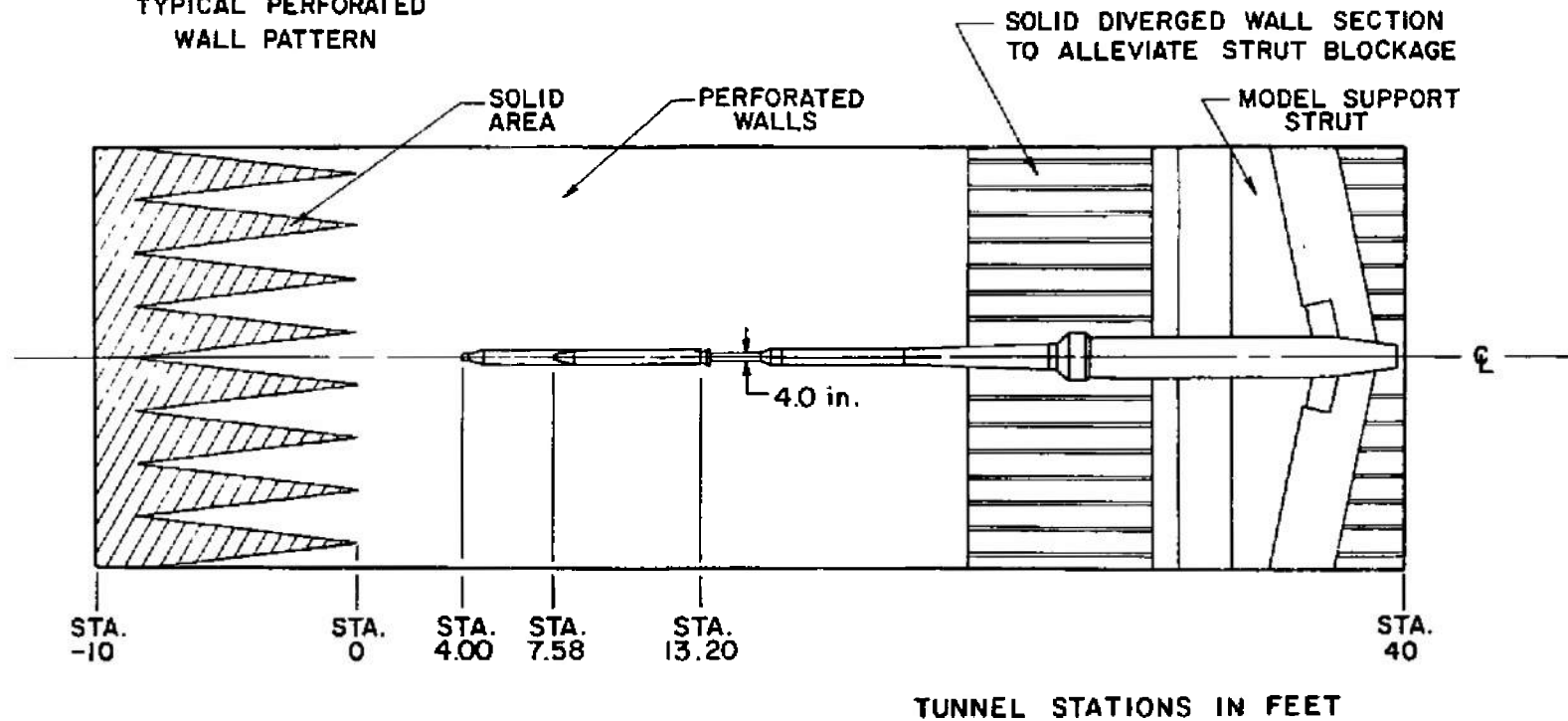
Fig. 2 Photograph of Titan III/MOL Pressure Model Installed in Tunnel 16S



TYPICAL PERFORATED WALL PATTERN



6% Open Area
 Hole Diameter = 0.75 In.
 Plate Thickness = 0.75 In.



TUNNEL STATIONS IN FEET

Fig. 3 Sketch of Titan III/MOL Installation in Tunnel 16T

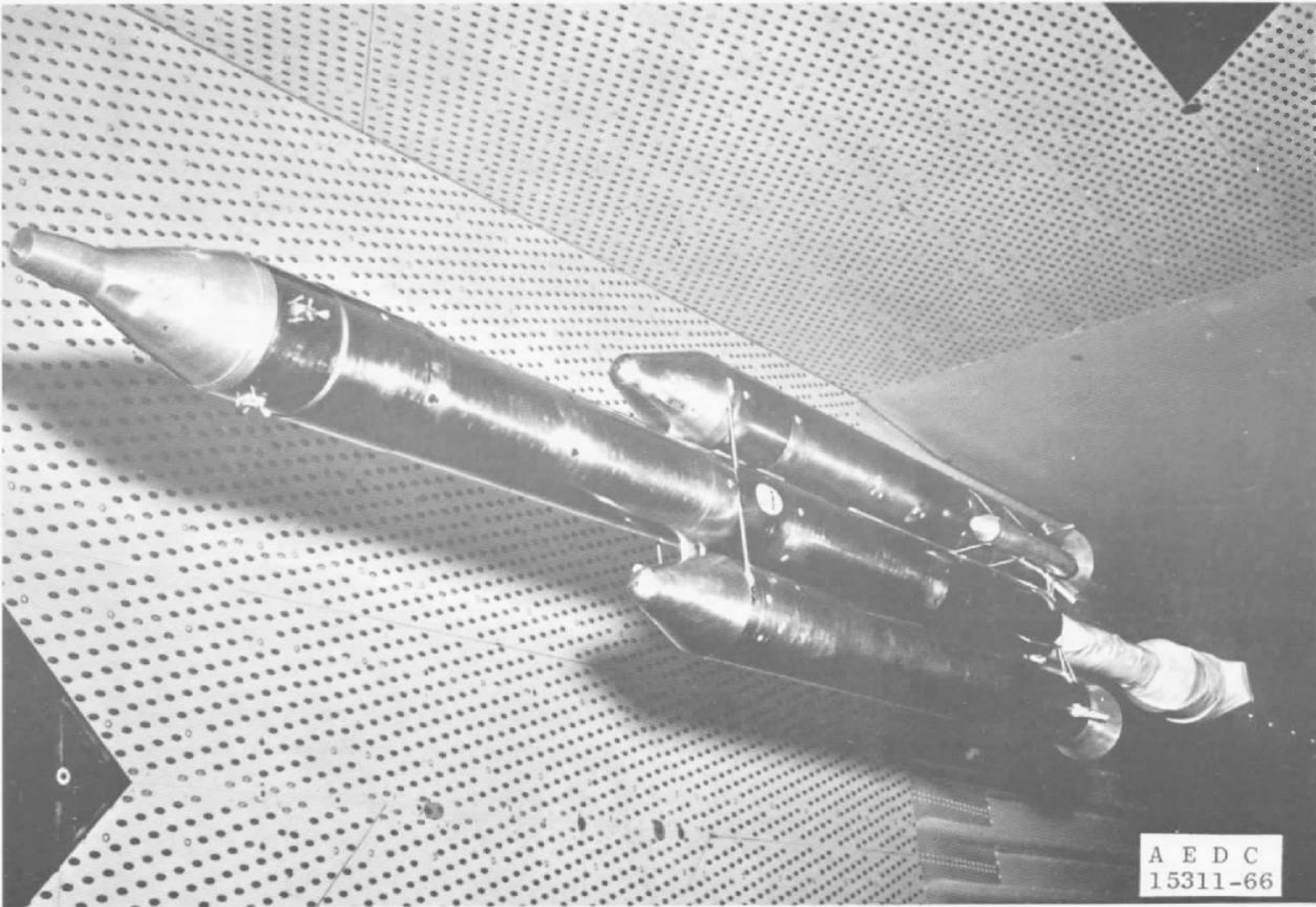


Fig. 4 Photograph of Titan III/MOL Force Model Installed in Tunnel 16T

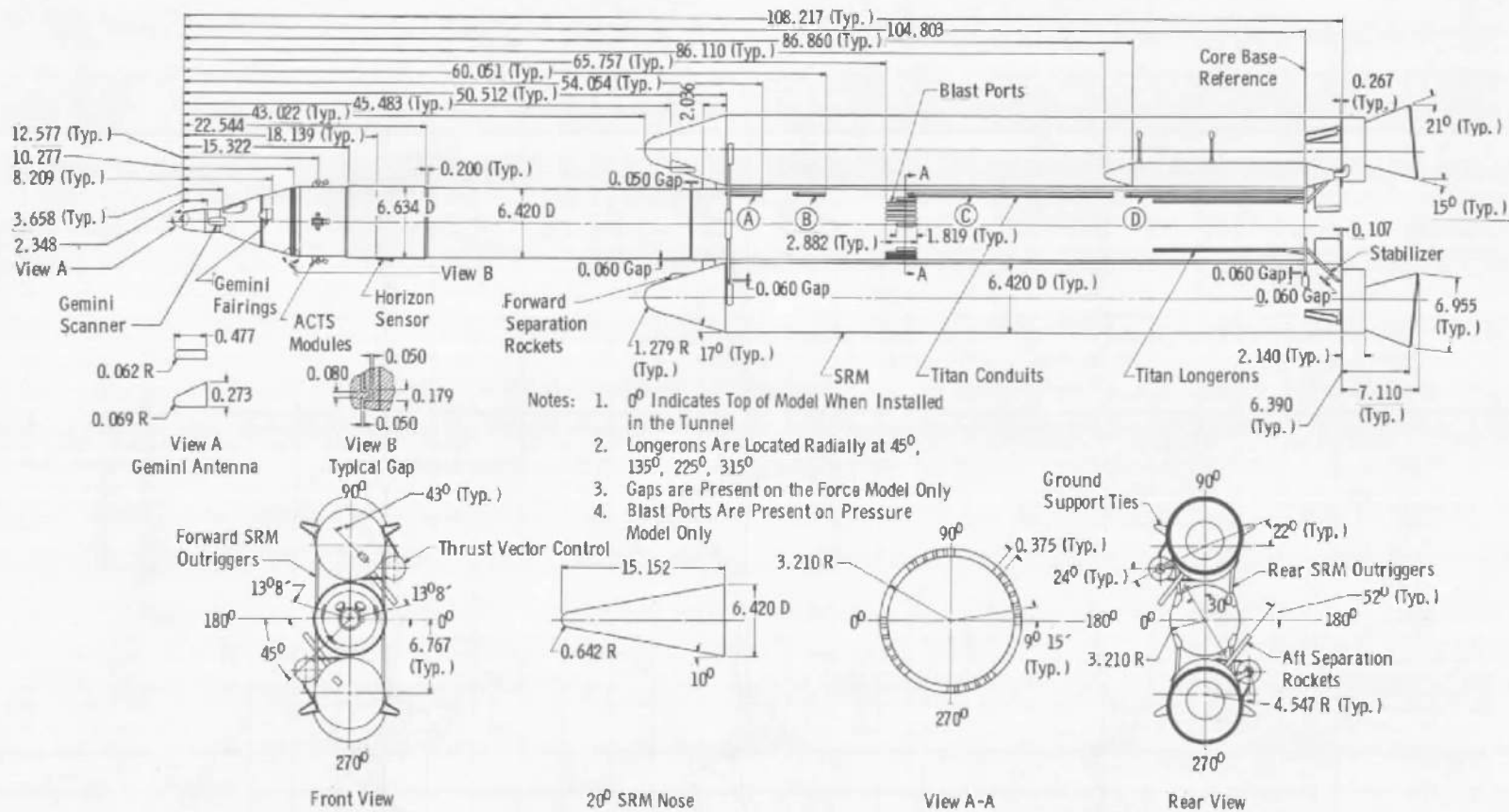
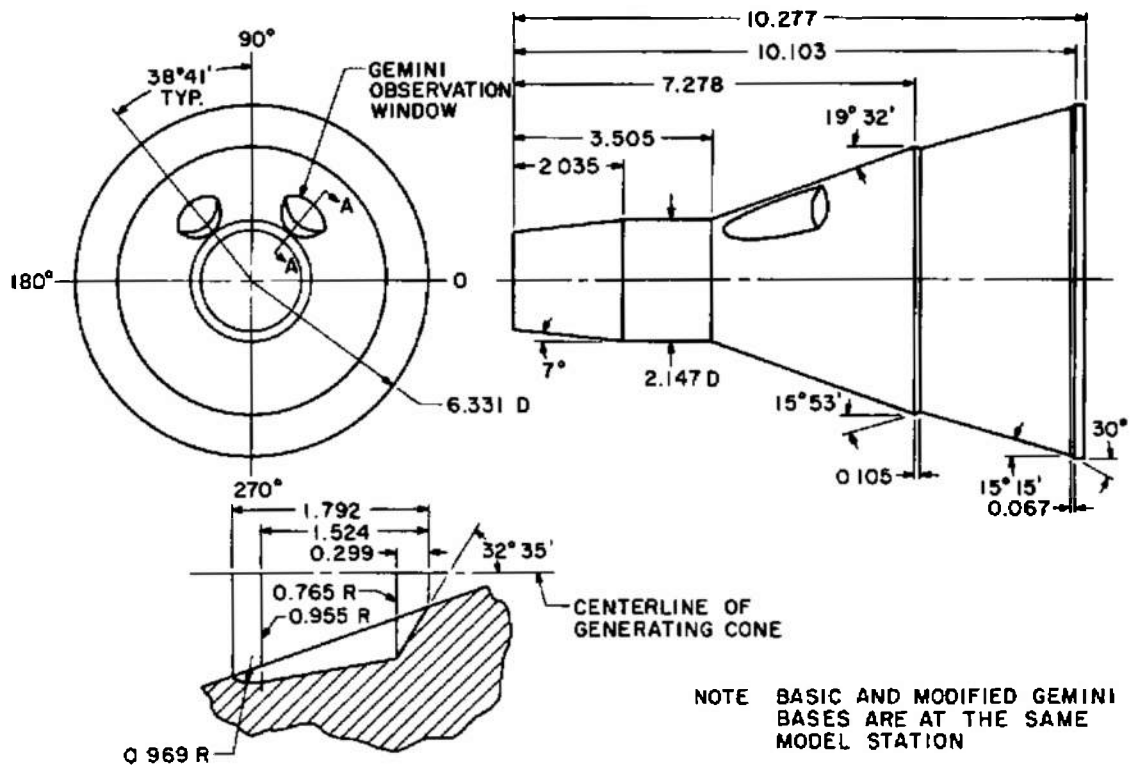


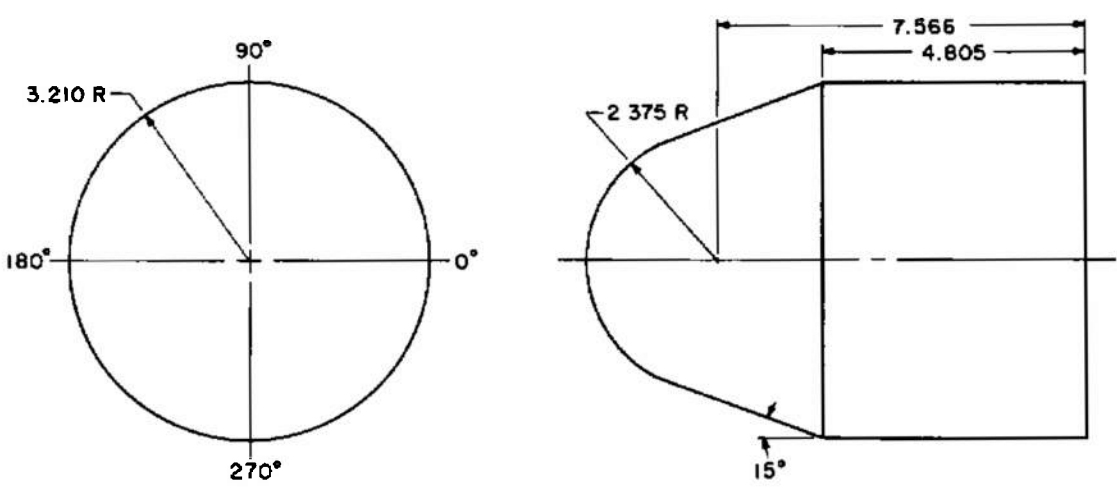
Fig. 5 Titan III/MOL Geometry

All Dimensions In Inches



VIEW A-A

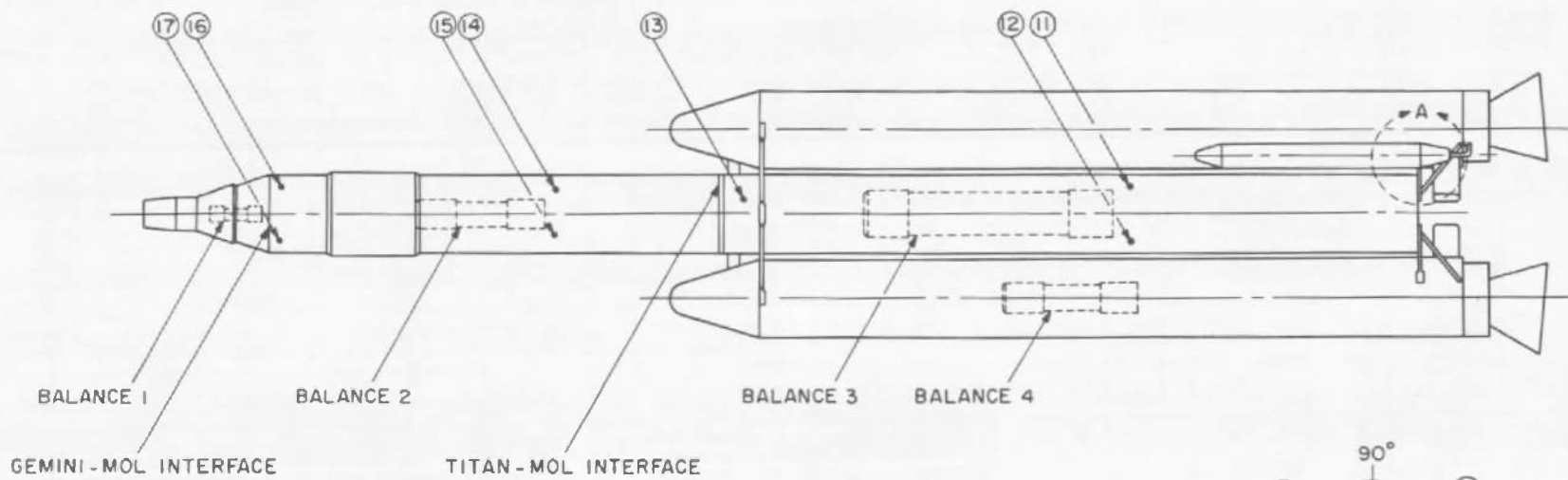
BASIC GEMINI DETAILS



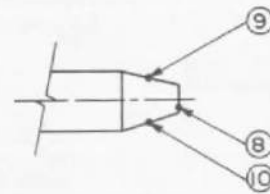
MODIFIED GEMINI DETAILS

ALL DIMENSIONS IN INCHES

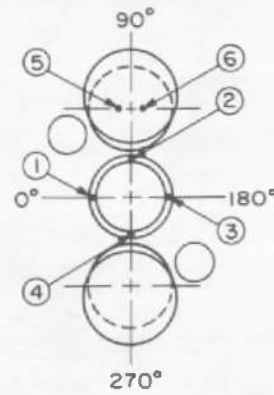
Fig. 6 Details of Modified and Basic Gemini Configurations



NOTES: PRESSURES 1 - 10 ARE BASE PRESSURES
 PRESSURES 11 - 17 ARE CAVITY PRESSURES

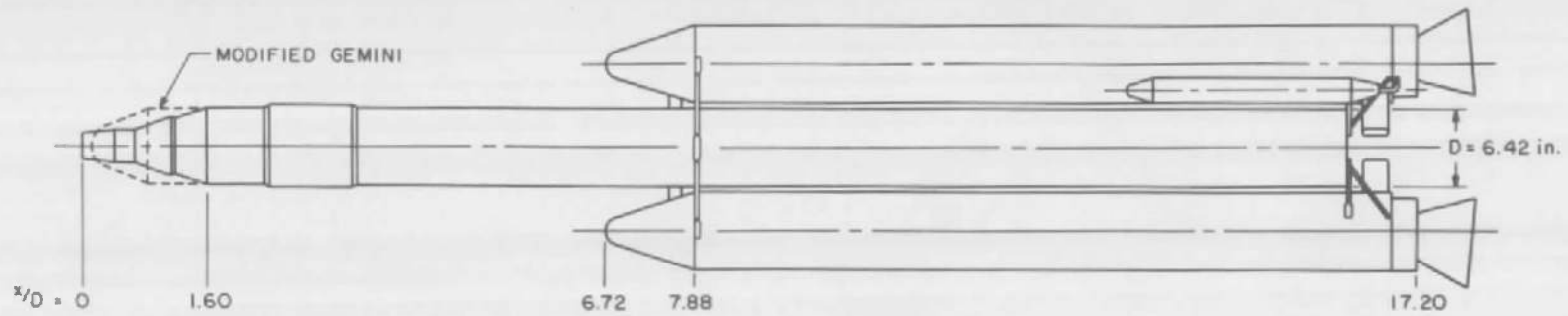


VIEW A



REAR VIEW

Fig. 7 Sketch of Force Model Showing Balance and Cavity Pressure Locations



X/D	A	X/D	A	X/D	A
*0.05	A	2.15	D	8.04	D
*0.17	B	2.32	D	8.20	E
*0.32	C	2.48	D	8.49	D
*0.50	C	2.81	D	8.69	D
*0.68	C	3.23	D	9.65	D
*0.82	C	3.65	D	10.16	G
*0.88	C	4.11	D	10.78	G
*0.96	C	4.56	D	11.02	D
*1.08	C	5.02	D	11.81	D
*1.34	C	5.48	D	12.40	F
		5.94	D	13.18	D
0.94	D	6.40	D	13.38	D
1.11	D	6.61	E	13.59	D
1.19	D	6.81	D	13.67	D
1.40	D	7.02	D	13.76	D
1.54	D	7.23	D	13.92	D
1.65	D	7.48	D	14.05	D
1.77	D	7.60	F	14.46	D
1.92	D	7.70	F	15.02	D
2.01	D	7.81	D	16.19	D

NOTE: ASTERISK DENOTES MODIFIED GEMINI

X/D	θ	X/D	θ
*0.81	A	2.69	C
*0.89	B	2.81	A
*0.97	A	3.16	C
*1.13	A	3.59	C
*1.79	C	3.77	C
*1.90	D	5.57	C
1.19	A	6.44	C
1.40	A	6.69	F
1.52	C	6.90	C
1.77	B	7.11	C
1.90	A	7.42	C
2.11	A	7.94	G
2.15	C	8.34	H
2.52	E	9.10	G

PRESSURE LEGEND

A: Nose Stagnation
 B: 0, 30 deg
 C: 0, 30, 60, 90 deg
 D: 0, 30, 60, 90, 120, 150, 180 deg
 E: 30, 60, 90, 120, 150, 180 deg
 F: 30, 60, 120, 150, 180 deg
 G: 0, 30, 60, 90, 120, 150, 180, 210, 240, 270, 300, 330 deg

MICROPHONE LEGEND

A: 315 deg
 B: 292, 315 deg
 C: 270 deg
 D: 292 deg
 E: 270, 292, 315 deg
 F: 0, 270, 285, 300, 330 deg
 G: 300 deg
 H: 0, 270, 300 deg

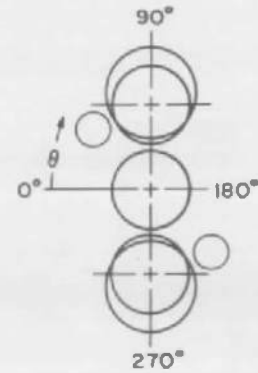


Fig. 8 Sketch of Pressure Model Showing Locations of Pressure Orifices and Microphones

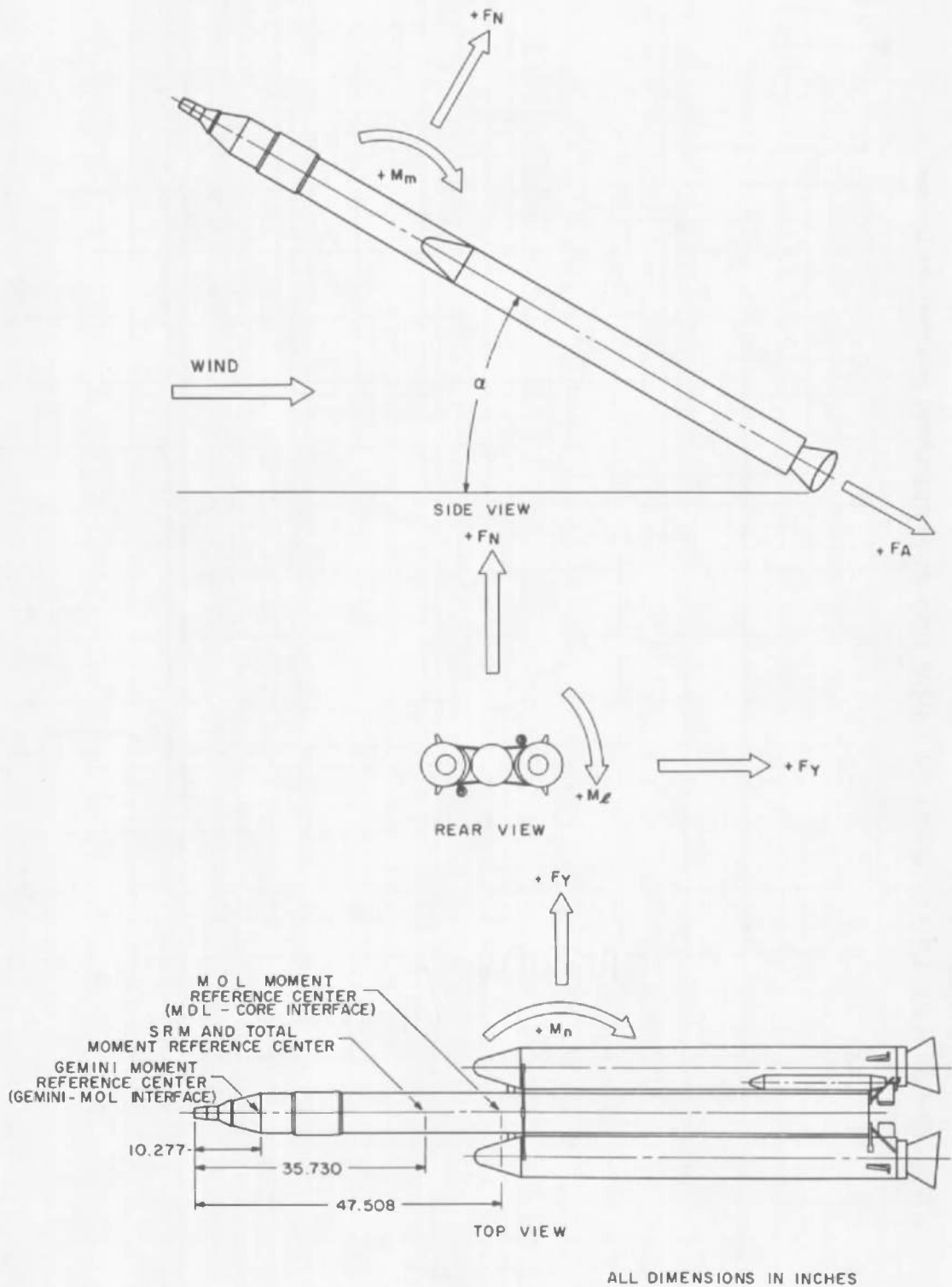


Fig. 9 Orientation of Forces and Moments

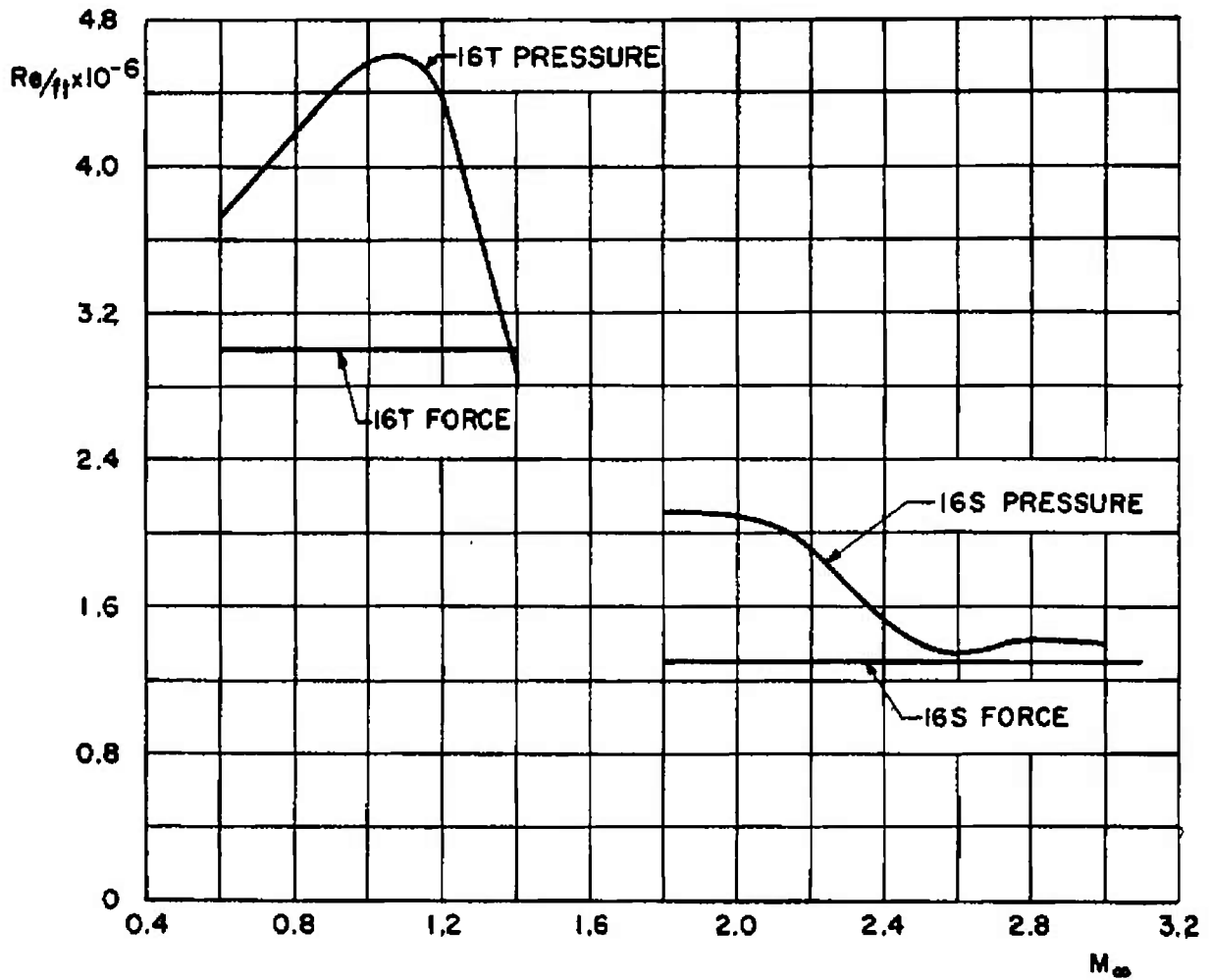


Fig. 10 Variation of Reynolds Number with Mach Number

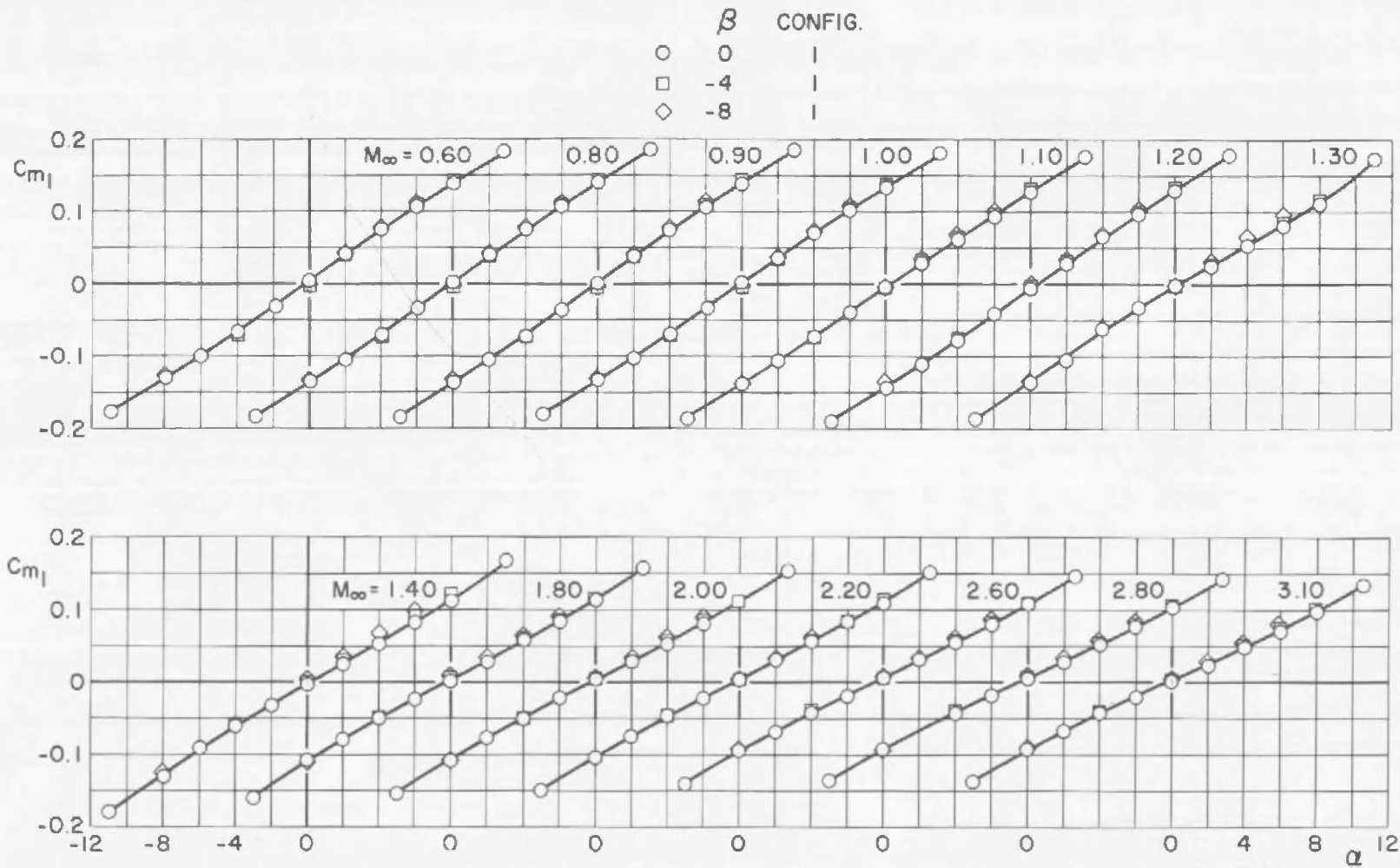


Fig. 11 Variation of Pitching-Moment Coefficient with Angle of Attack for the Gemini Section

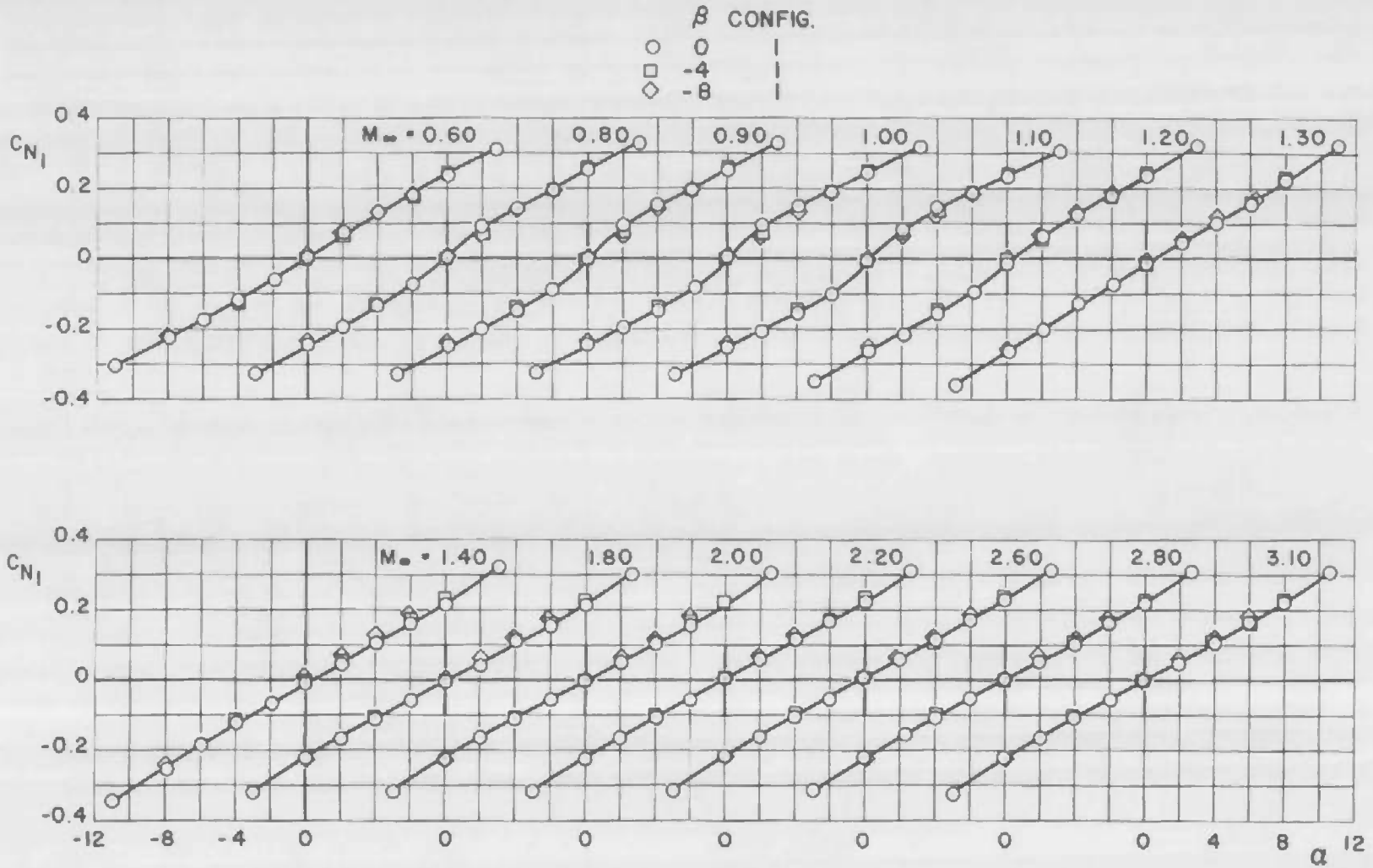


Fig. 12 Variation of Normal-Force Coefficient with Angle of Attack for the Gemini Section

	α	CONFIG
○	0	1
□	4	1
◇	8	1

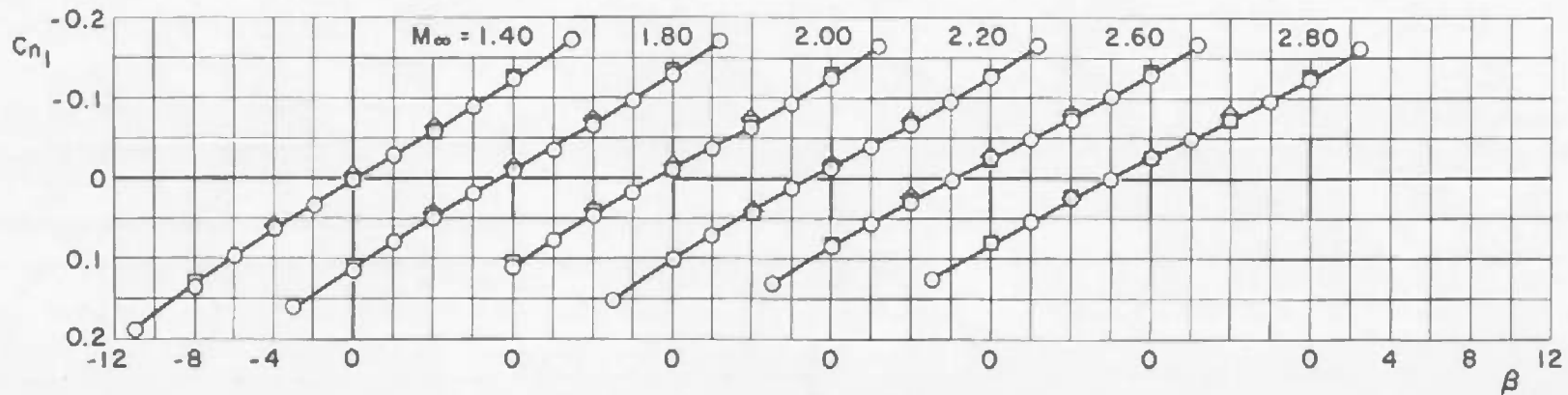
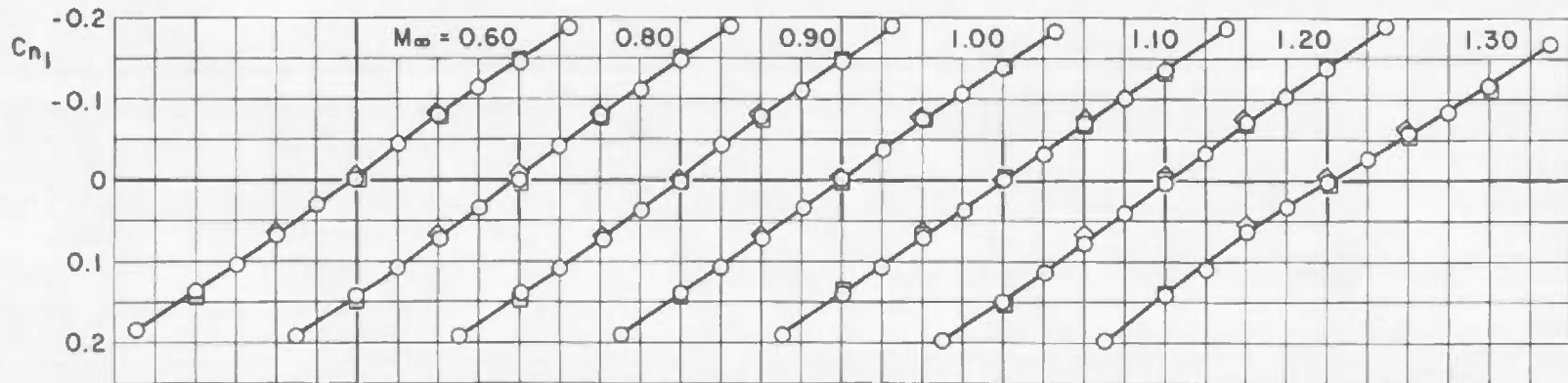


Fig. 13 Variation of Yawing-Moment Coefficient with Sideslip Angle for the Gemini Section

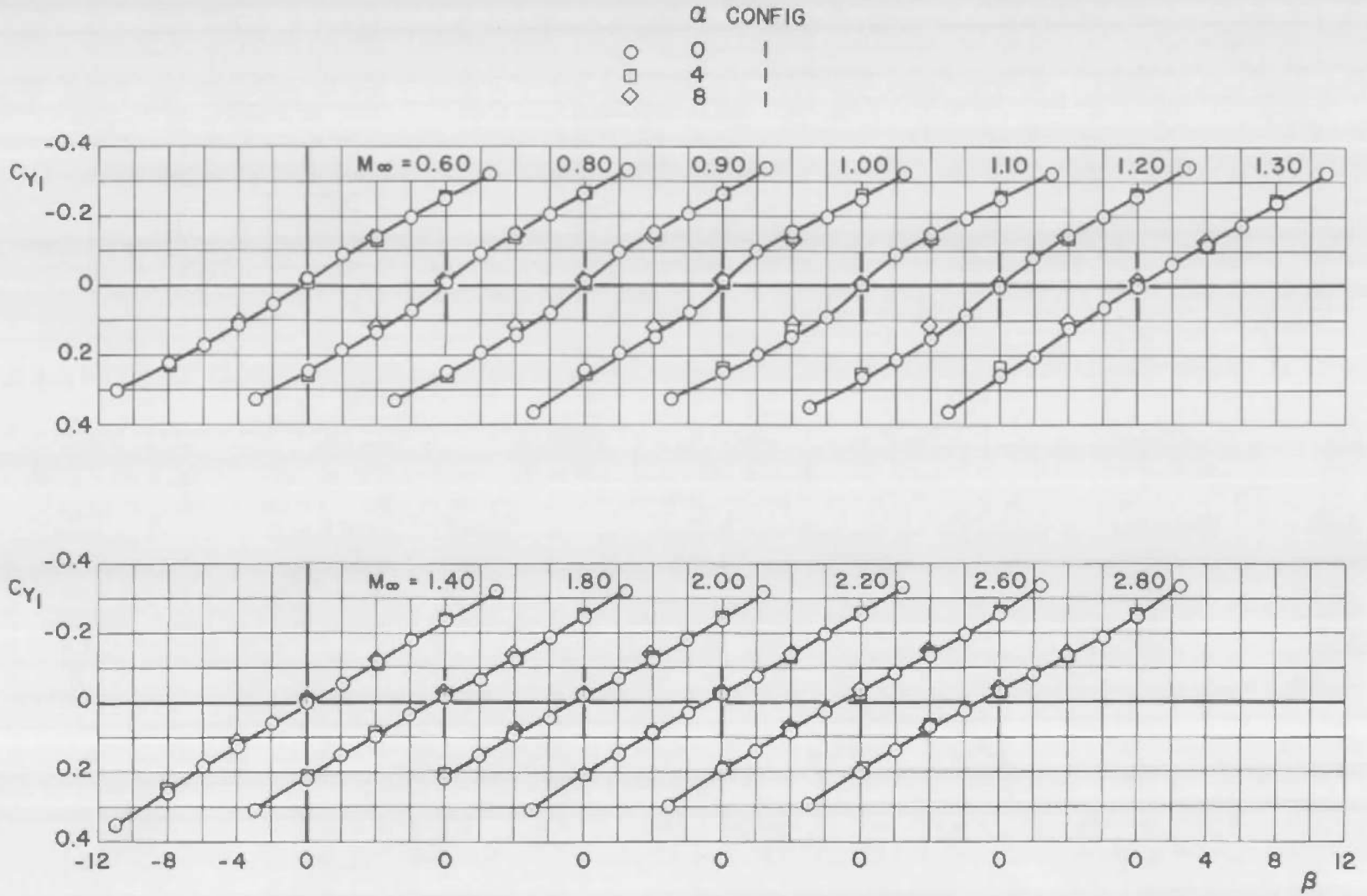
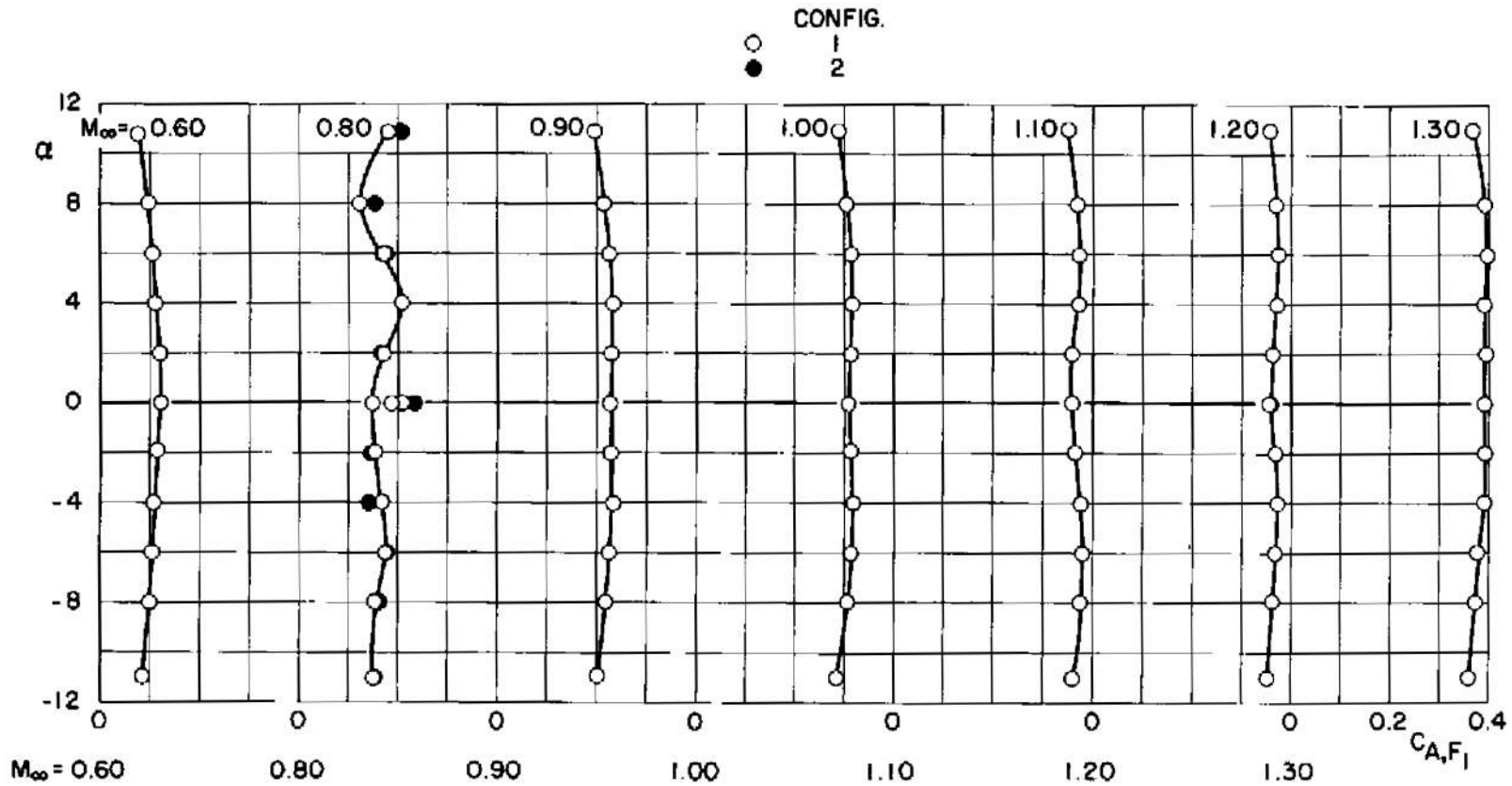
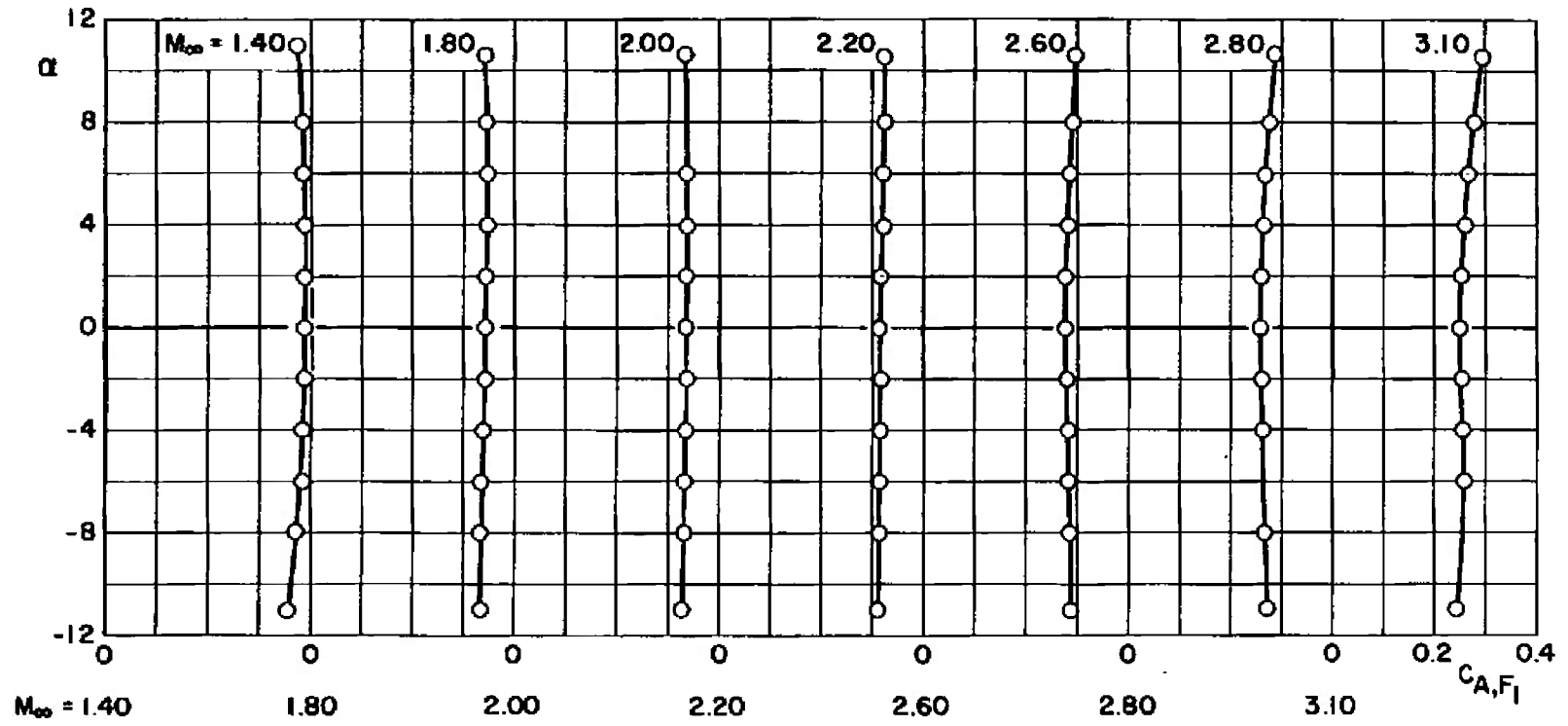


Fig. 14 Variation of Side-Force Coefficient with Sideslip Angle for the Gemini Section



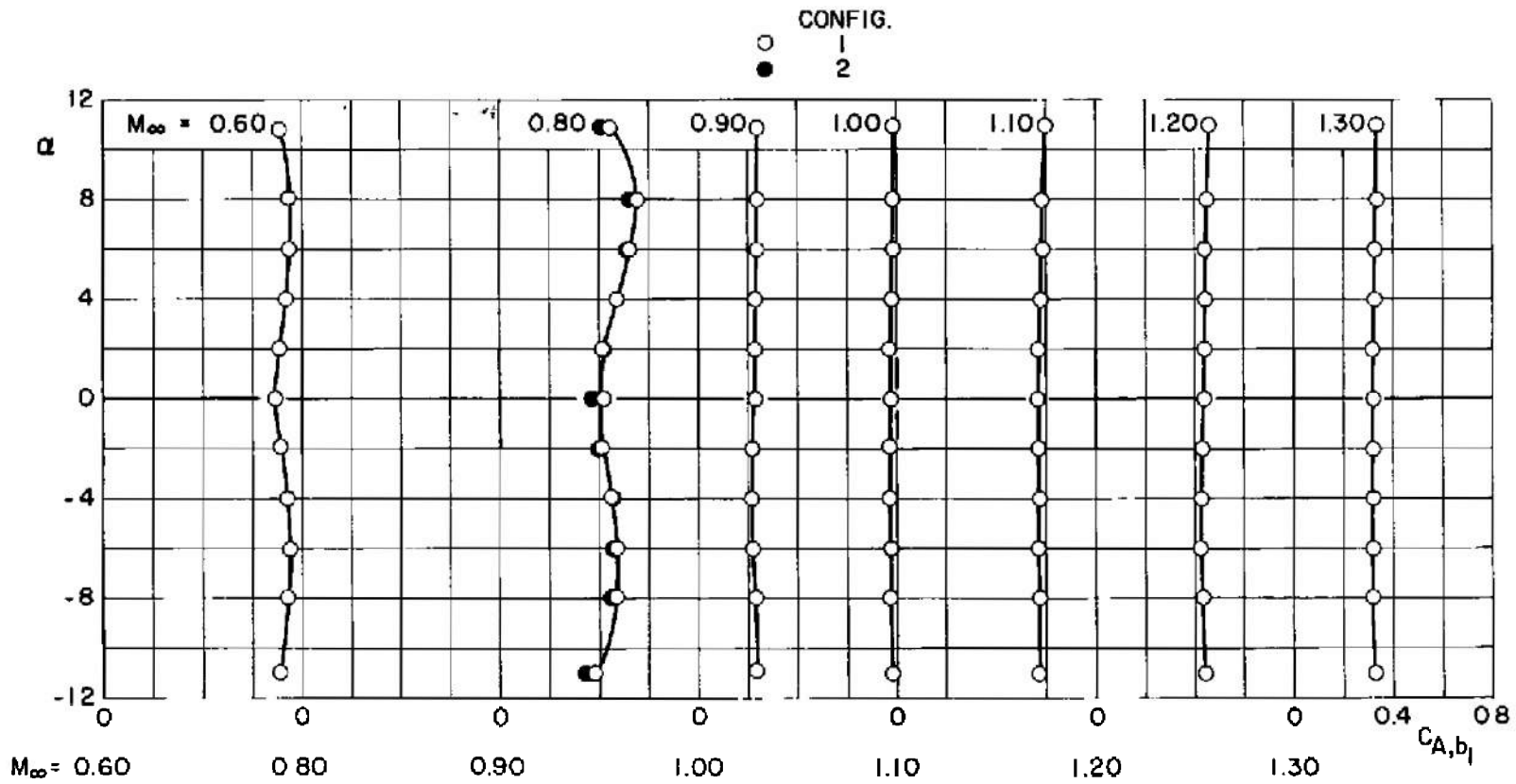
a. Mach Numbers 0.60 through 1.30

Fig. 15 Variation of Forebody Axial-Force Coefficient with Angle of Attack for the Gemini Section, $\beta = 0$



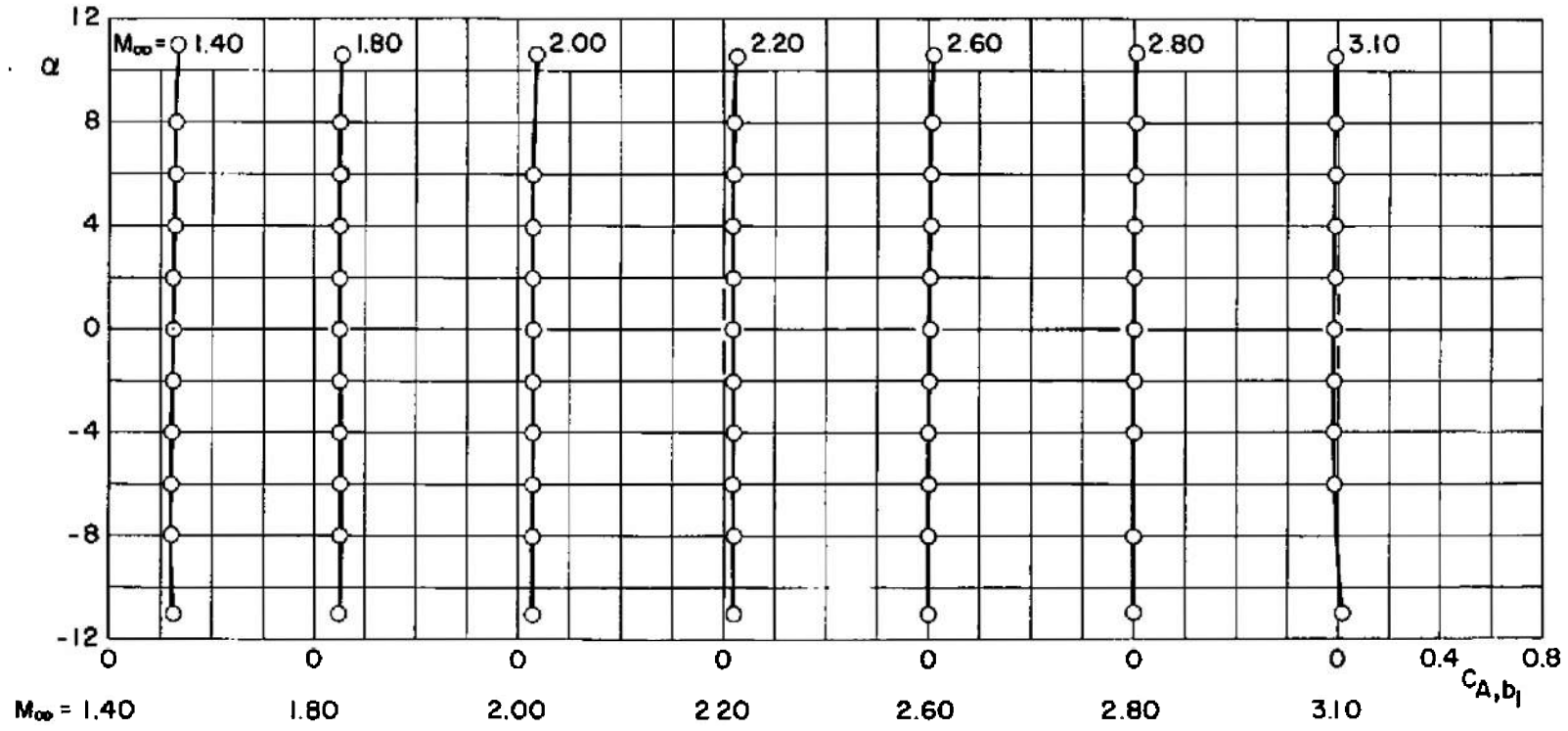
b. Mach Numbers 1.40 through 3.10

Fig. 15 Concluded



a. Mach Numbers 0.60 through 1.30

Fig. 16 Variation of Base Axial-Force Coefficient with Angle of Attack for the Gemini Section, $\beta = 0$



b. Mach Numbers 1.40 through 3.10
 Fig. 16 Concluded

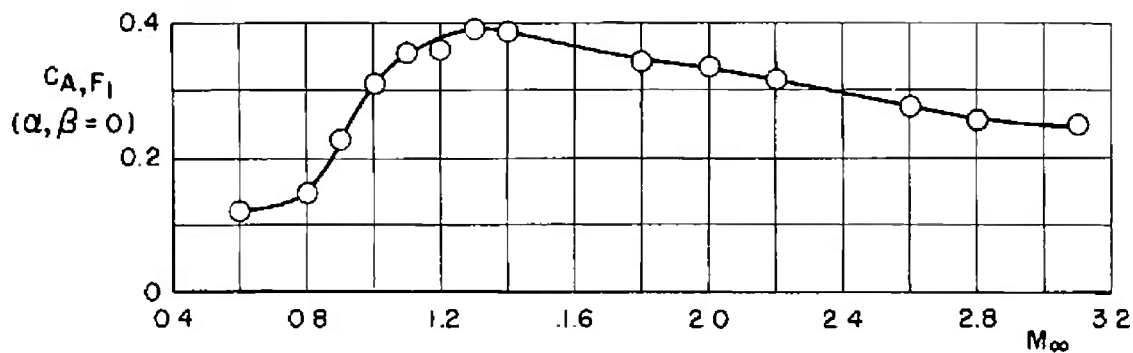


Fig. 17 Variation of Forebody Axial-Force Coefficient with Mach Number for the Gemini Section

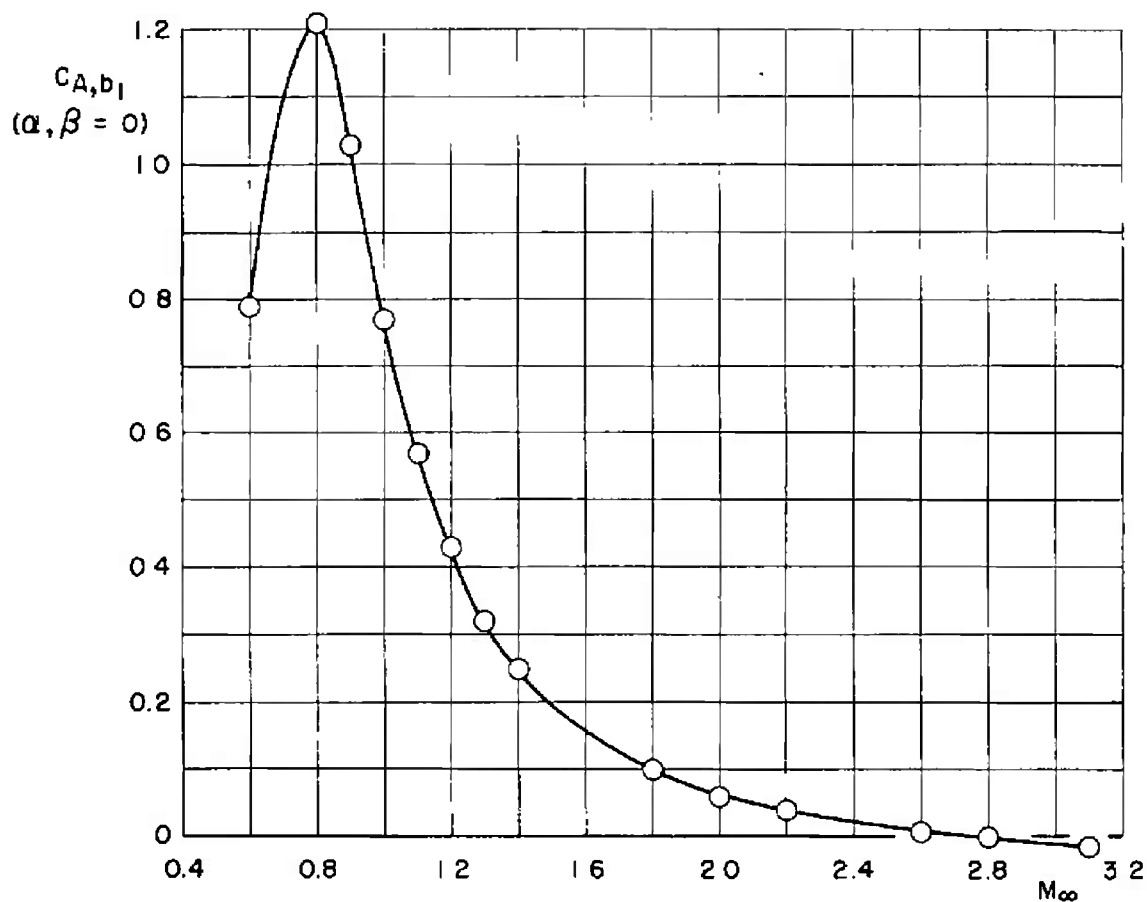


Fig. 18 Variation of Base Axial-Force Coefficient with Mach Number for the Gemini Section

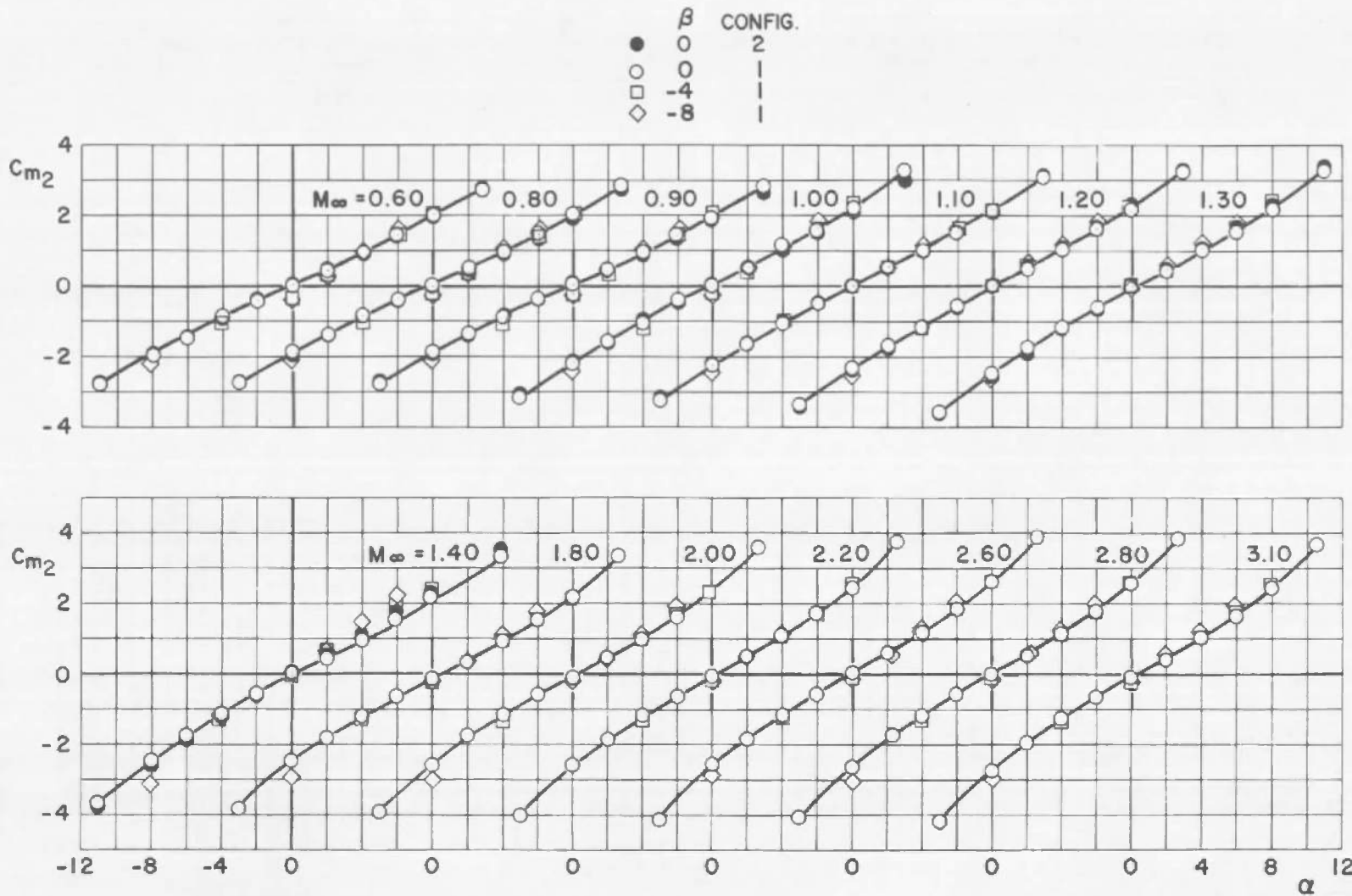


Fig. 19 Variation of Pitching-Moment Coefficient with Angle of Attack for the MOL-Gemini Section in the Presence of SRM Configurations 1 and 2

	β	CONFIG
●	0	2
○	0	1
□	-4	1
◇	-8	

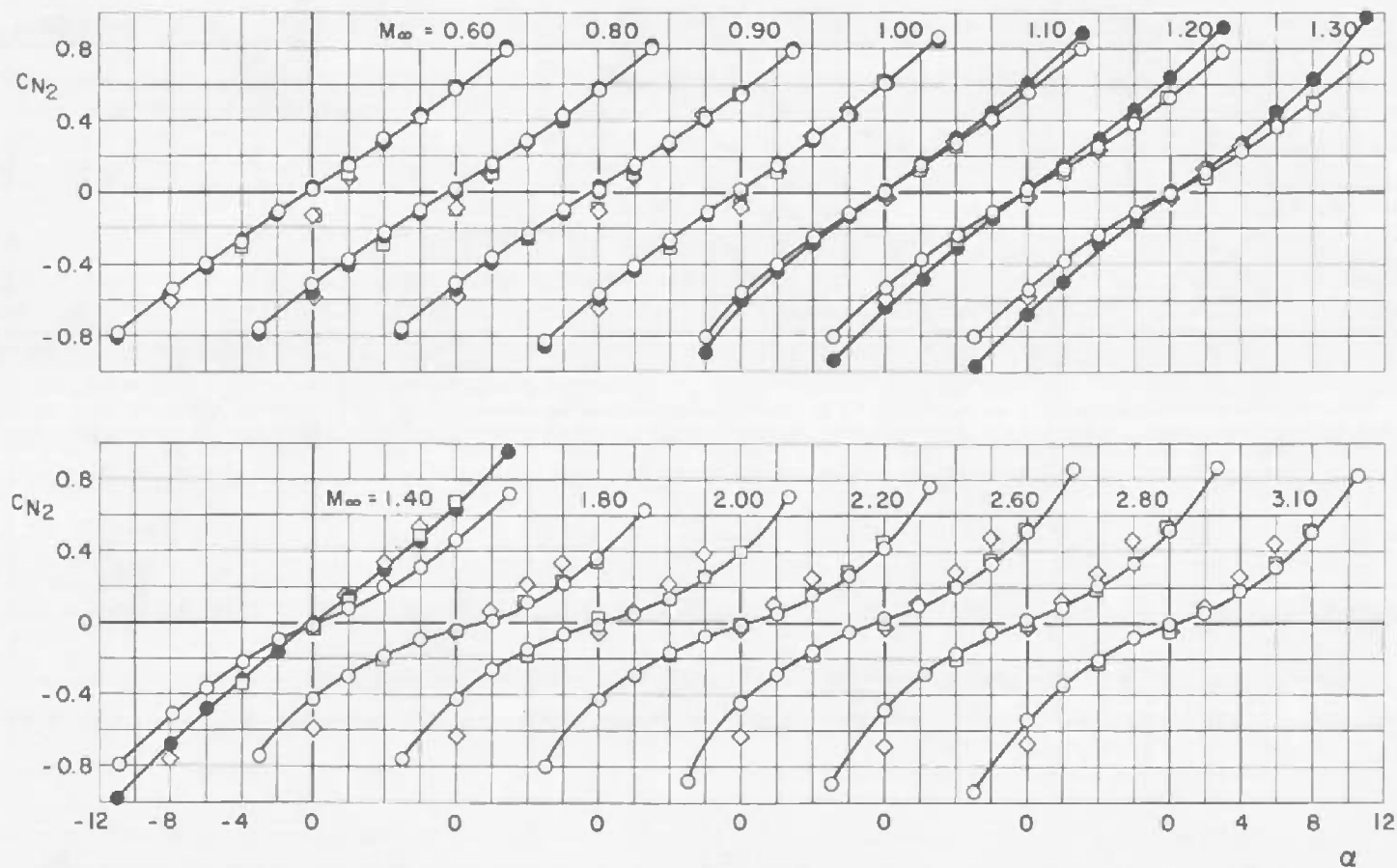


Fig. 20 Variation of Normal-Force Coefficient with Angle of Attack for the MOL-Gemini Section in the Presence of SRM Configurations 1 and 2

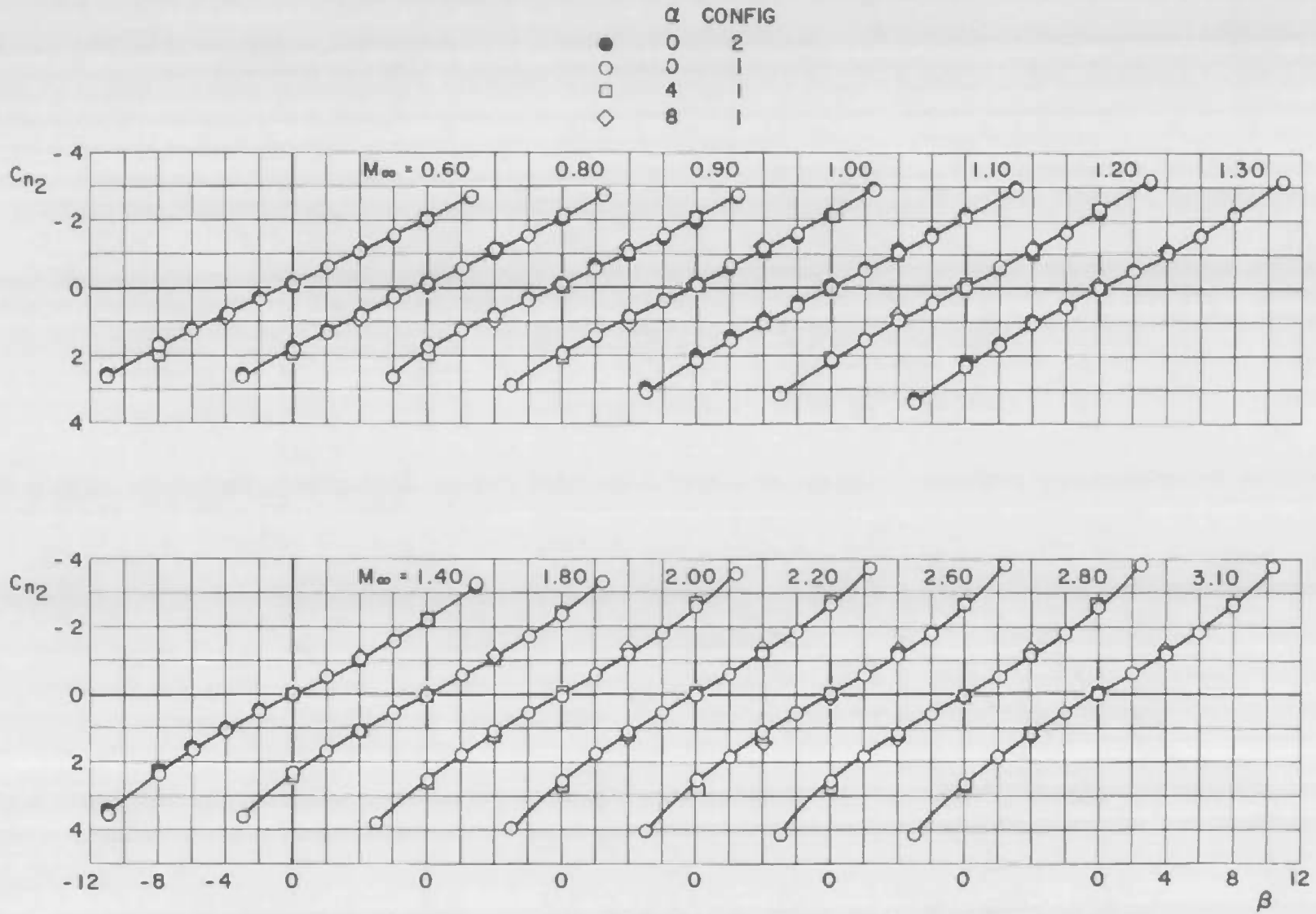


Fig. 21 Variation of Yawing-Moment Coefficient with Sideslip Angle for the MOL-Gemini Section in the Presence of SRM Configurations 1 and 2

α	CONFIG
●	0 2
○	0 1
□	4 1
◇	8 1

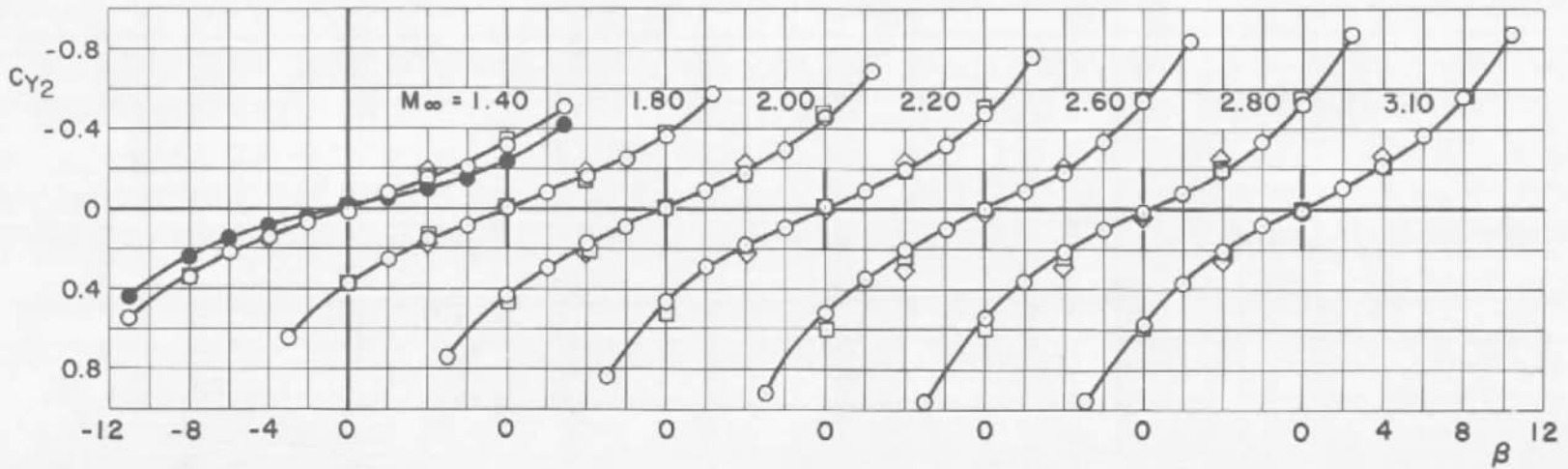
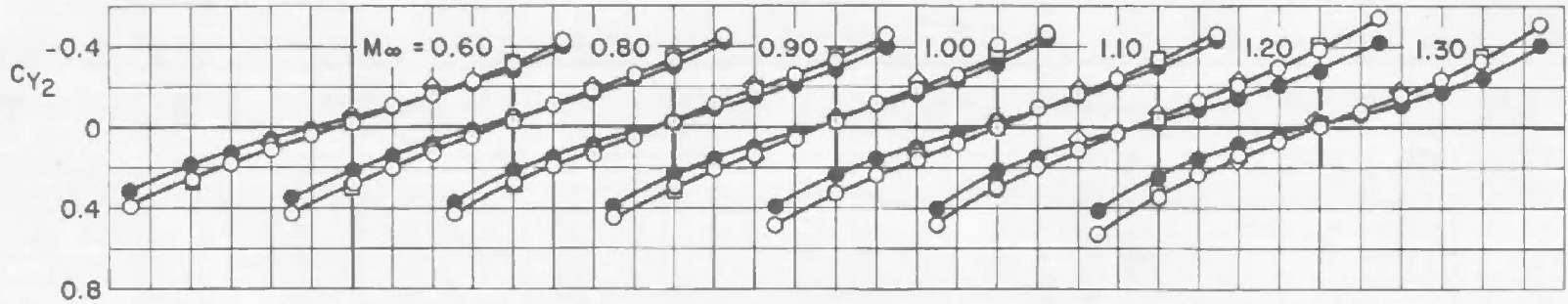
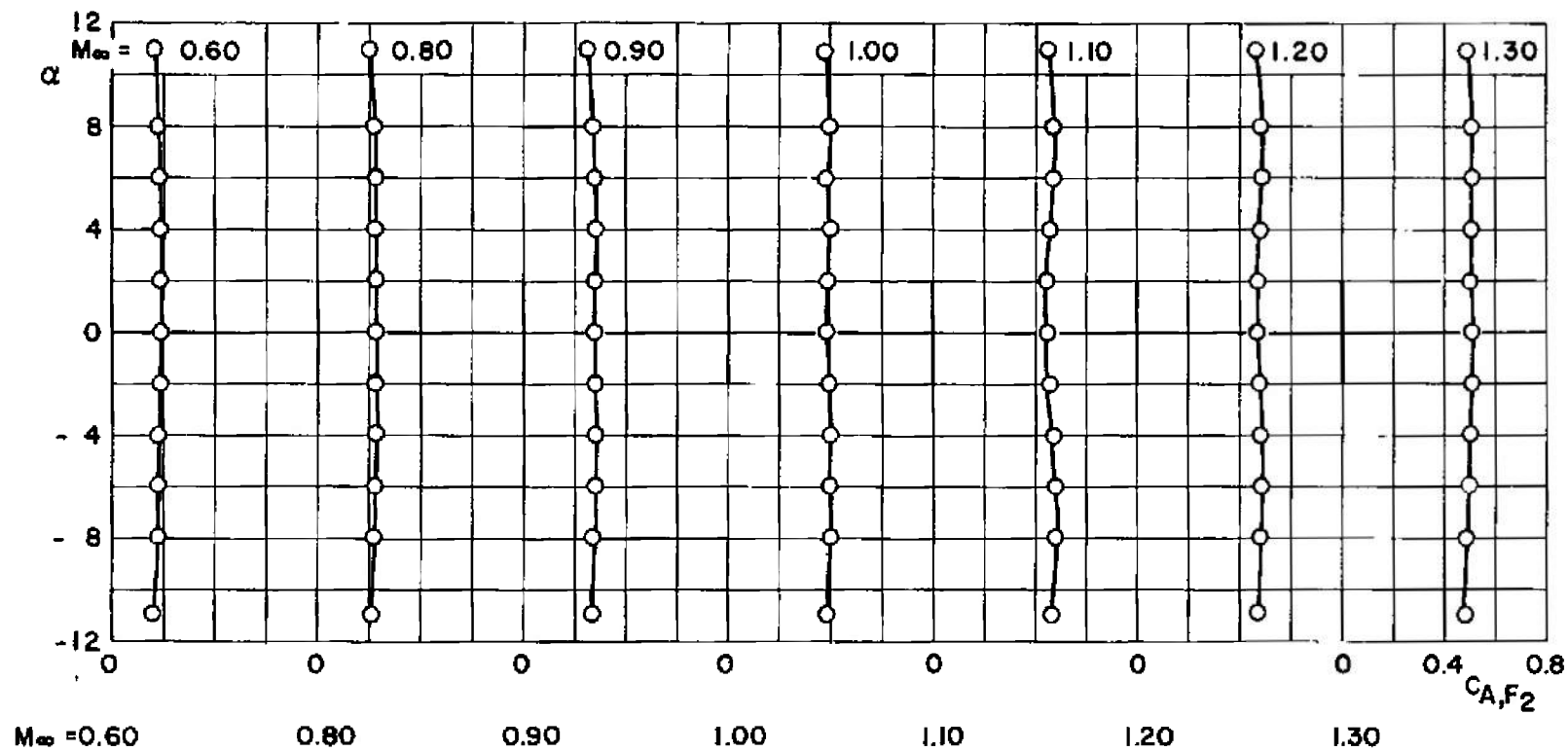
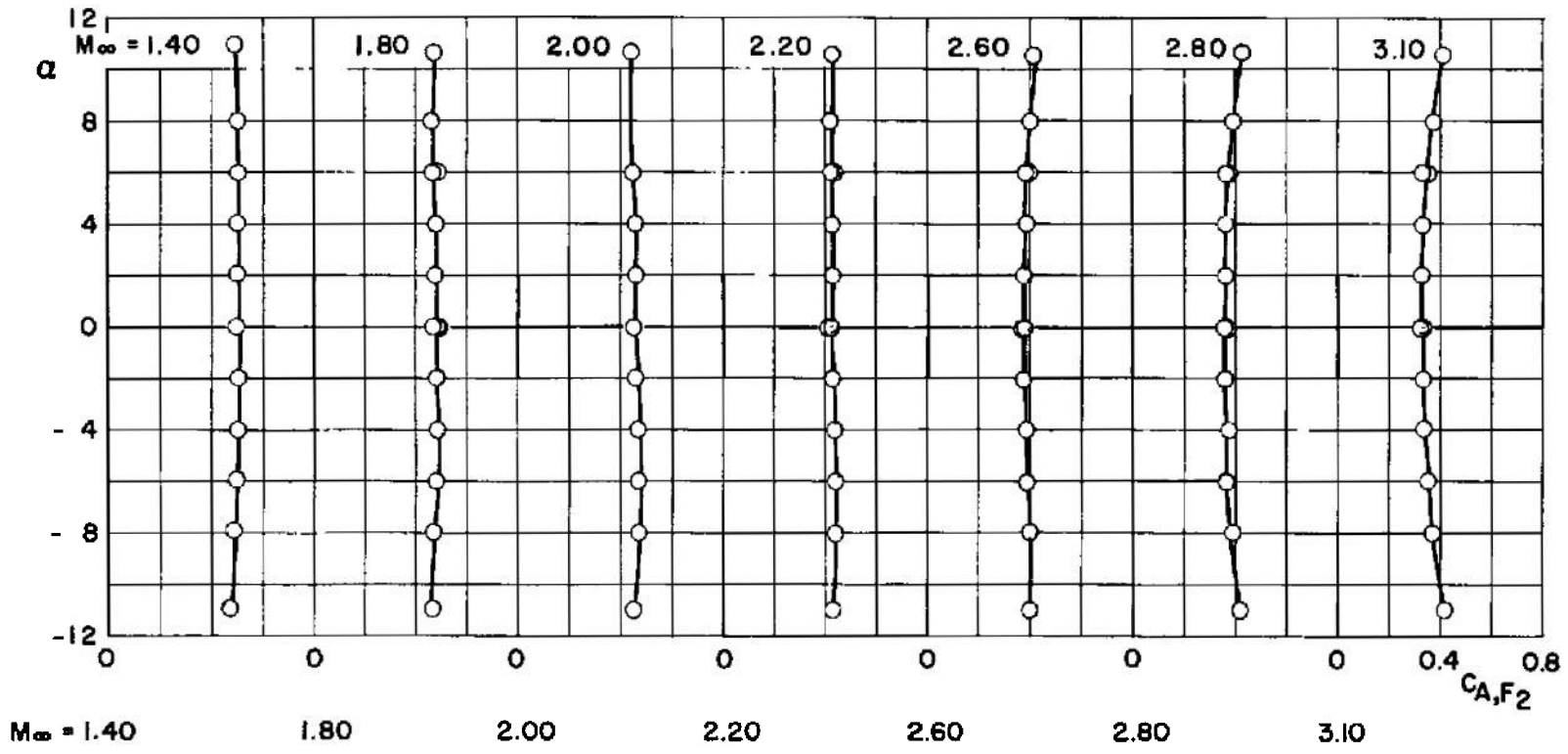


Fig. 22 Variation of Side-Force Coefficient with Sideslip Angle for the MOL-Gemini Section in the Presence of SRM Configurations 1 and 2

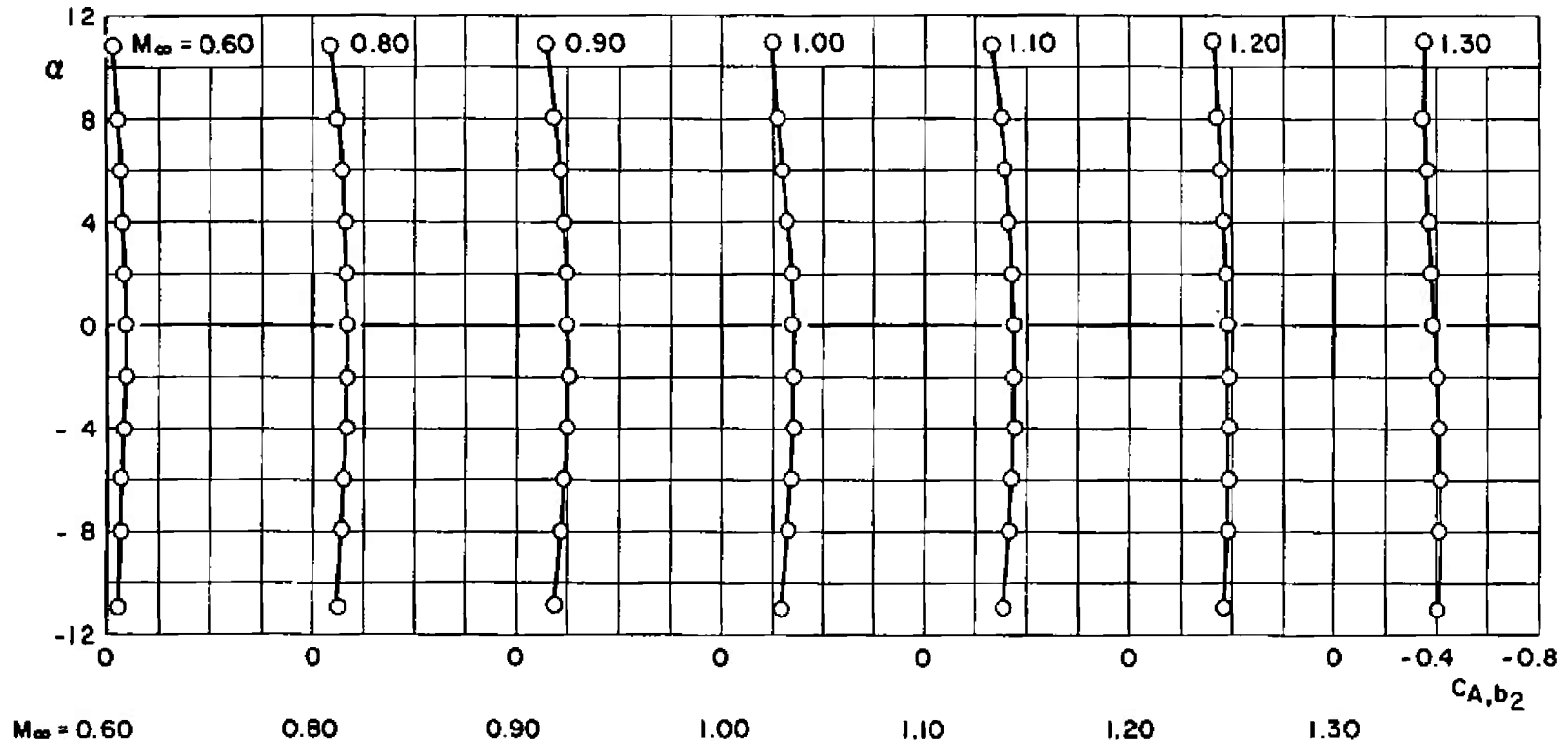


a. Mach Numbers 0.60 through 1.30

Fig. 23 Variation of Forebody Axial-Force Coefficient with Angle of Attack for the MOL-Gemini Section in the Presence of SRM Configuration 1, $\beta = 0$

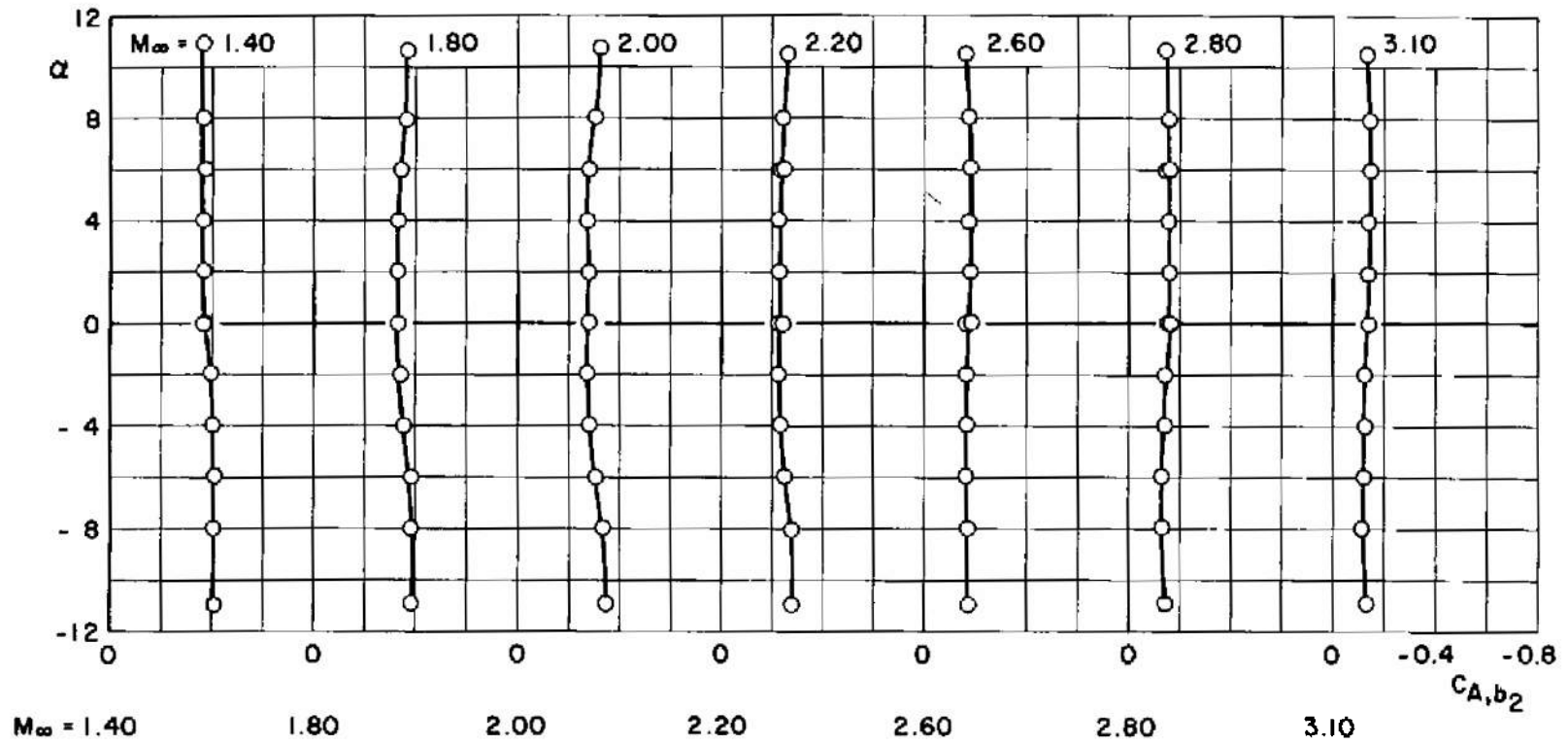


b. Mach Numbers 1.40 through 3.10
 Fig. 23 Concluded



a. Mach Numbers 0.60 through 1.30

Fig. 24 Variation of Base Axial-Force Coefficient with Angle of Attack for the MOL-Gemini Section in the Presence of SRM Configuration 1, $\beta = 0$



b. Mach Numbers 1.40 through 3.10
 Fig. 24 Concluded

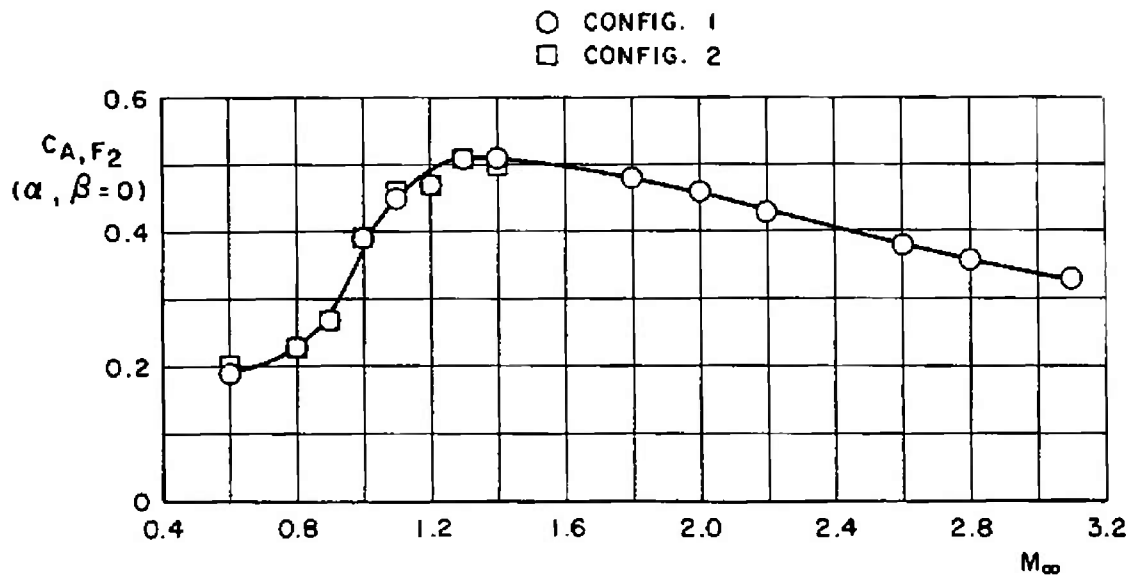


Fig. 25 Variation of Forebody Axial-Force Coefficient with Mach Number for the MOL-Gemini Section in the Presence of SRM Configurations 1 and 2

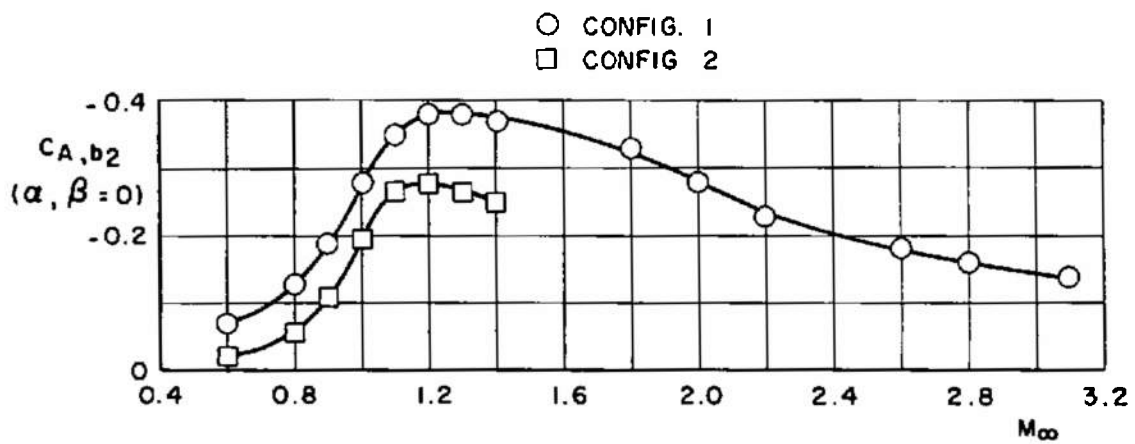


Fig. 26 Variation of Base Axial-Force Coefficient with Mach Number for the MOL-Gemini Section in the Presence of SRM Configurations 1 and 2

β	CONFIG.
●	0 2
○	0 1
□	-4 1
◇	-8 1

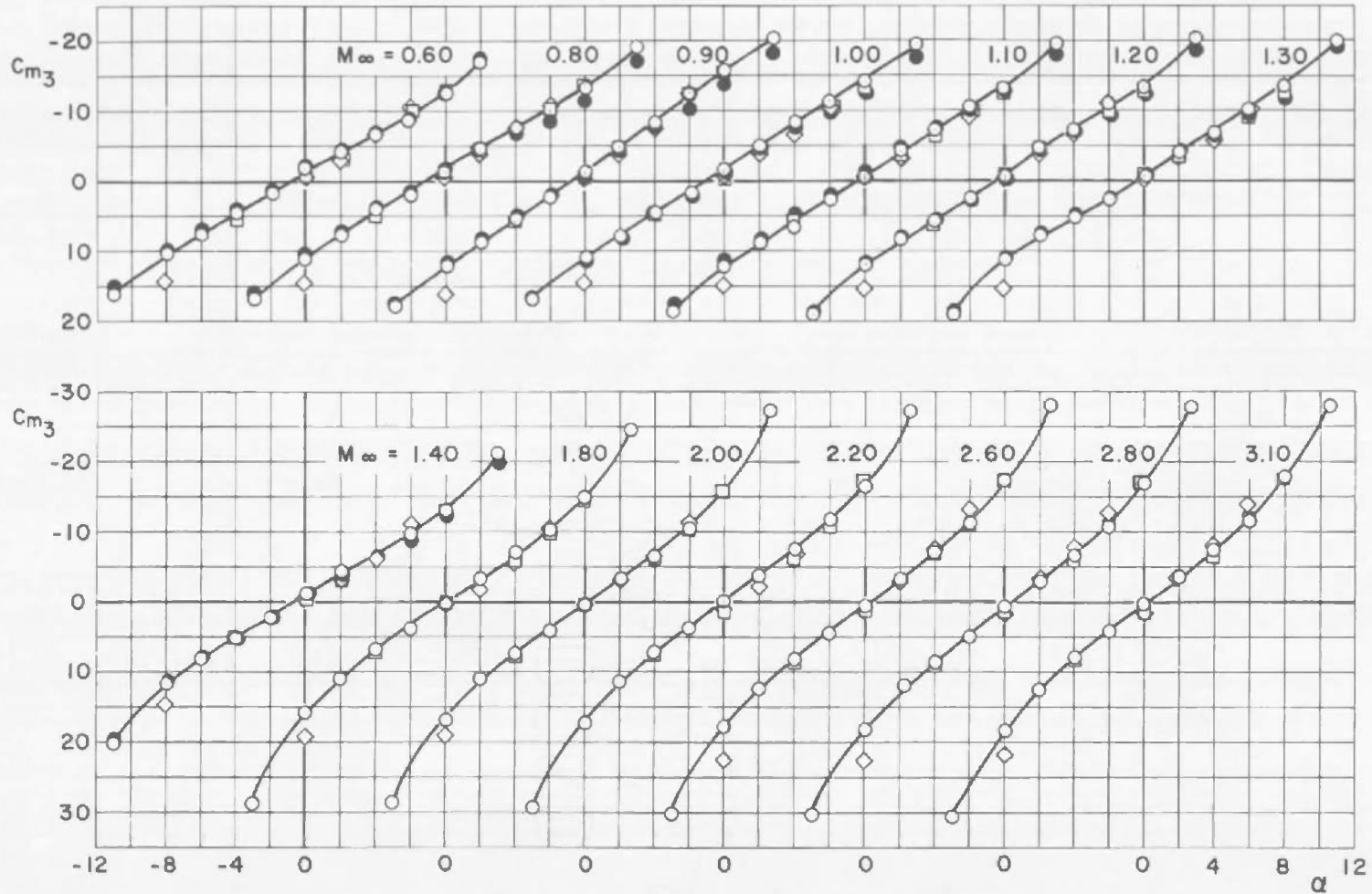


Fig. 27 Variation of Pitching-Moment Coefficient with Angle of Attack for Configurations 1 and 2 of the Composite Model

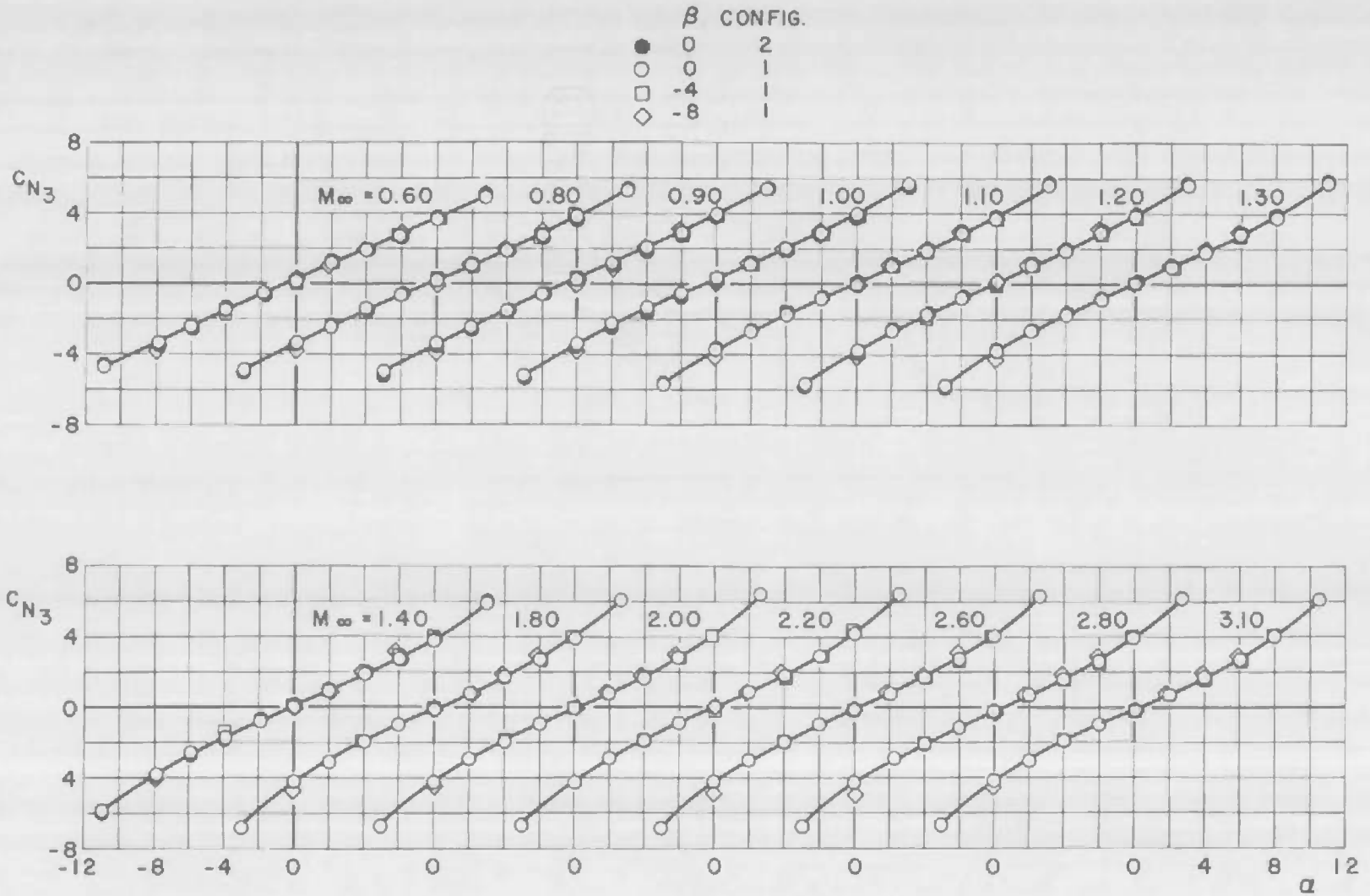


Fig. 28 Variation of Normal-Force Coefficient with Angle of Attack for Configurations 1 and 2 of the Composite Model

α CONFIG	
●	0 2
○	0 1
□	4 1
◇	8 1

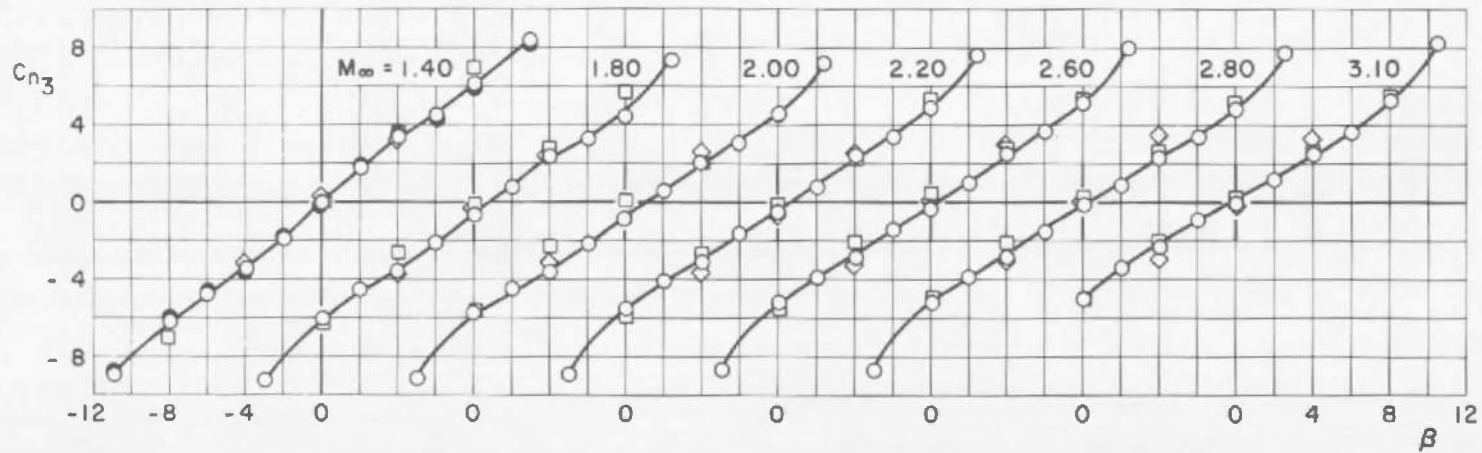
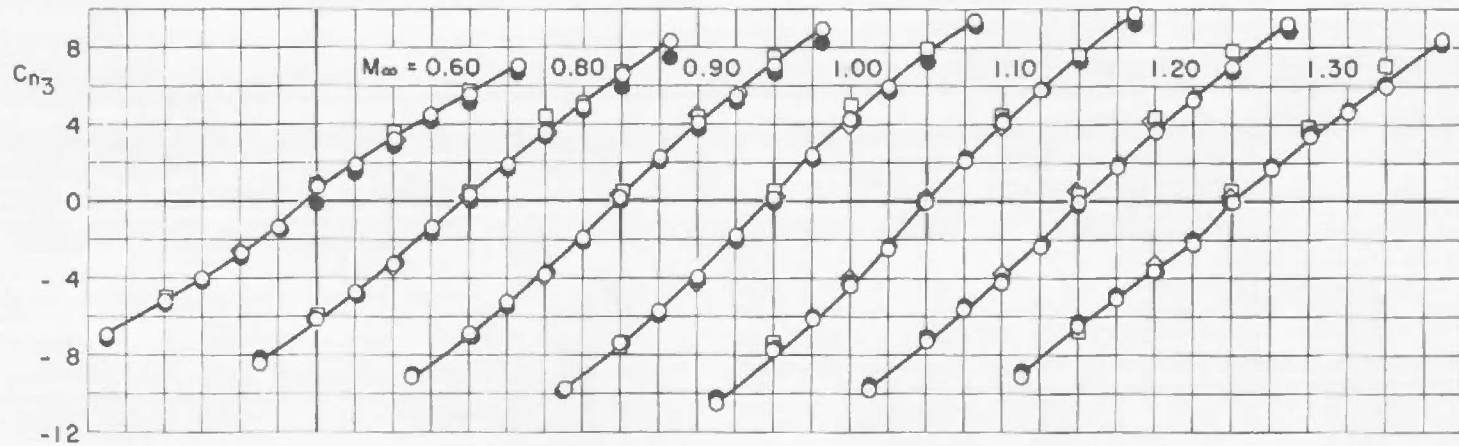


Fig. 29 Variation of Yawing-Moment Coefficient with Sideslip Angle for Configurations 1 and 2 of the Composite Model

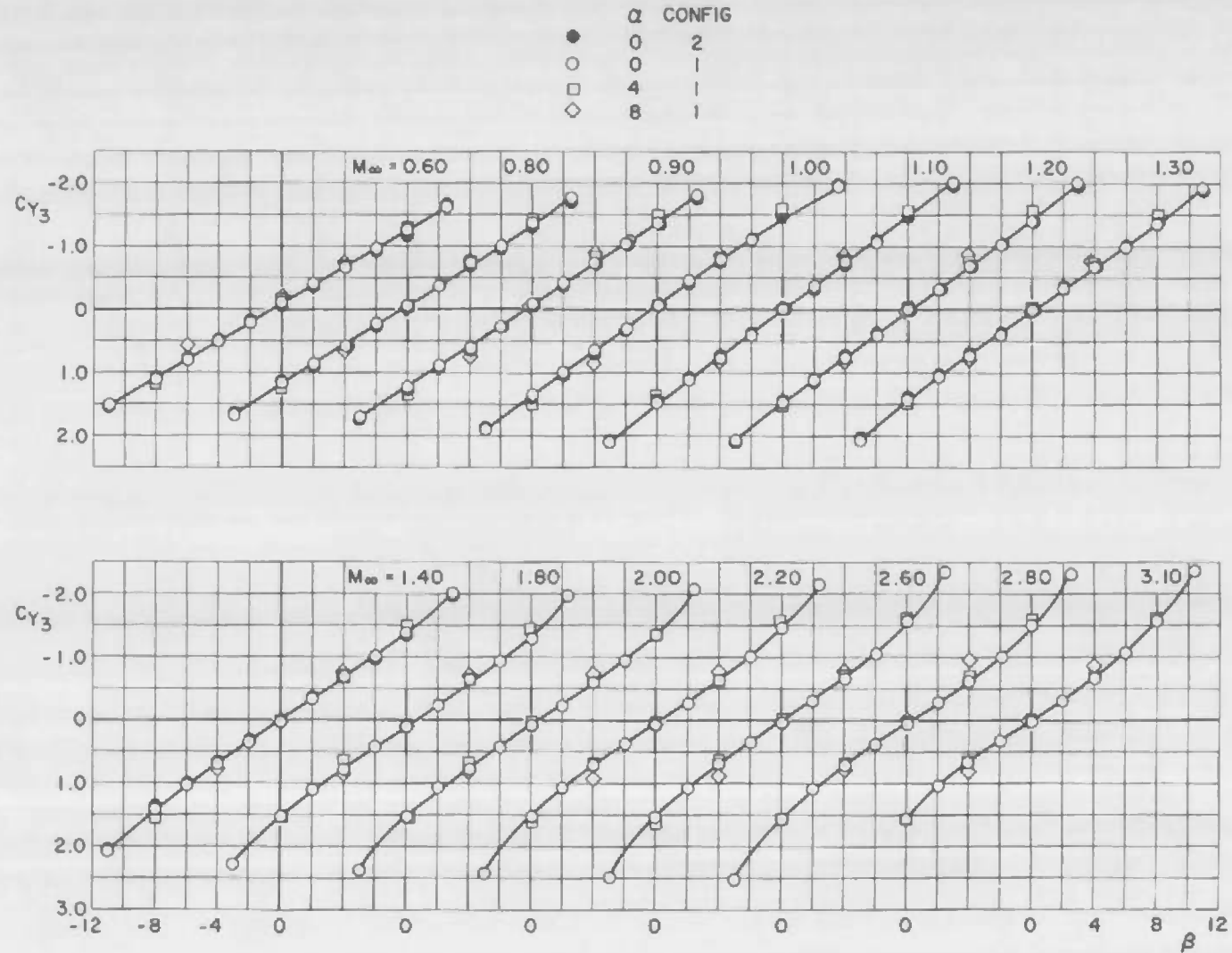


Fig. 30 Variation of Side-Force Coefficient with Sideslip Angle for Configurations 1 and 2 of the Composite Model

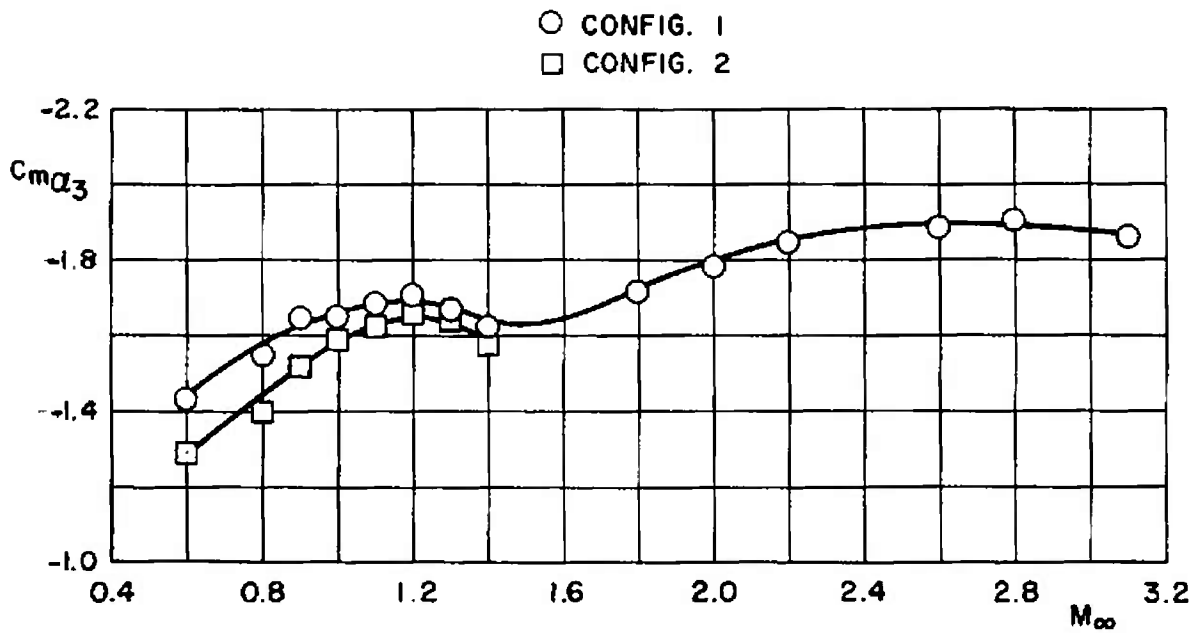


Fig. 31 Variation of Pitching-Moment Curve Slope with Mach Number for Configurations 1 and 2 of the Composite Model

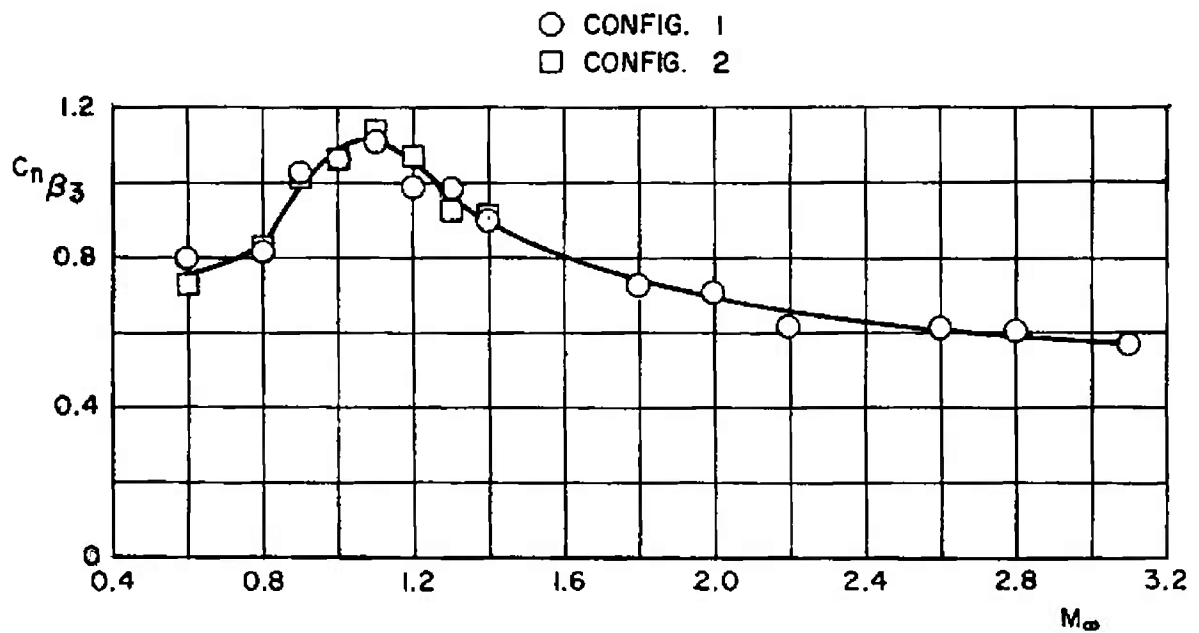
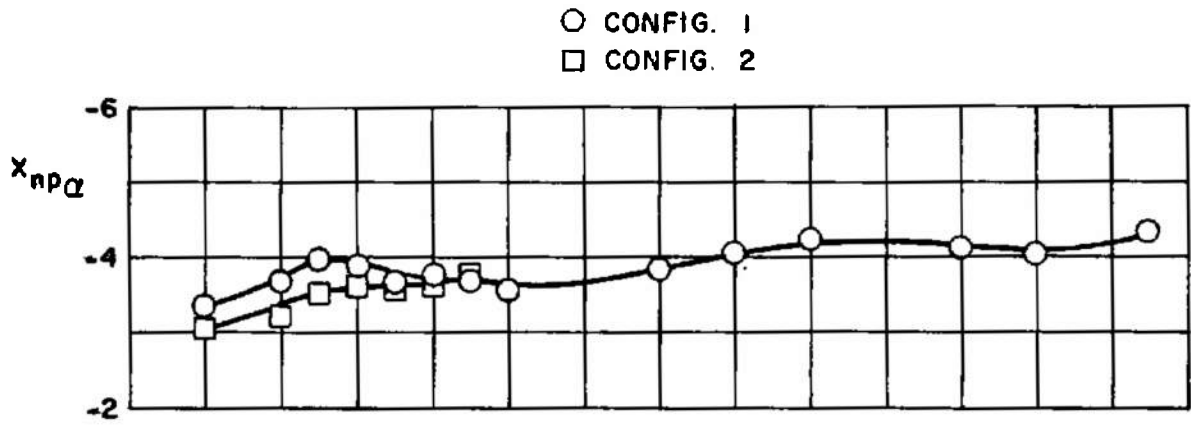
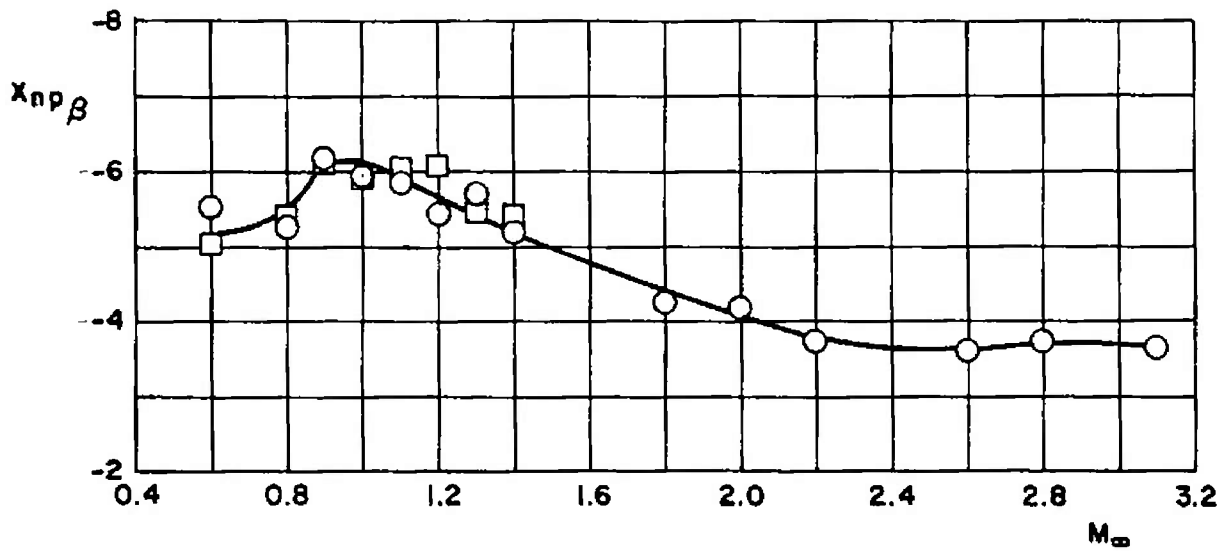


Fig. 32 Variation of Yawing-Moment Curve Slope with Mach Number for Configurations 1 and 2 of the Composite Model

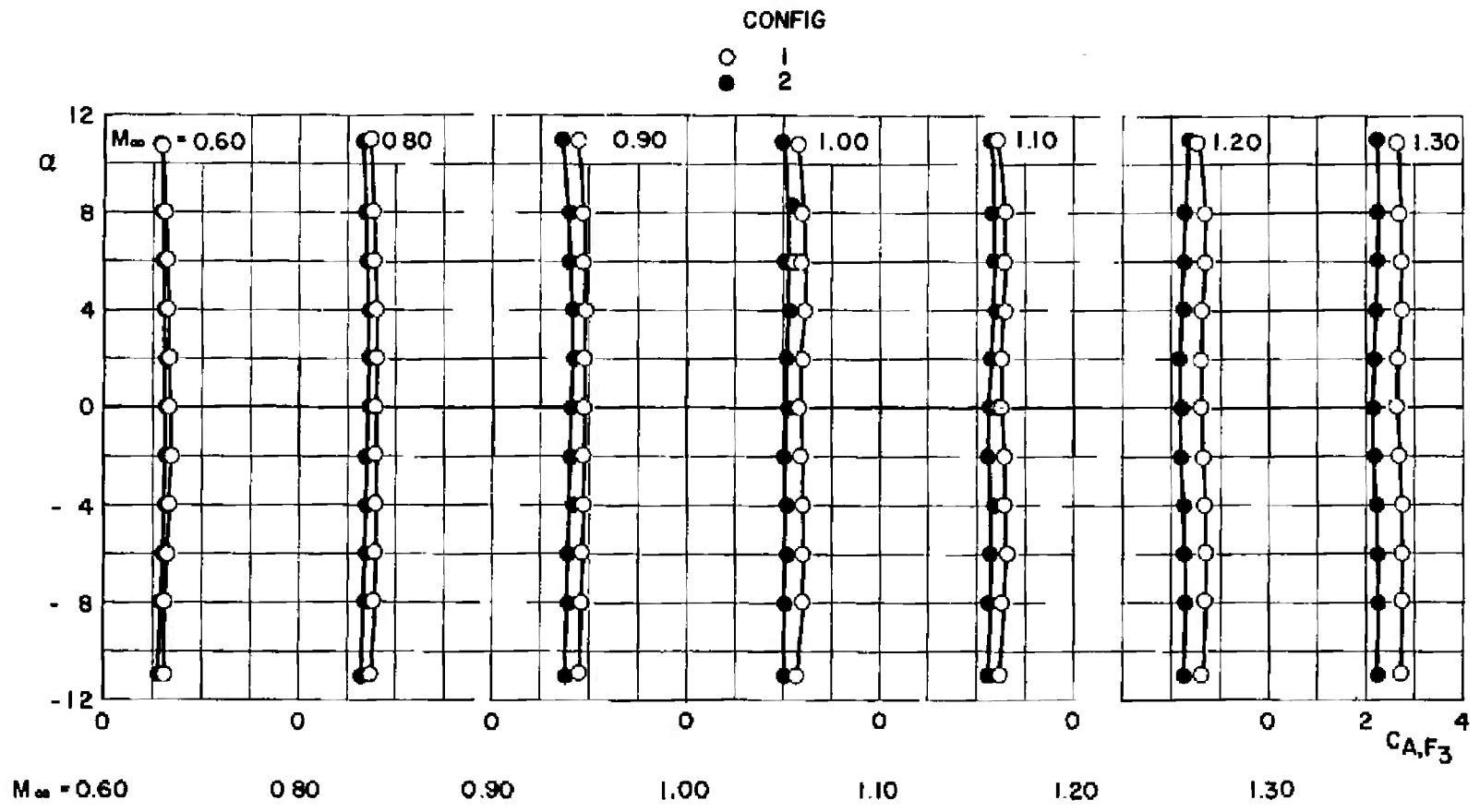


a. Longitudinal Neutral Point



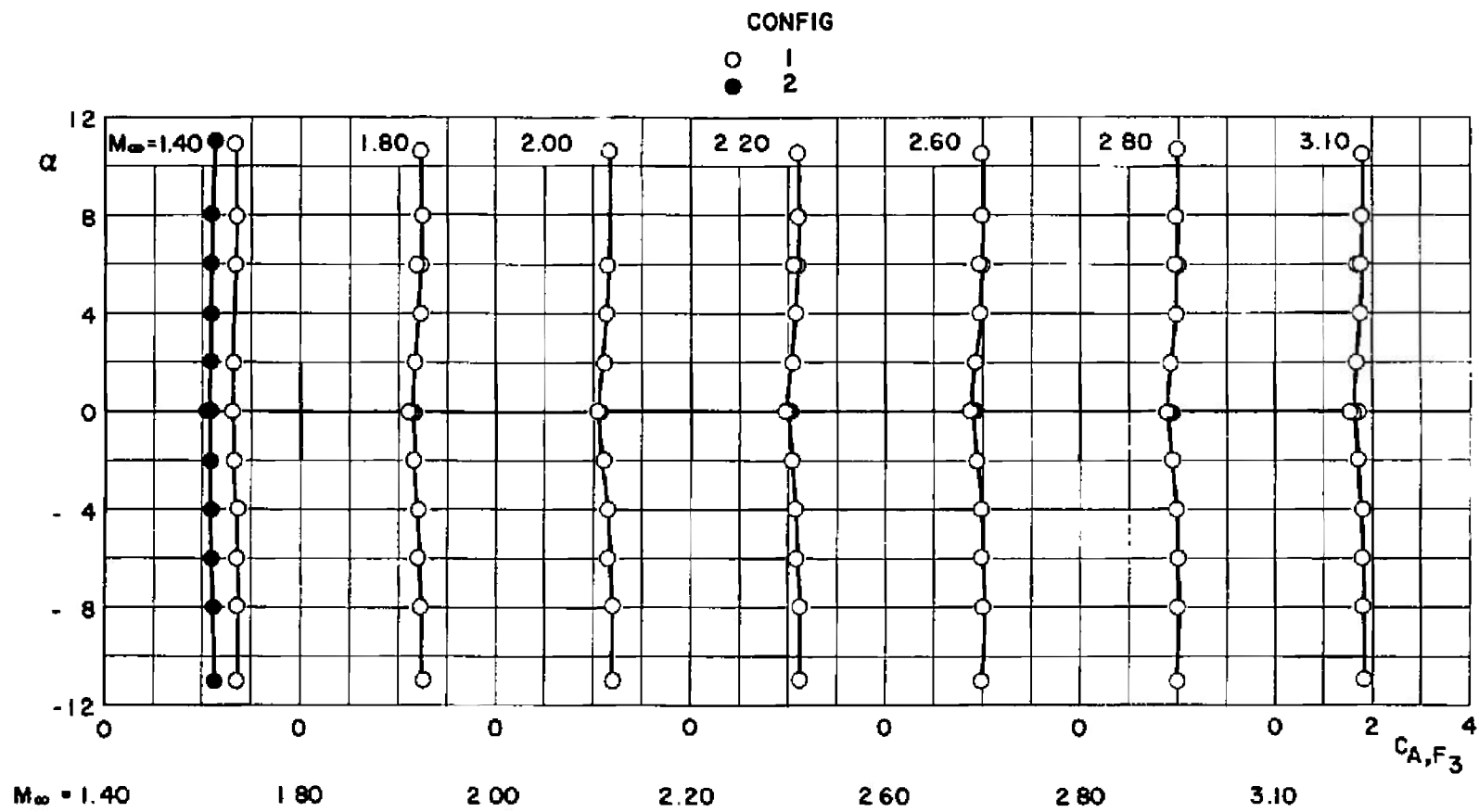
b. Lateral Neutral Point

Fig. 33 Variation of Neutral-Point Location with Mach Number for Configurations 1 and 2 of the Composite Model



a. Mach Numbers 0.60 through 1.30

Fig. 34 Variation of Forebody Axial-Force Coefficient with Angle of Attack for Configurations 1 and 2 of the Composite Model, $\beta = 0$



b. Mach Numbers 1.40 through 3.10

Fig. 34 Concluded

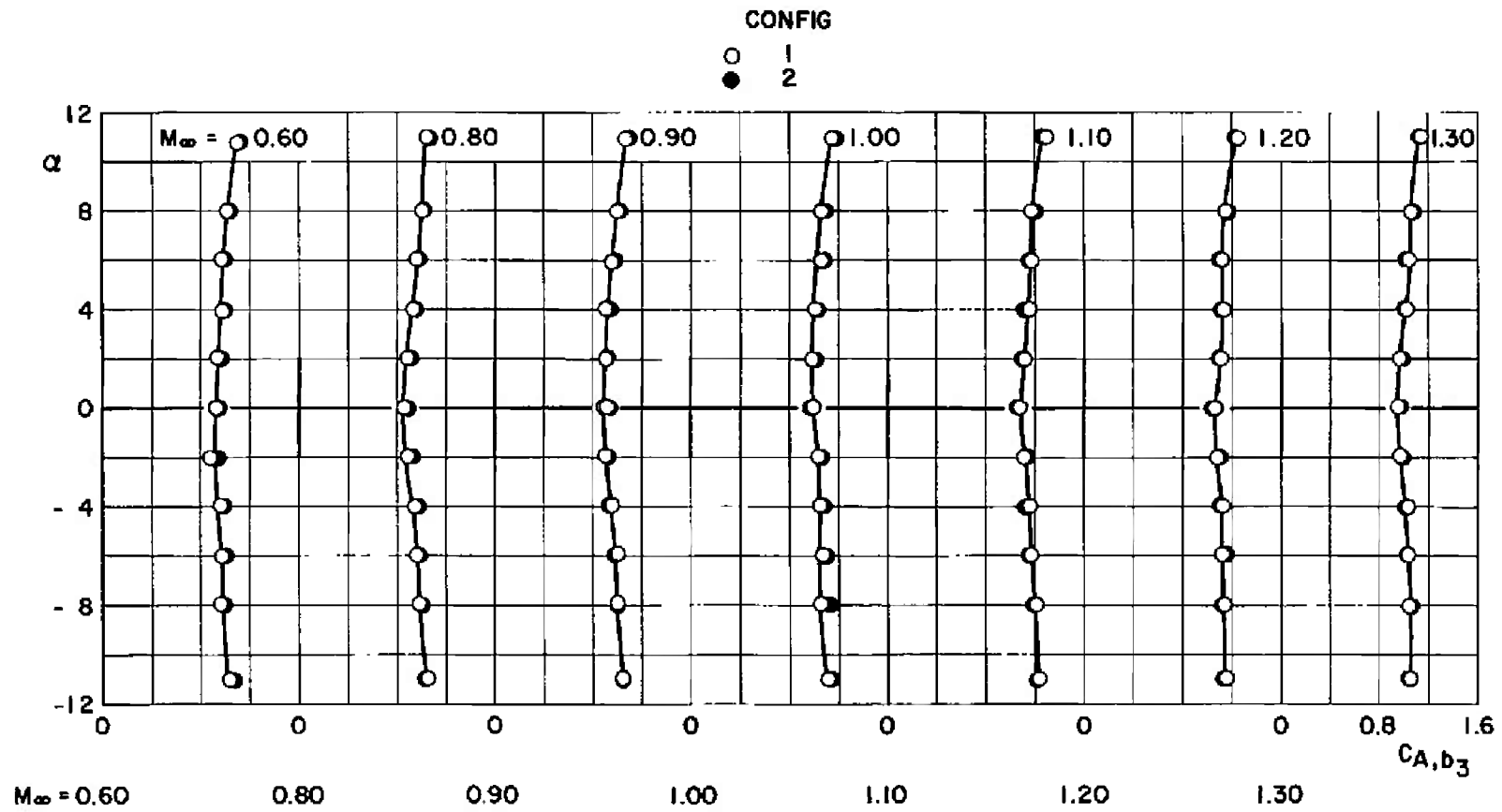
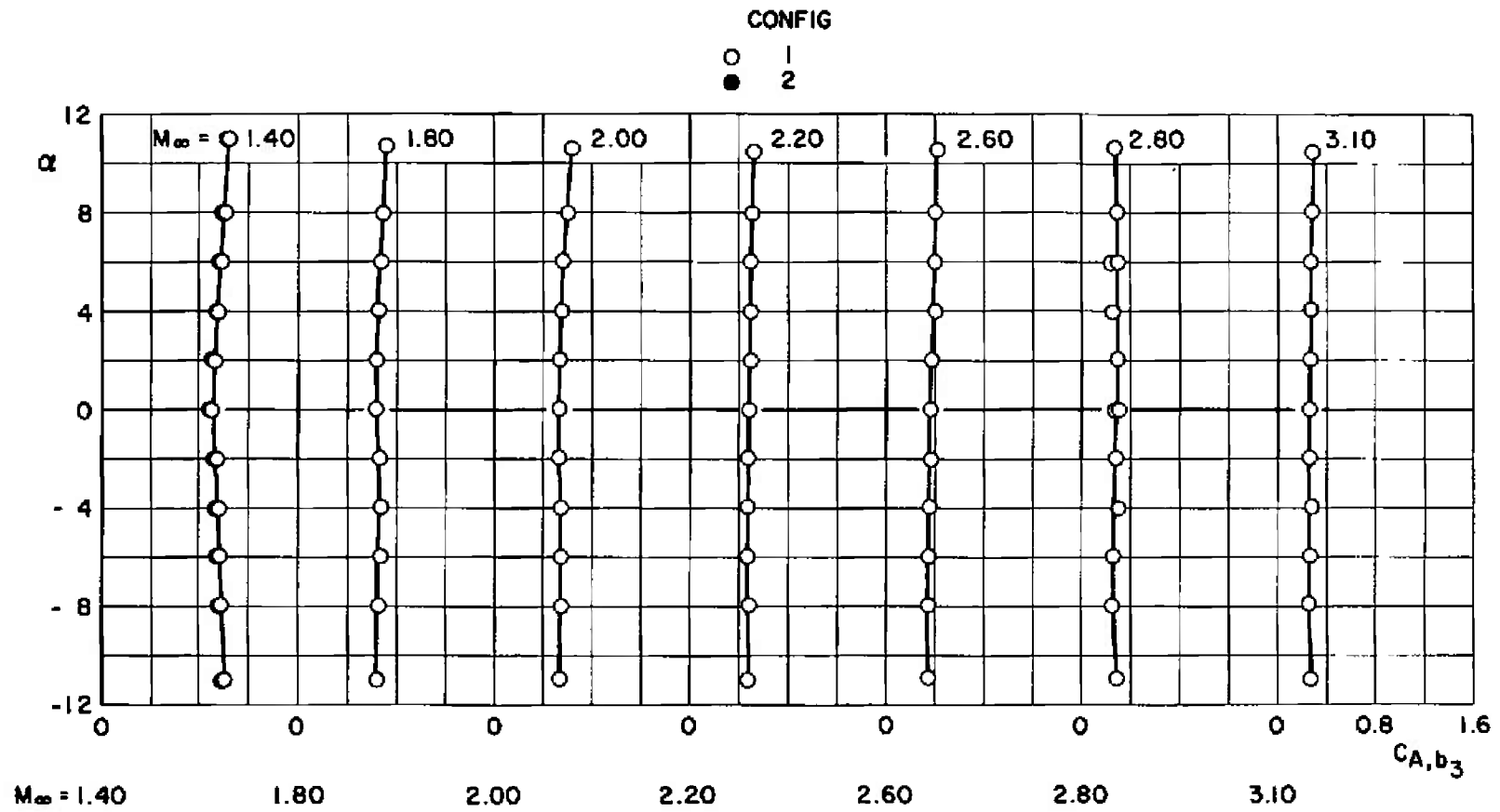


Fig. 35 Variation of Base Axial-Force Coefficient with Angle of Attack for Configurations 1 and 2 of the Composite Model, $\beta = 0$



b. Mach Numbers 1.40 through 3.10

Fig. 35 Concluded

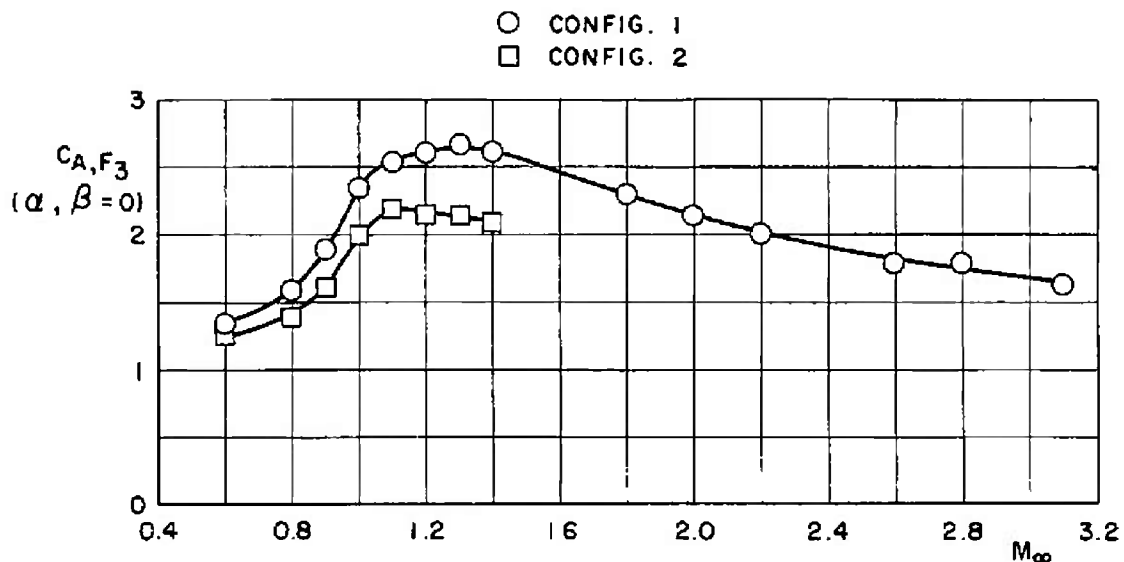


Fig. 36 Variation of Forebody Axial-Force Coefficient with Mach Number for Configurations 1 and 2 of the Composite Model

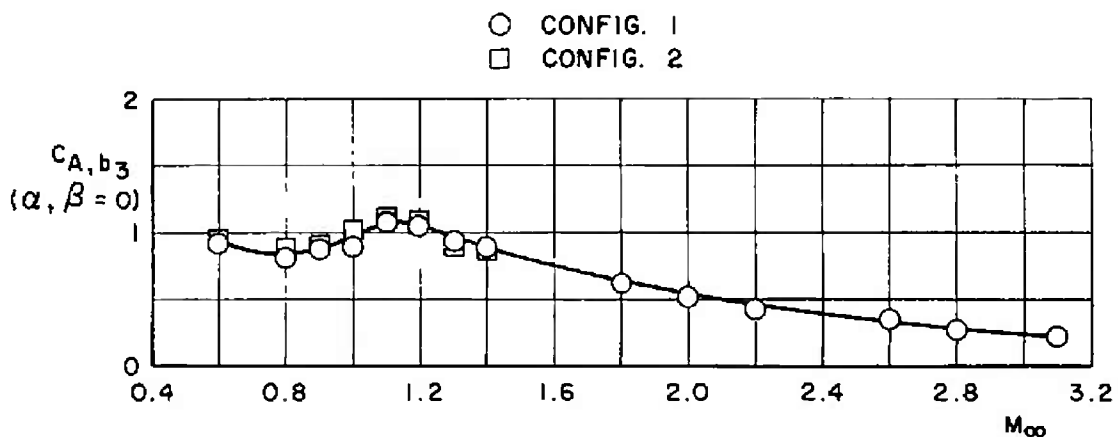
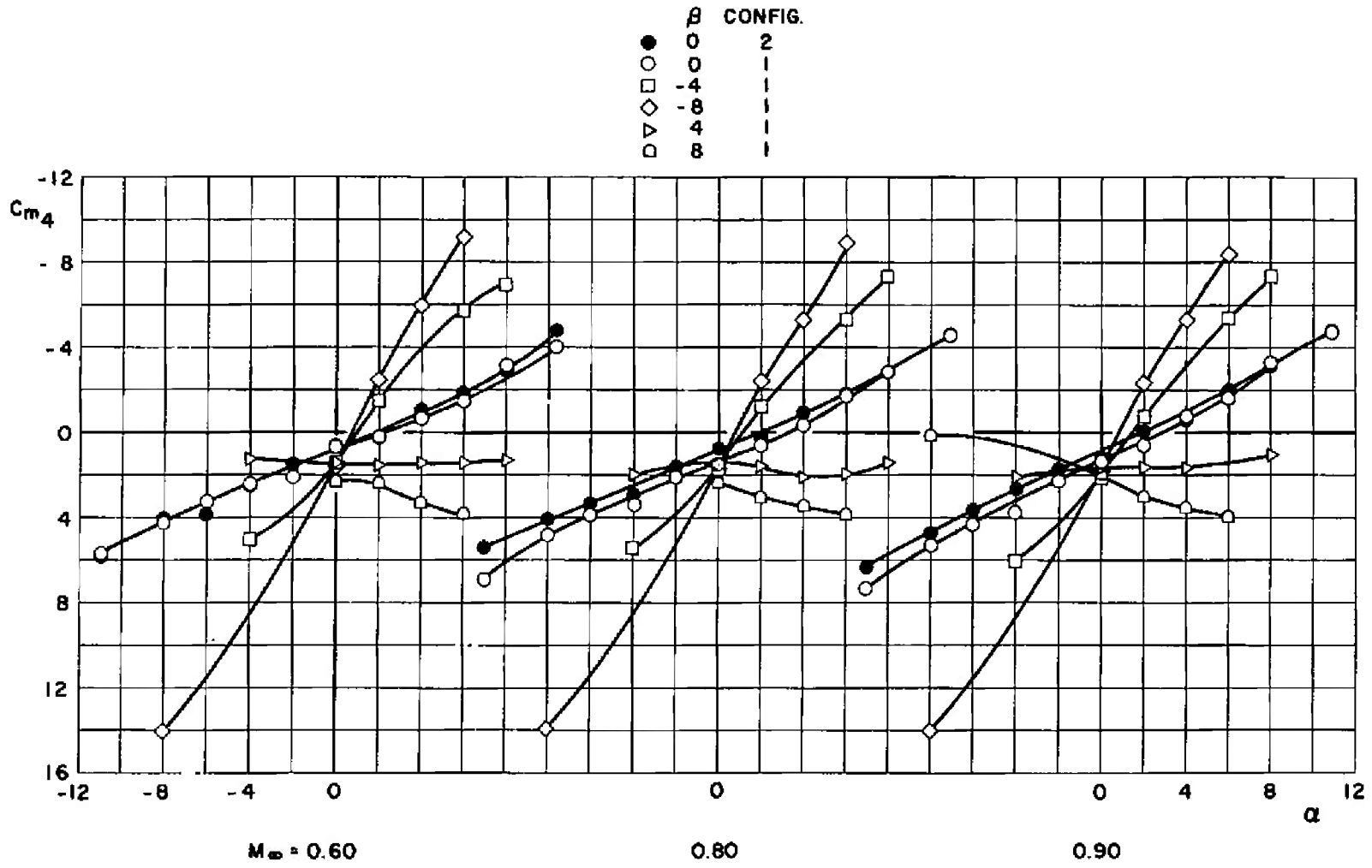
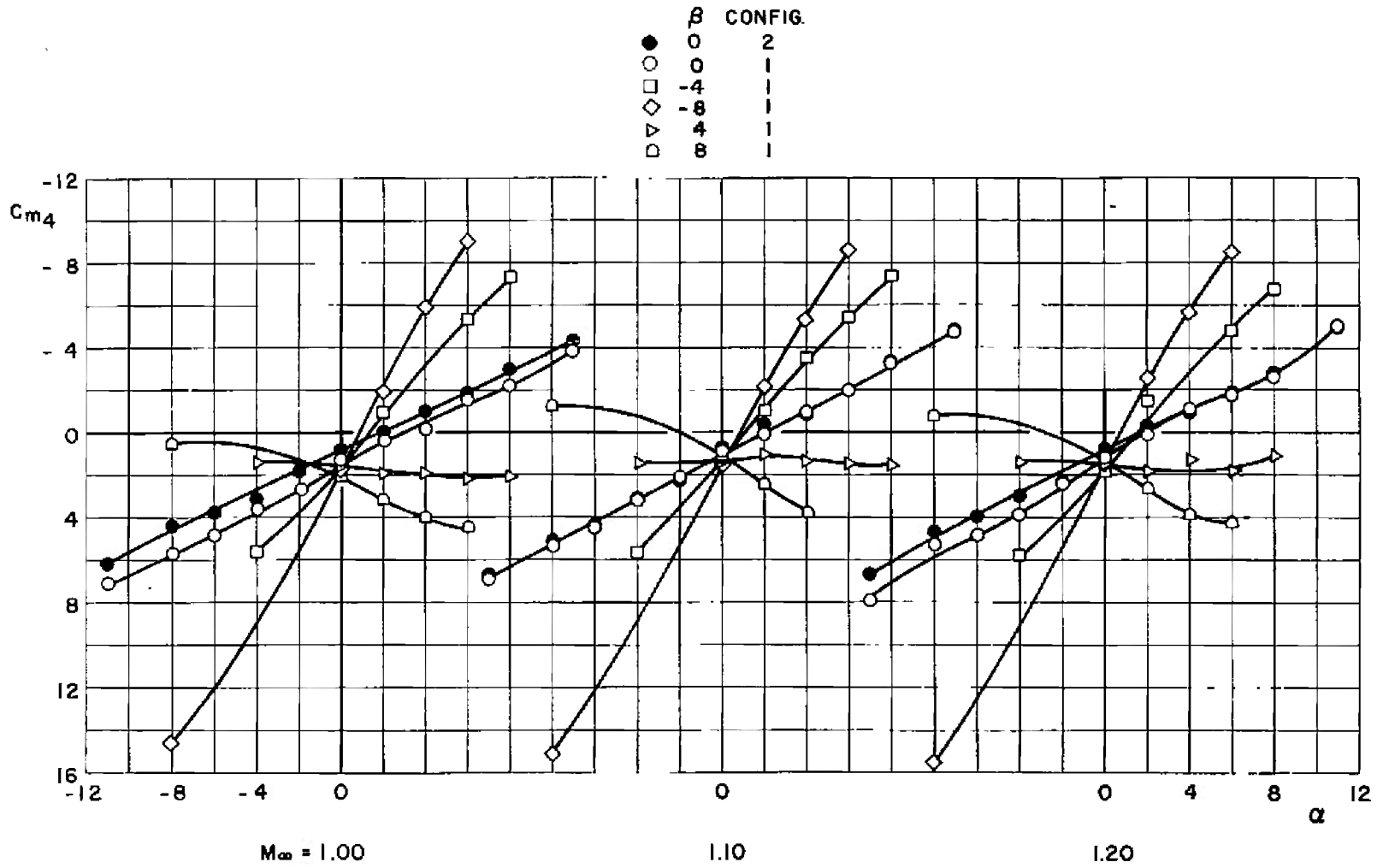


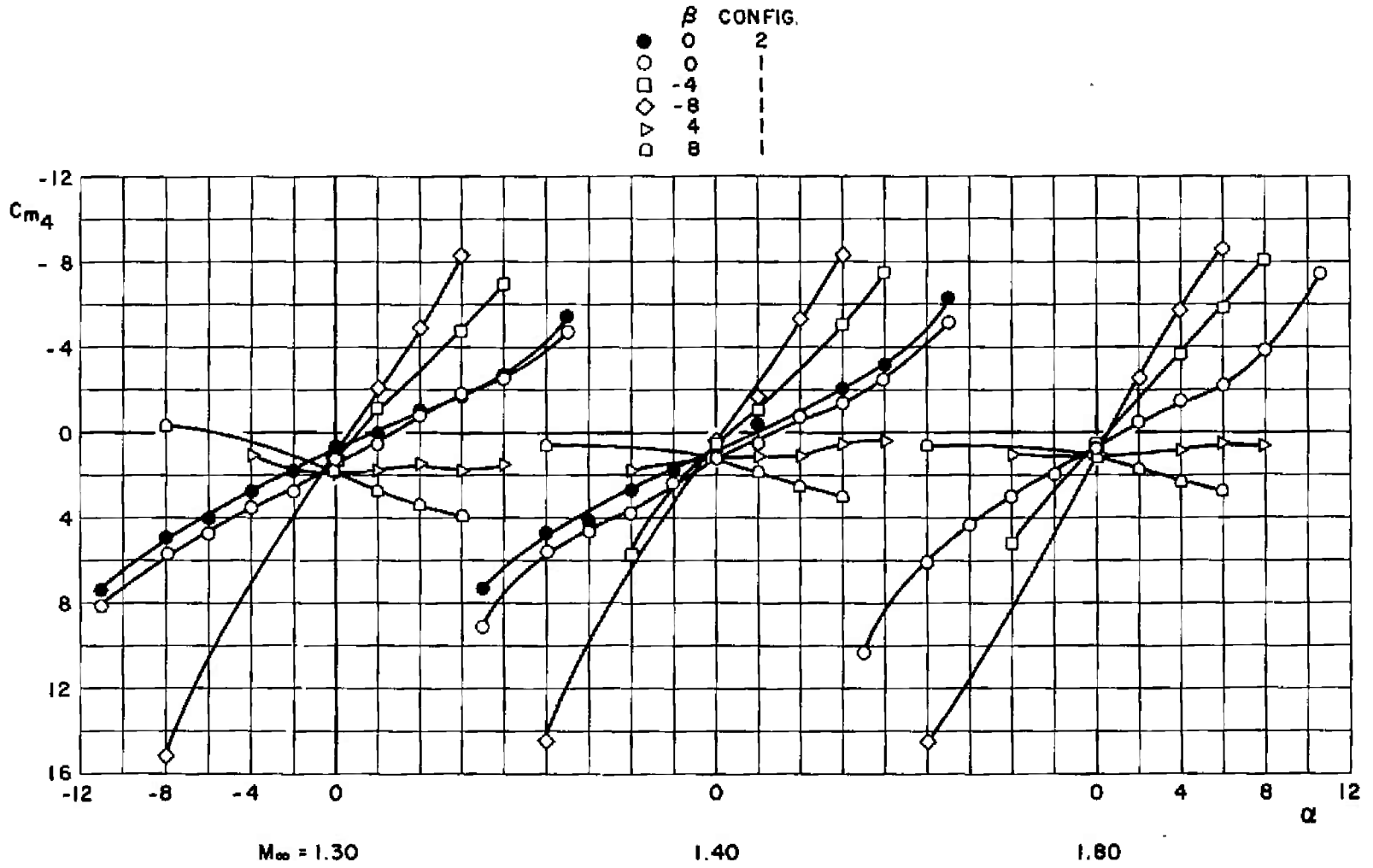
Fig. 37 Variation of Base Axial-Force Coefficient with Mach Number for Configurations 1 and 2 of the Composite Model



a. Mach Numbers 0.60 through 0.90

Fig. 38 Variation of SRM Pitching-Moment Coefficient with Angle of Attack for Configurations 1 and 2

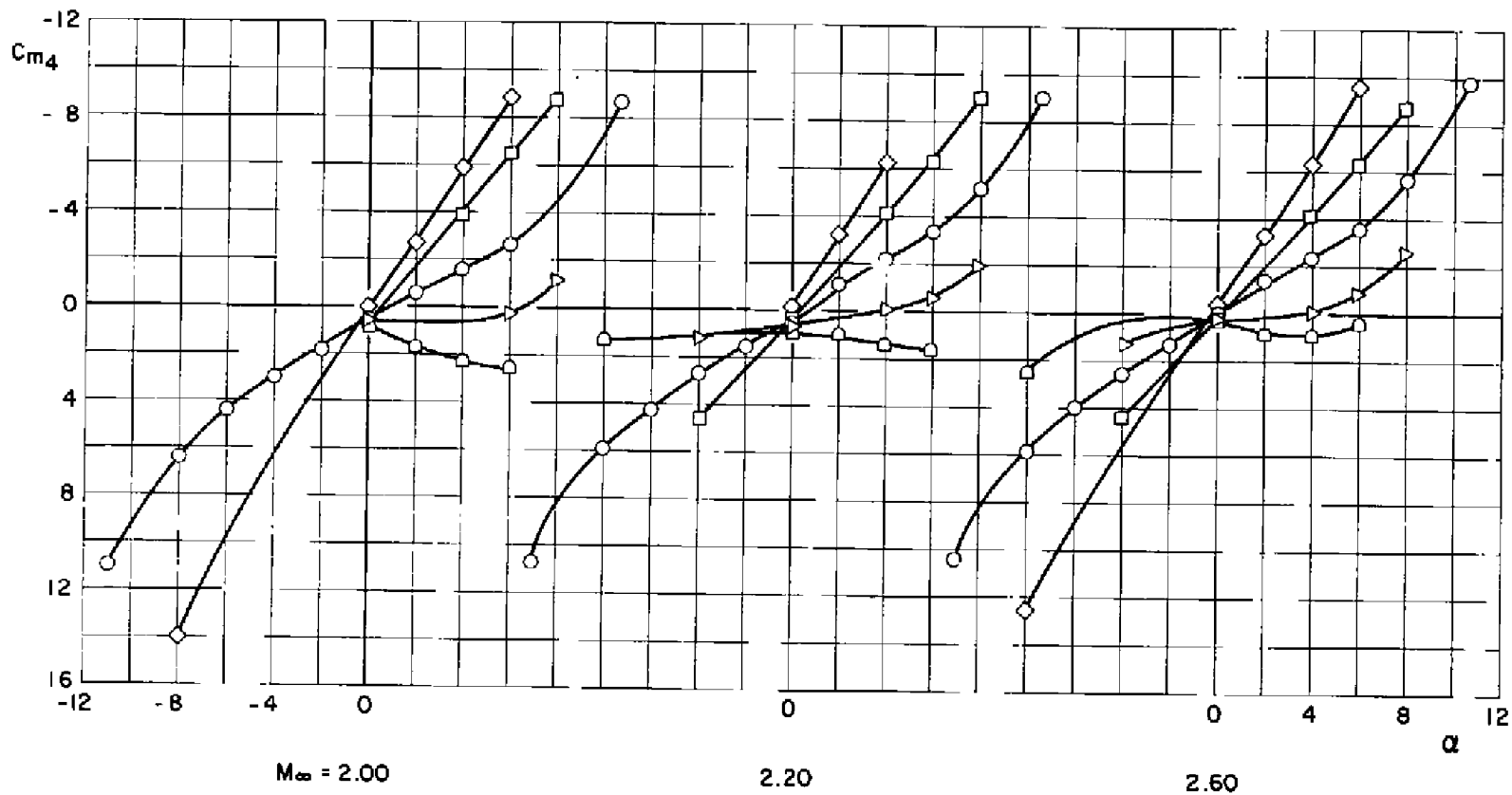




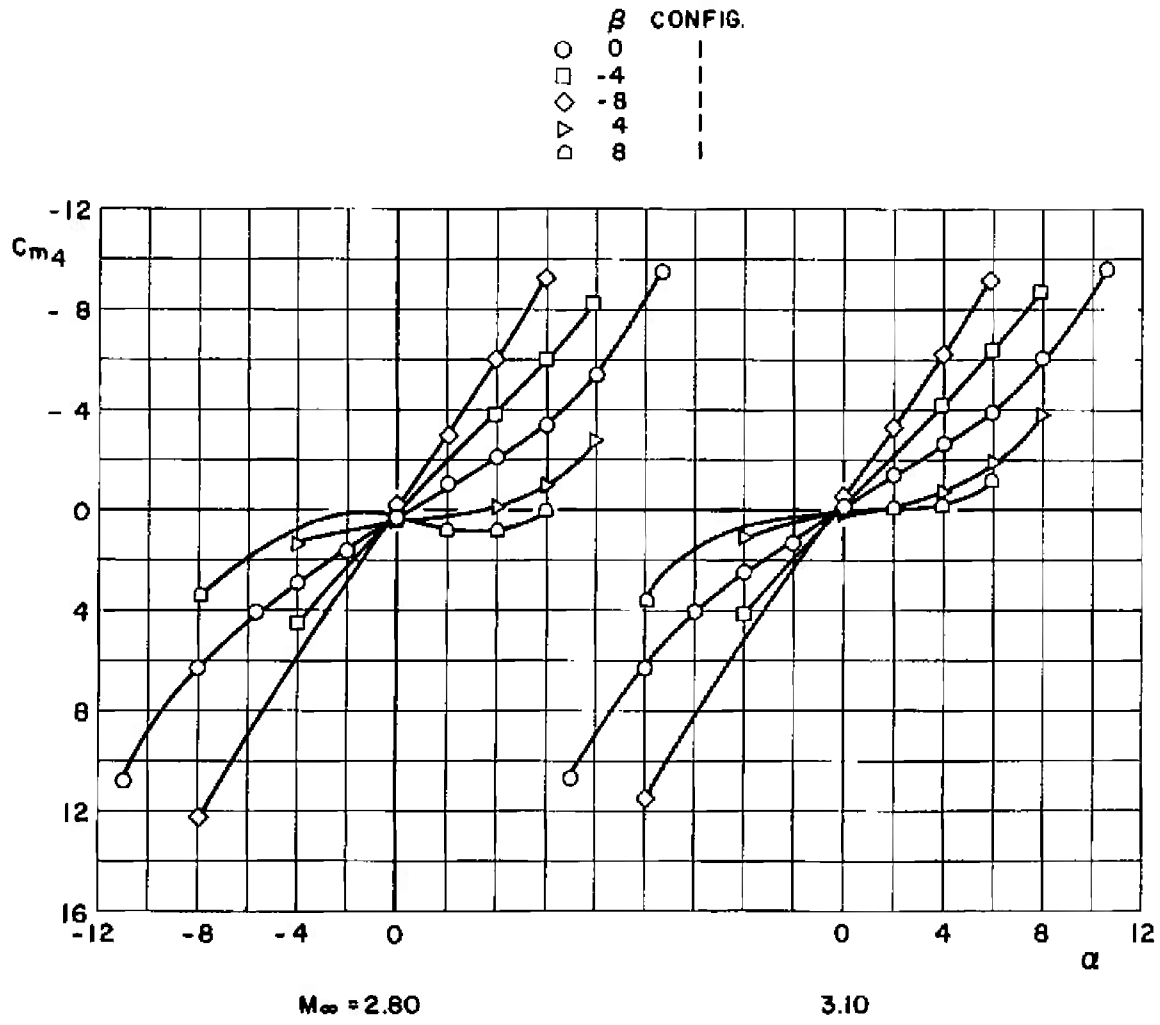
c. Mach Numbers 1.30 through 1.80

Fig. 38 Continued

	β	CONFIG.
○	0	
□	-4	
◇	-8	
▽	4	
◇	8	

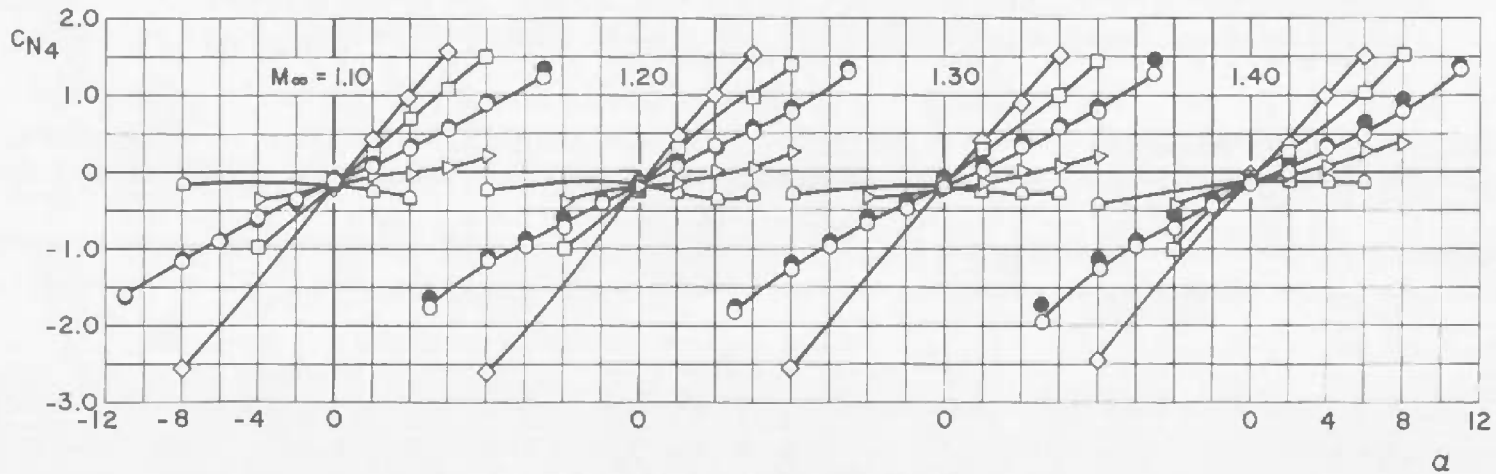
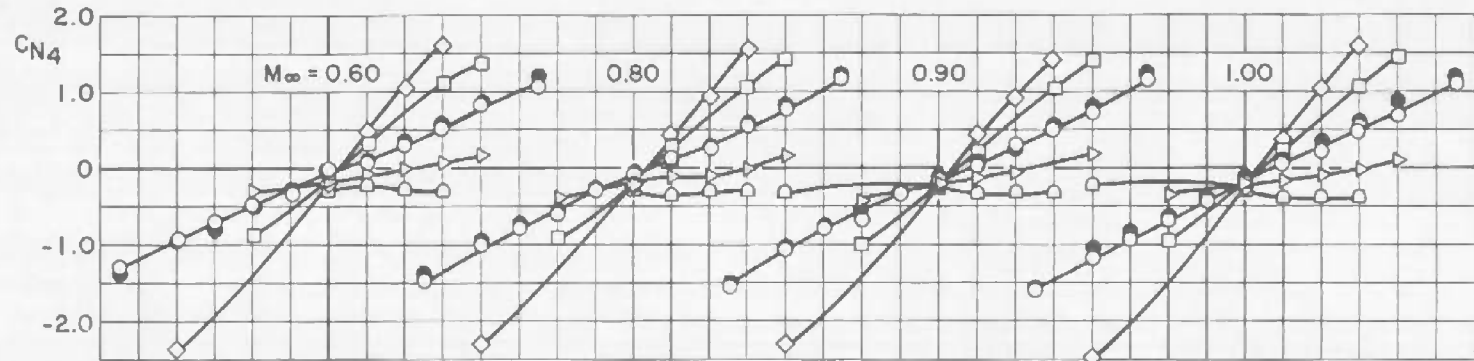


d. Mach Numbers 2.00 through 2.60
 Fig. 38 Continued



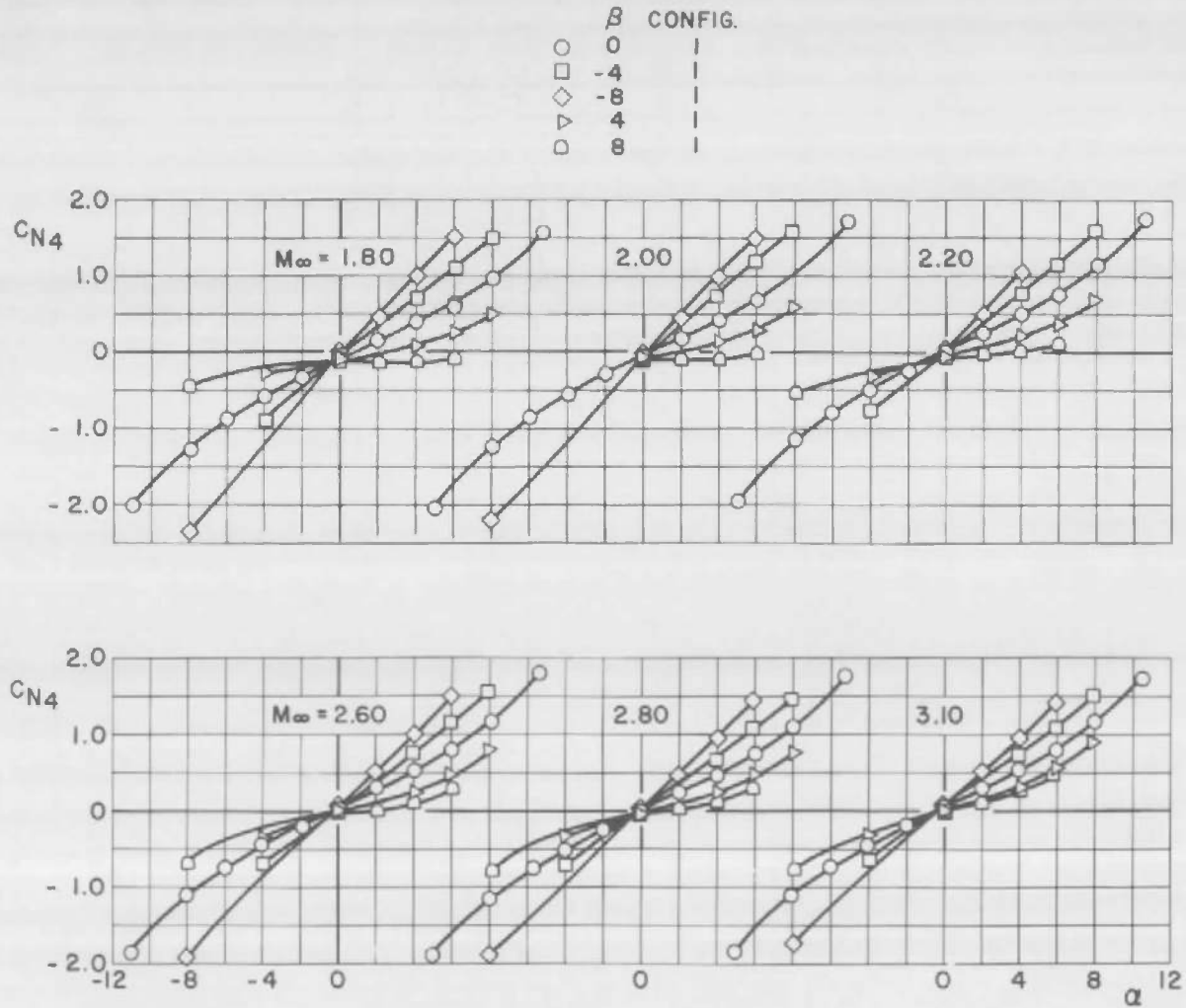
e. Mach Numbers 2.80 and 3.10
 Fig. 38 Concluded

β	CONFIG.
●	0 2
○	0 1
□	-4 1
◇	-8 1
▽	4 1
◇	8 1



a. Mach Numbers 0.60 through 1.40

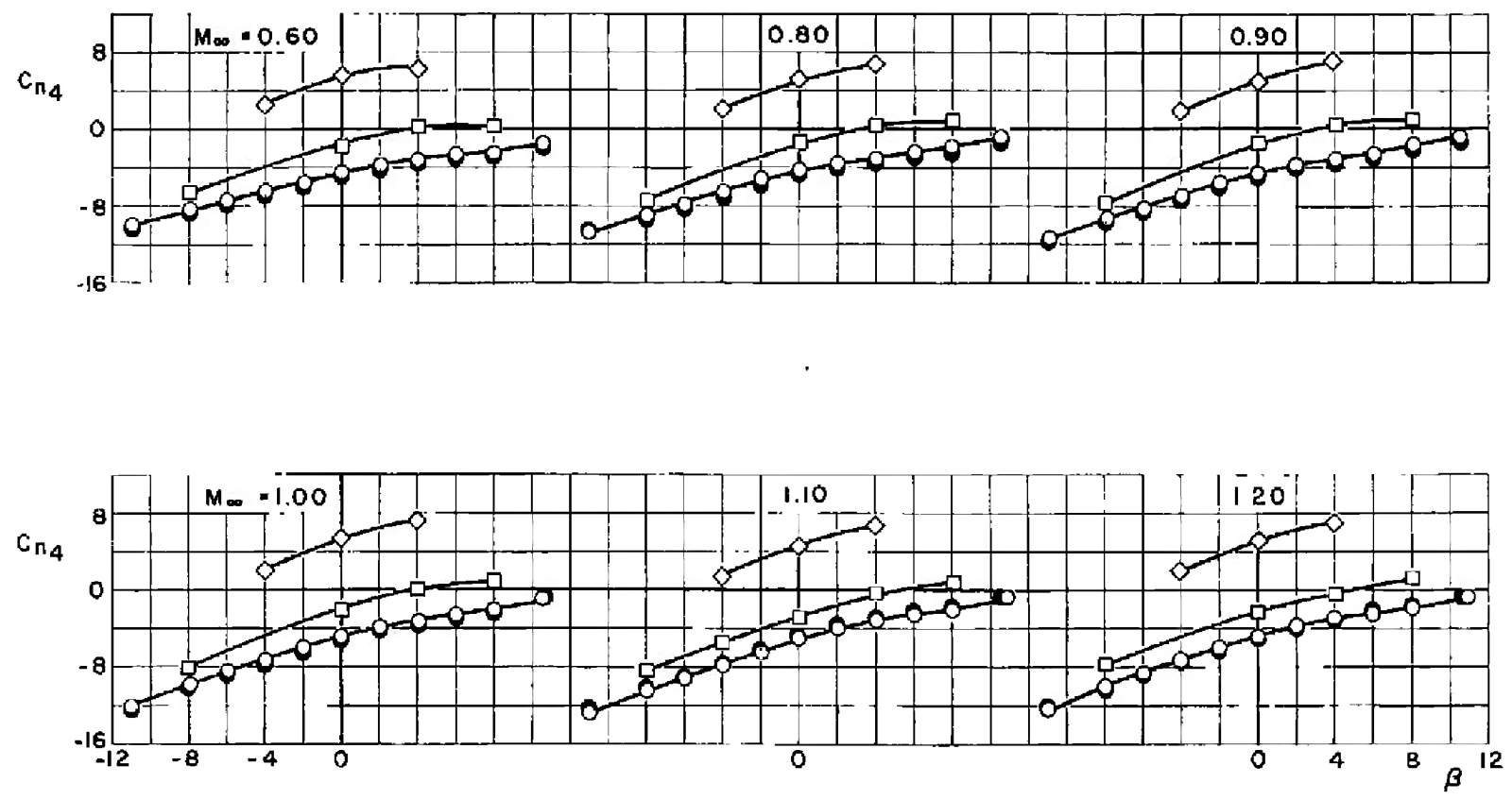
Fig. 39 Variation of SRM Normal-Force Coefficient with Angle of Attack for Configurations 1 and 2



b. Mach Numbers 1.80 through 3.10

Fig. 39 Concluded

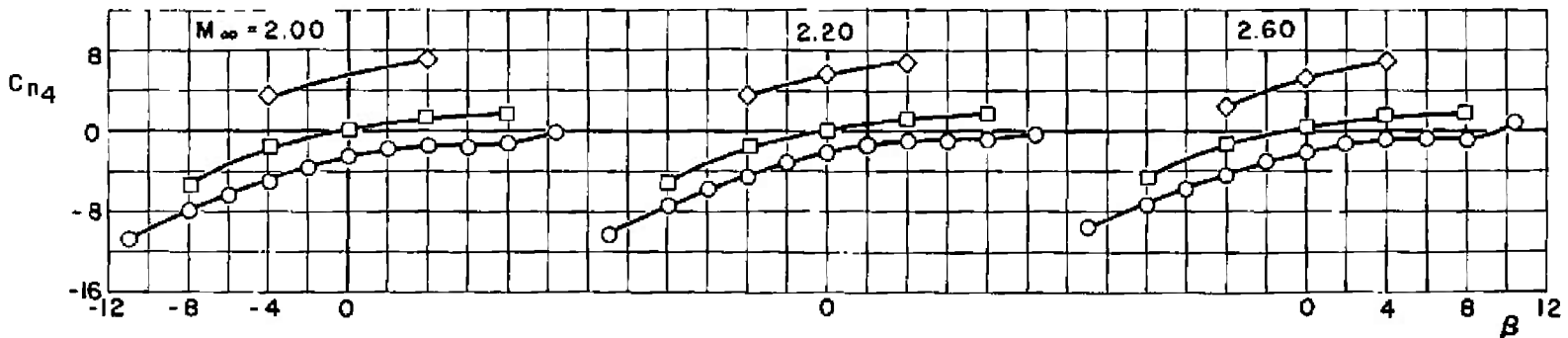
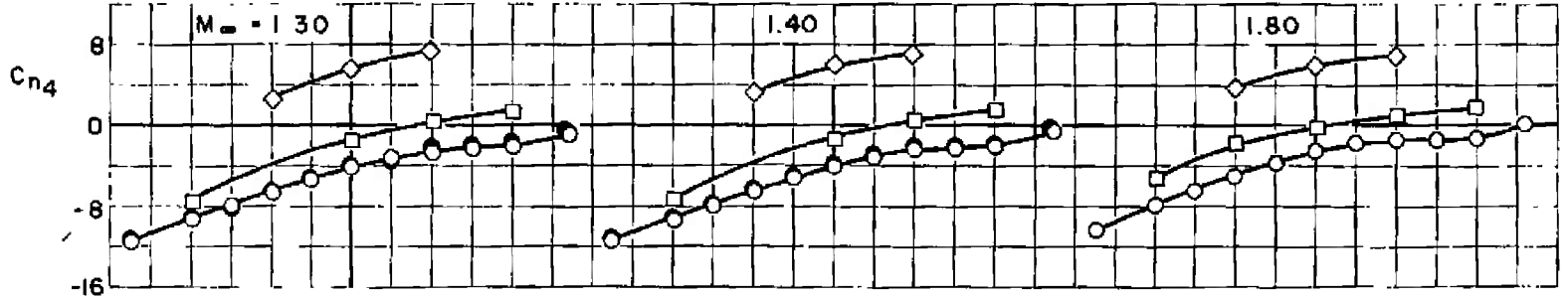
α CONFIG	
●	0 2
○	0 1
□	4 1
◇	8 1



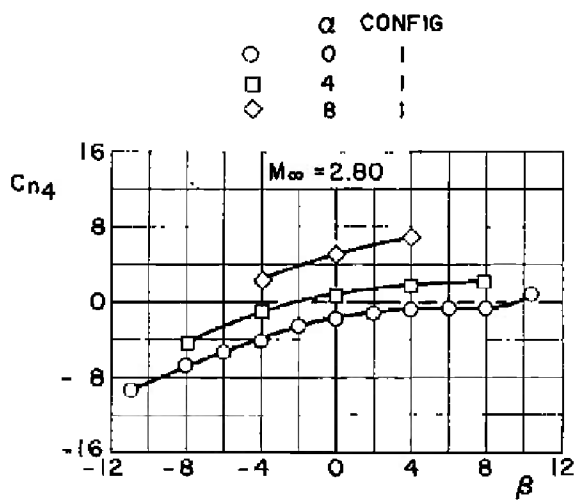
a. Mach Numbers 0.60 through 1.20

Fig. 40 Variation of SRM Yawing-Moment Coefficient with Sideslip Angle for Configurations 1 and 2

Symbol	α	CONFIG
●	0	2
○	0	1
□	4	1
◇	8	1



b. Mach Numbers 1.30 through 2.60
 Fig. 40 Continued



c. Mach Number 2.80

Fig. 40 Concluded

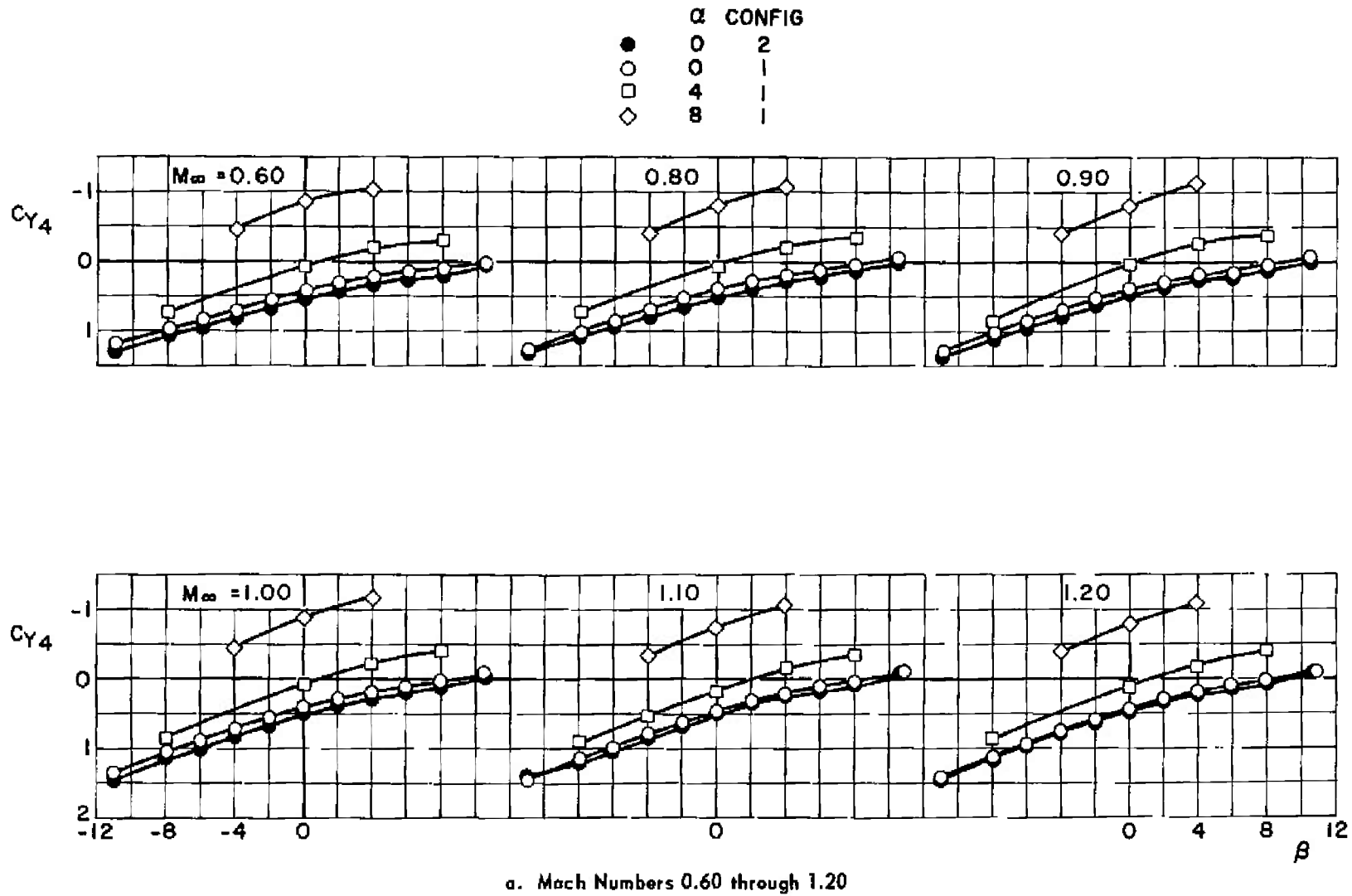
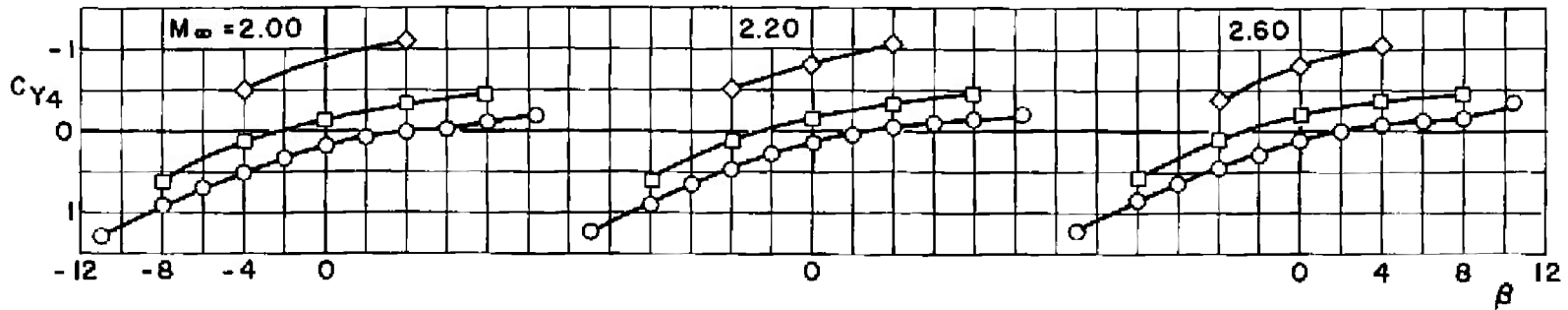
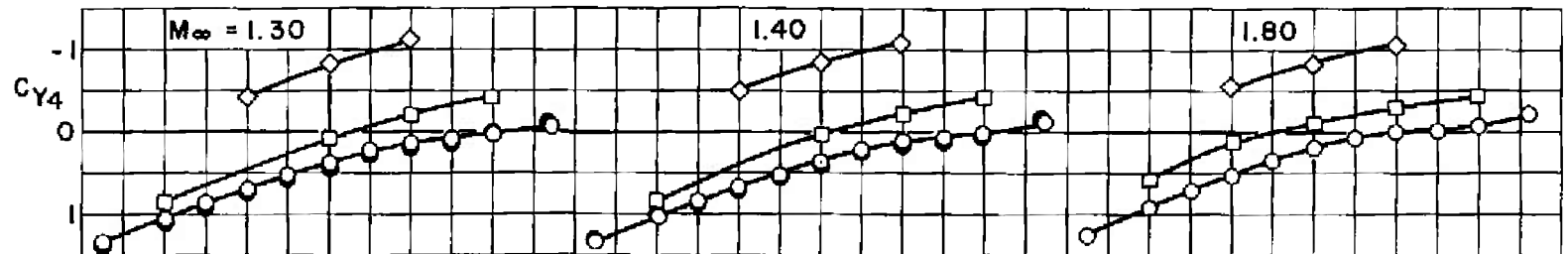


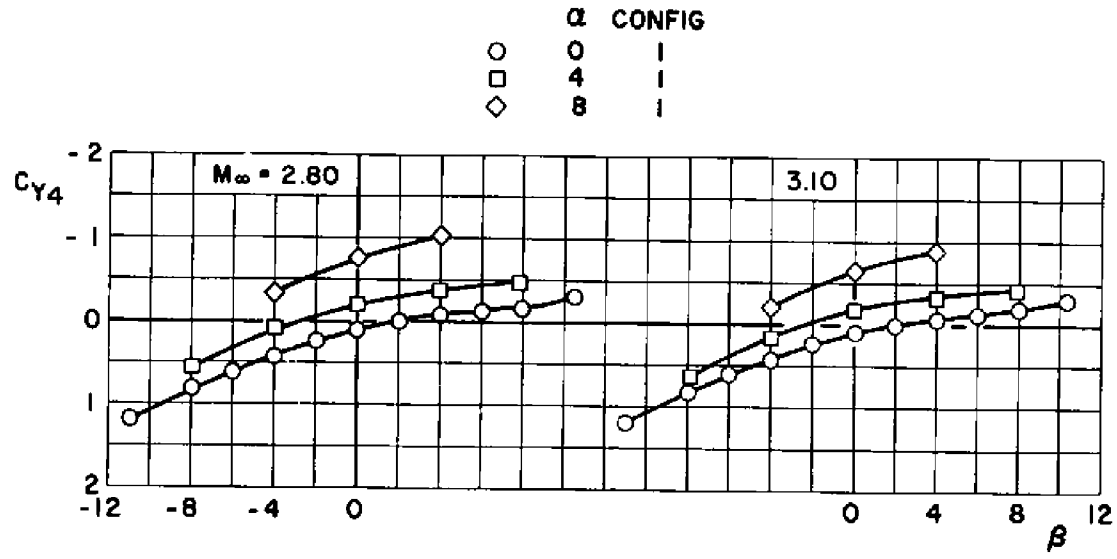
Fig. 41 Variation of SRM Side-Force Coefficient with Sideslip Angle for Configurations 1 and 2

	α	CONFIG
●	0	2
○	0	1
□	4	1
◇	8	1

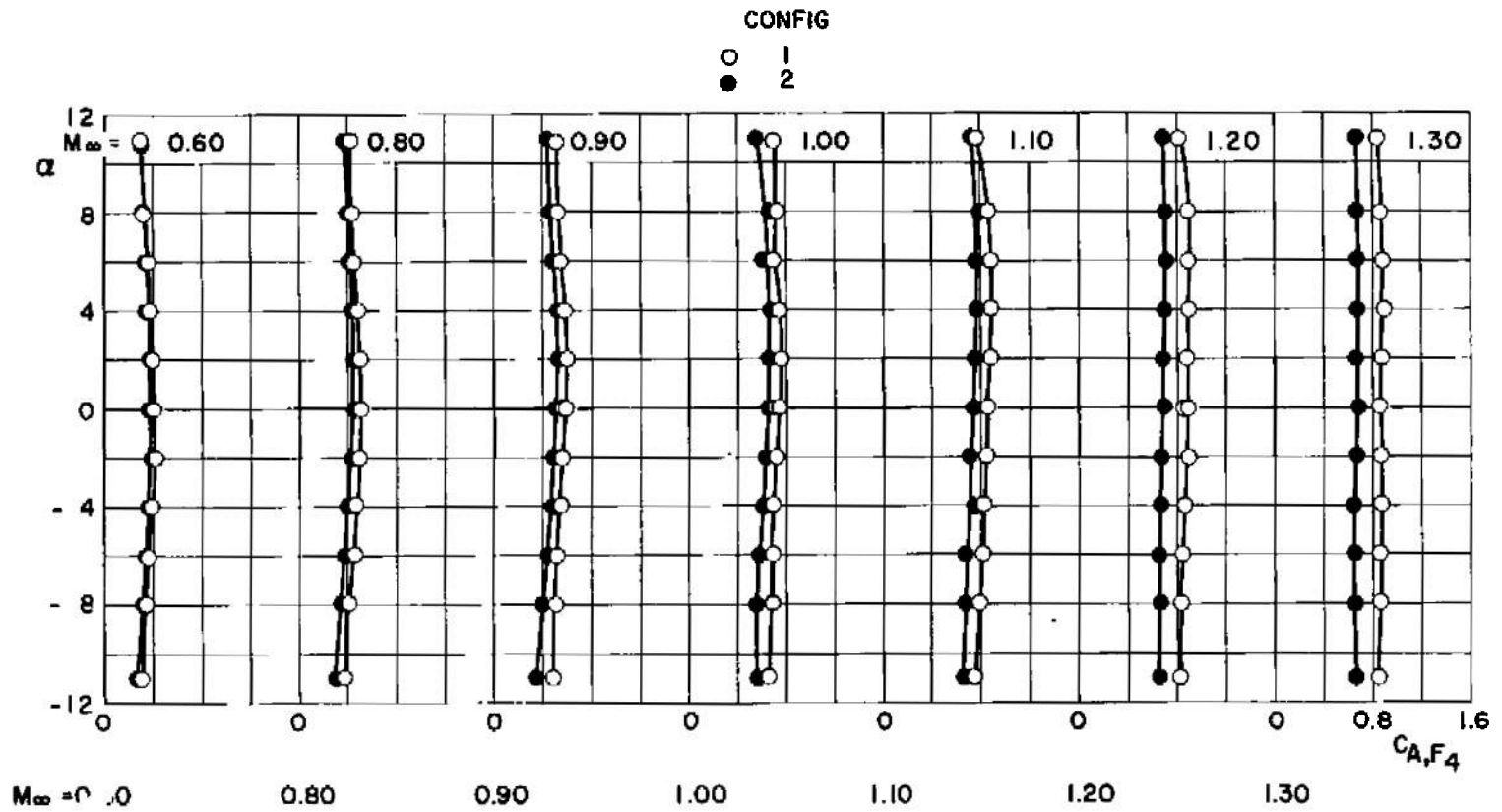


b. Mach Numbers 1.30 through 2.60

Fig. 41 Continued

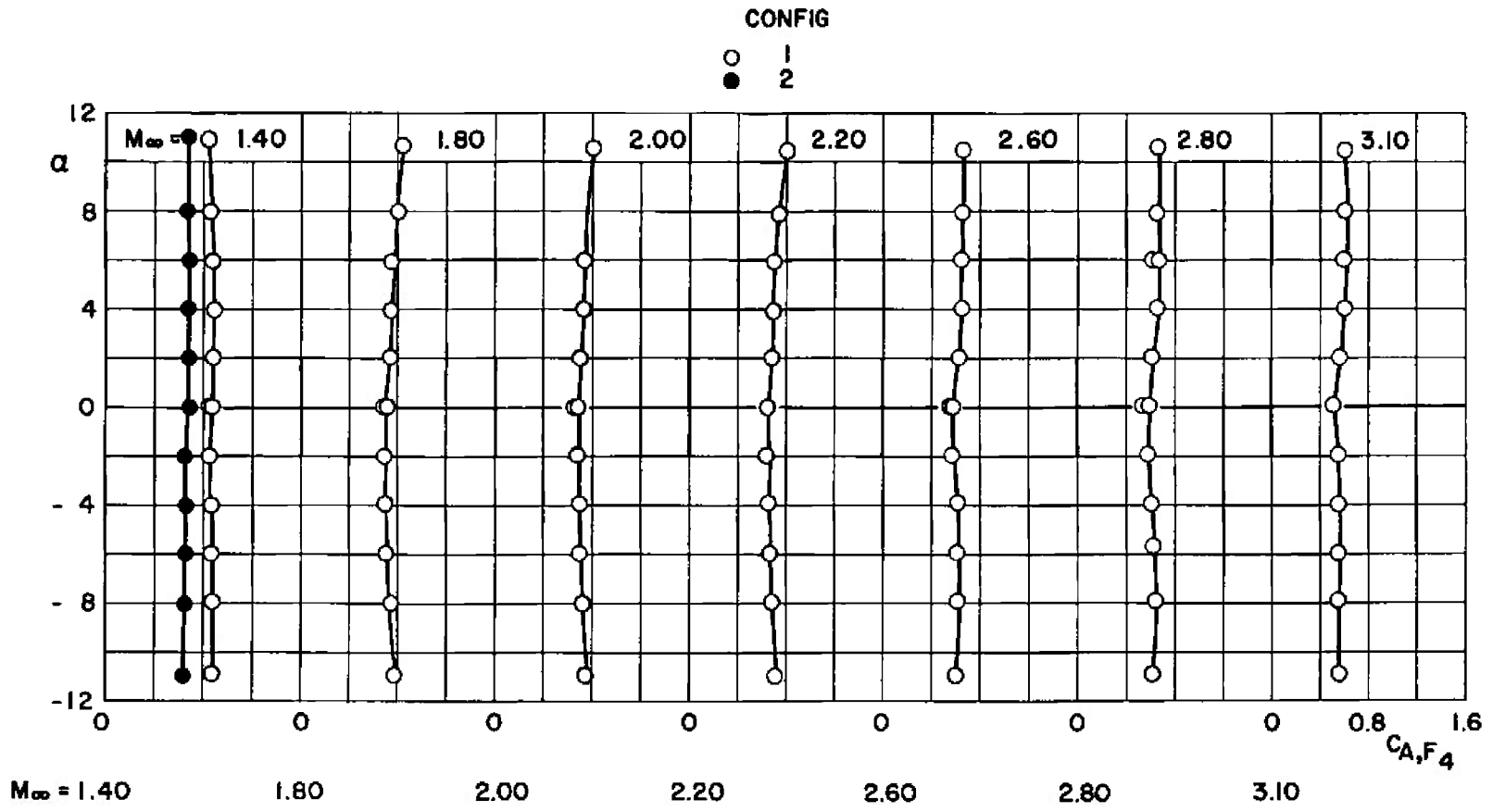


c. Mach Numbers 2.80 and 3.10
 Fig. 41 Concluded

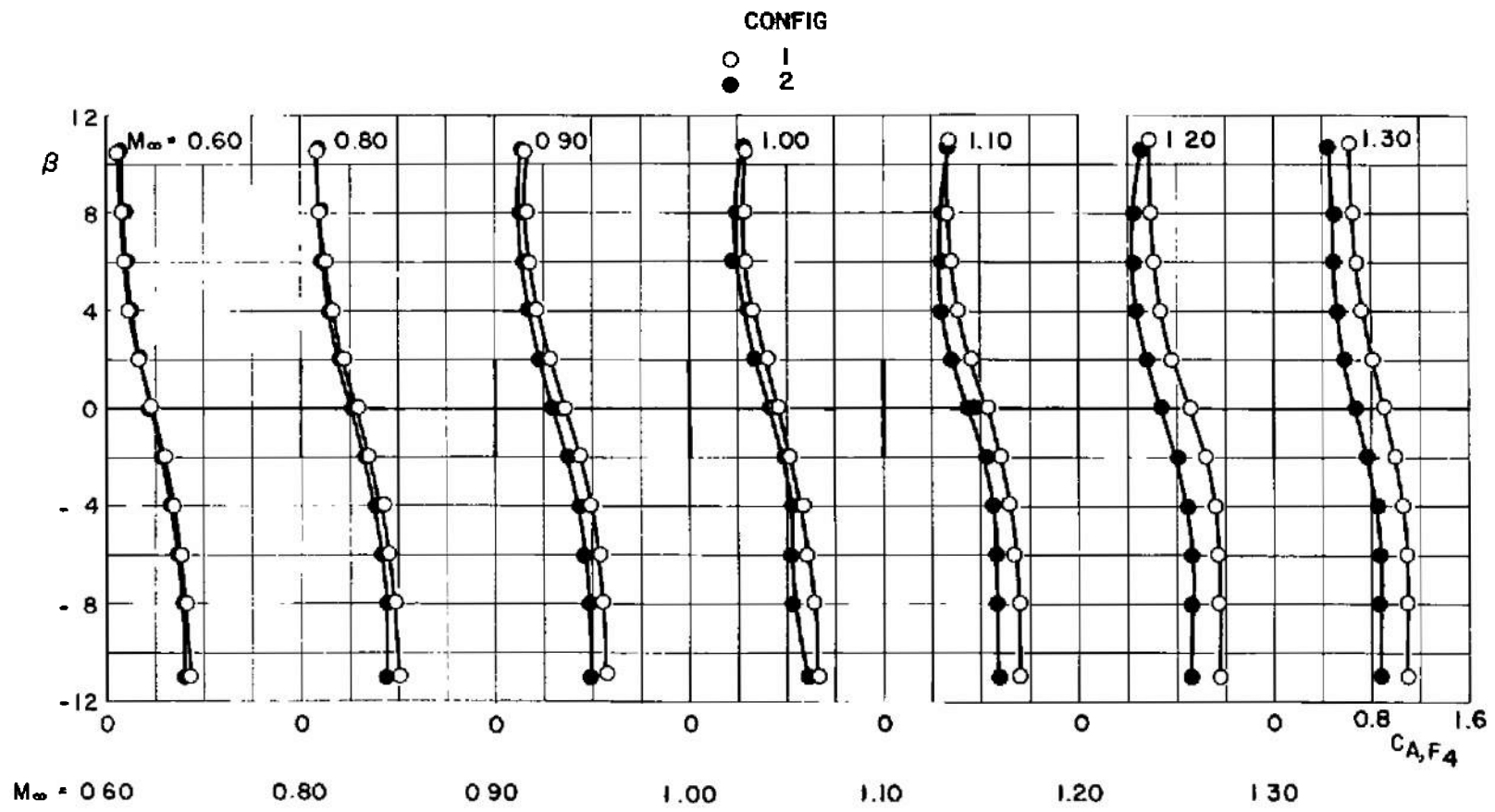


a. Mach Numbers 0.60 through 1.30

Fig. 42 Variation of SRM Forebody Axial-Force Coefficient with Angle of Attack for Configurations 1 and 2, $\beta = 0$



b. Mach Numbers 1.40 through 3.10
 Fig. 42 Concluded



a. Mach Numbers 0.60 through 1.30

Fig. 43 Variation of SRM Forebody Axial-Force Coefficient with Sideslip Angle for Configurations 1 and 2, $\alpha = 0$



b. Mach Numbers 1.40 through 3.10

Fig. 43 Concluded

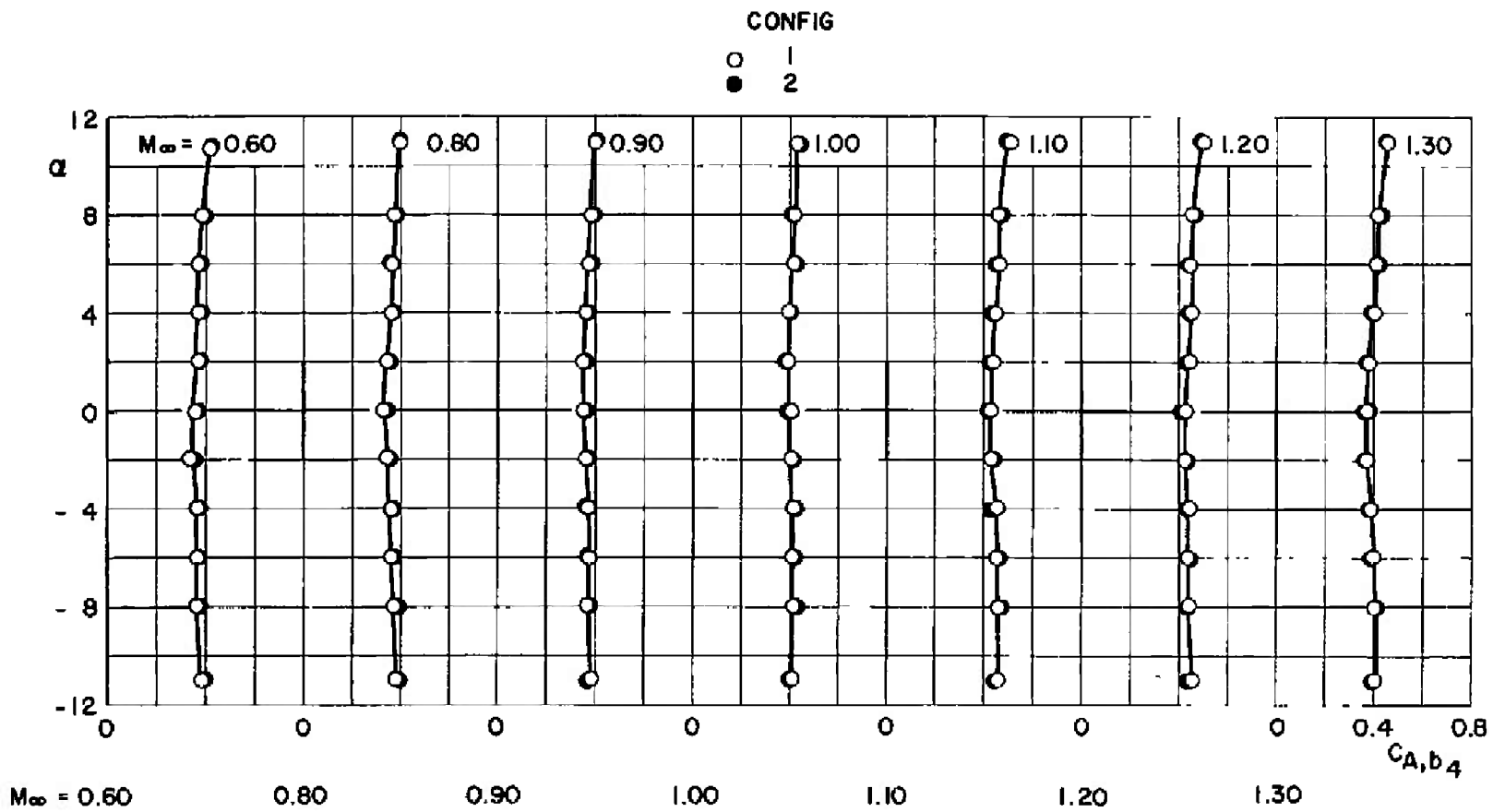
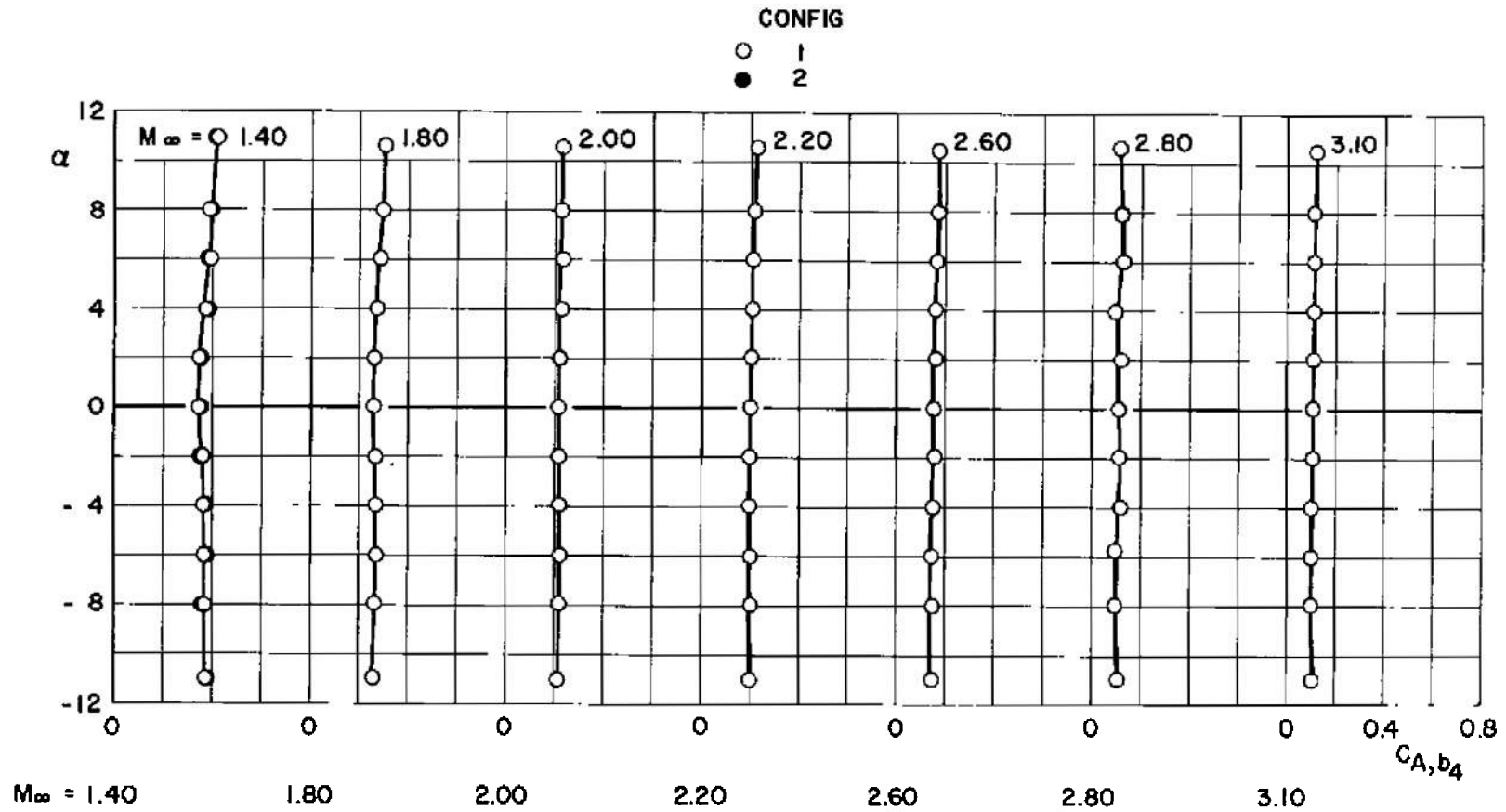


Fig. 44 Variation of SRM Base Axial-Force Coefficient with Angle of Attack for Configurations 1 and 2, $\beta = 0$



b. Mach Numbers 1.40 through 3.10

Fig. 44 Concluded

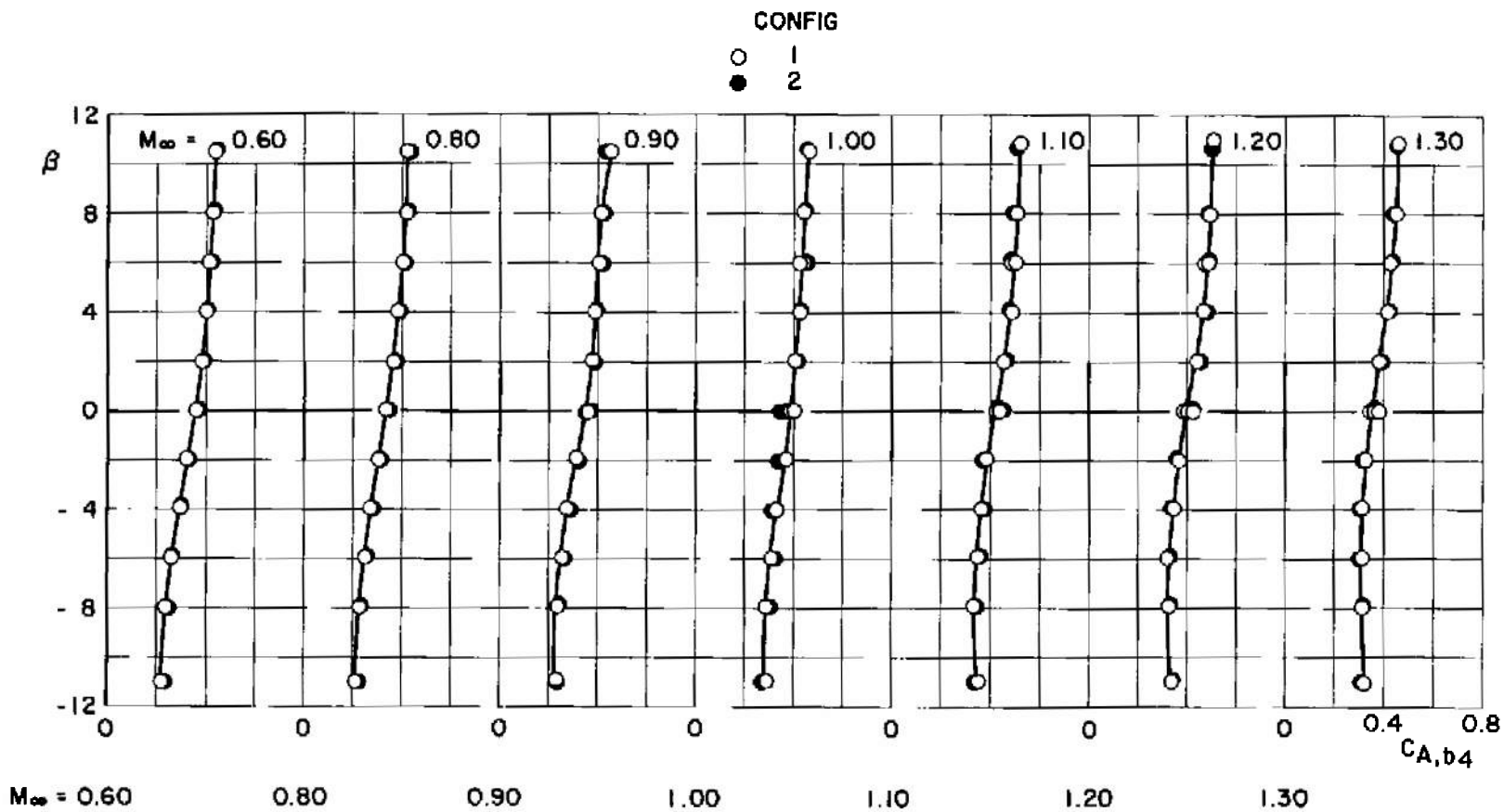
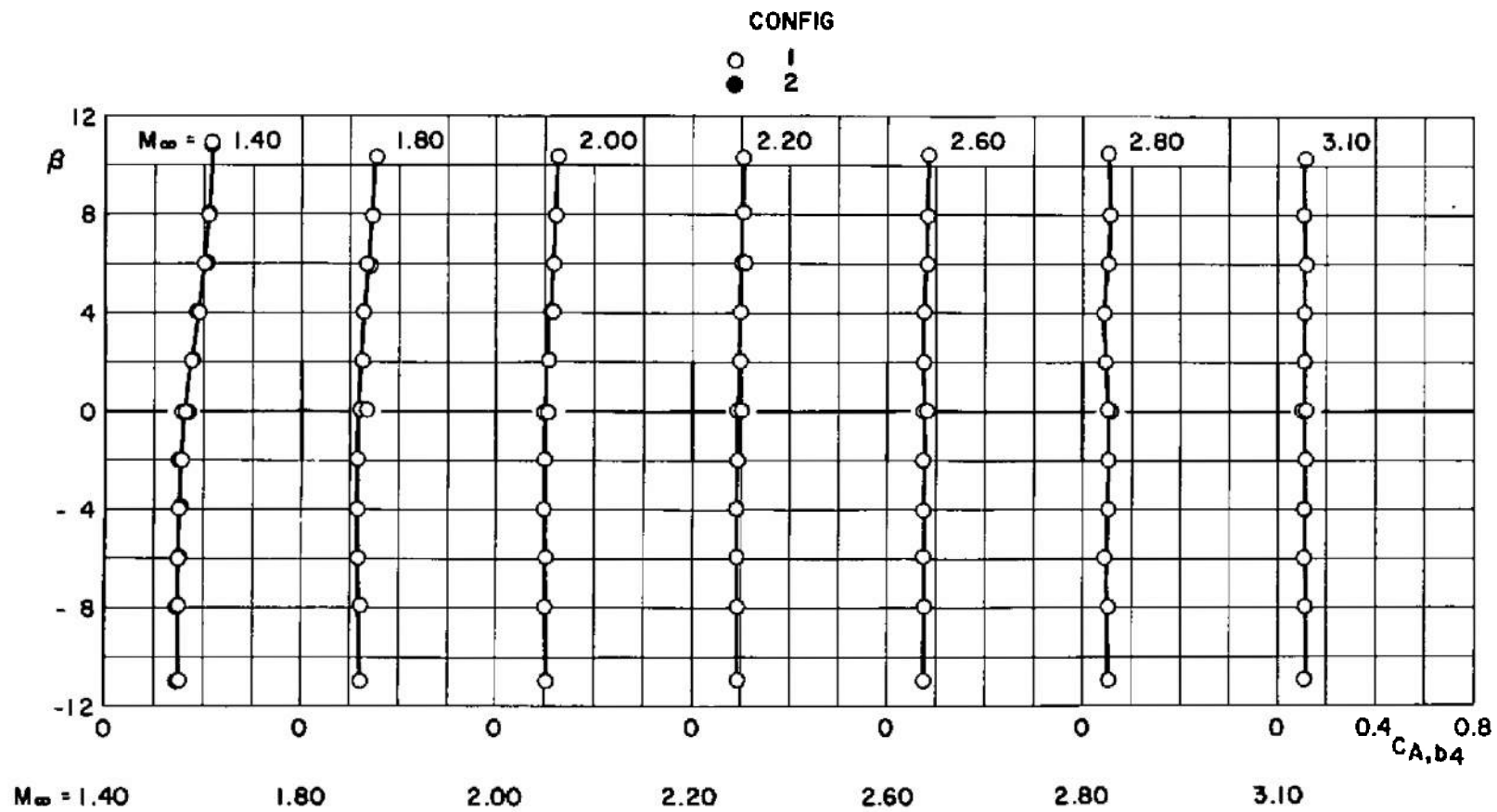


Fig. 45 Variation of SRM Base Axial-Force Coefficient with Sideslip Angle for Configurations 1 and 2, $\alpha = 0$



b. Mach Numbers 1.40 through 3.10

Fig. 45 Concluded

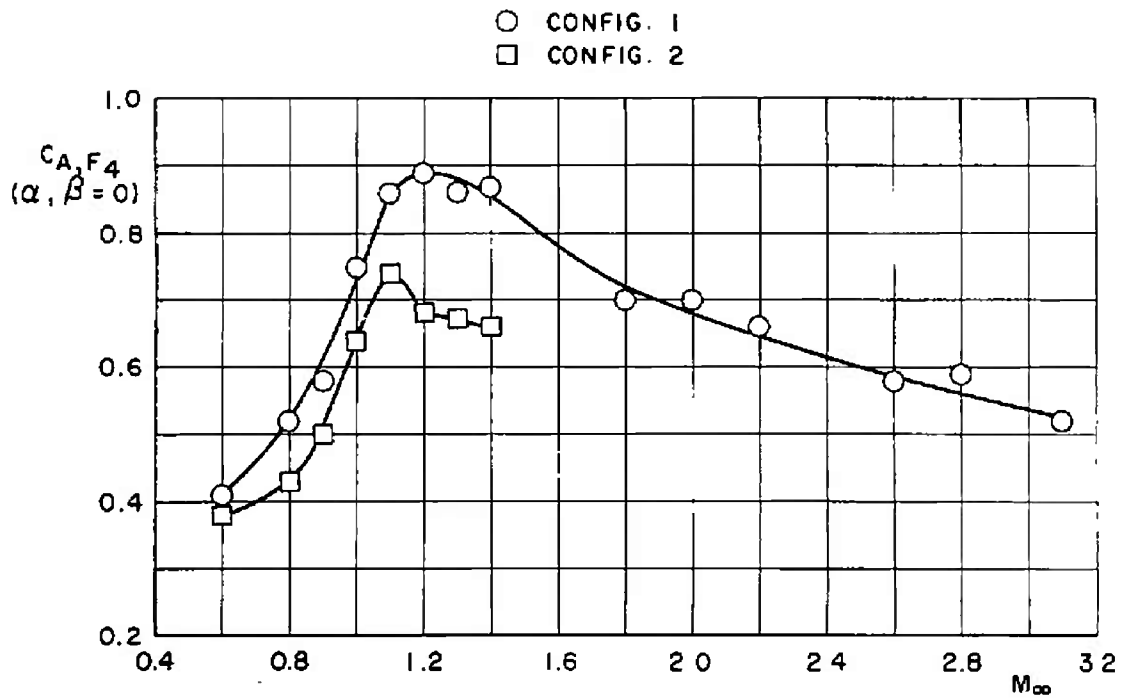


Fig. 46 Variation of SRM Forebody Axial-Force Coefficient with Mach Number for Configurations 1 and 2

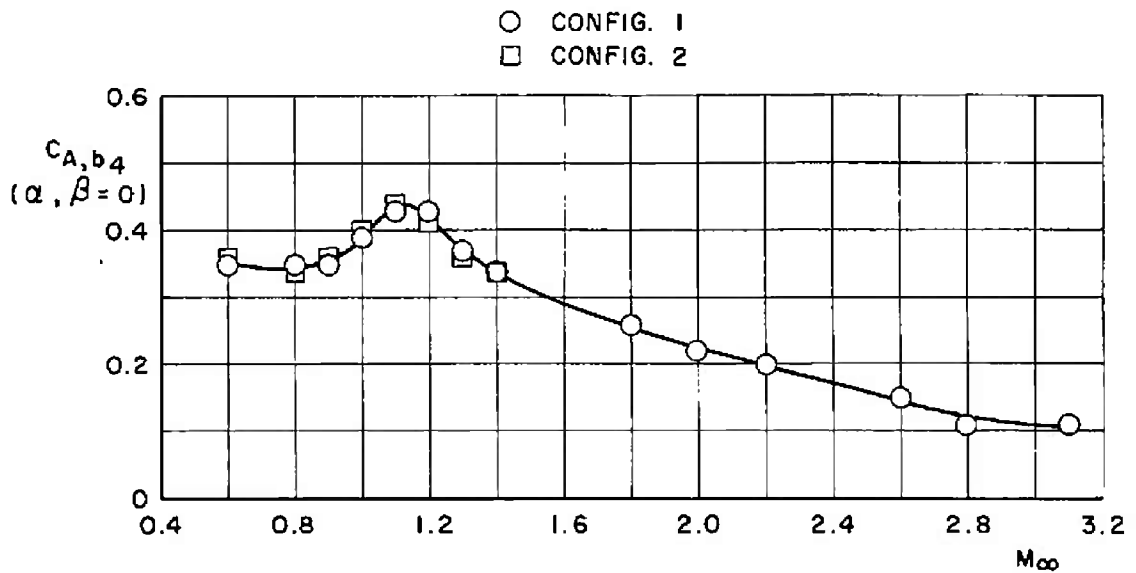
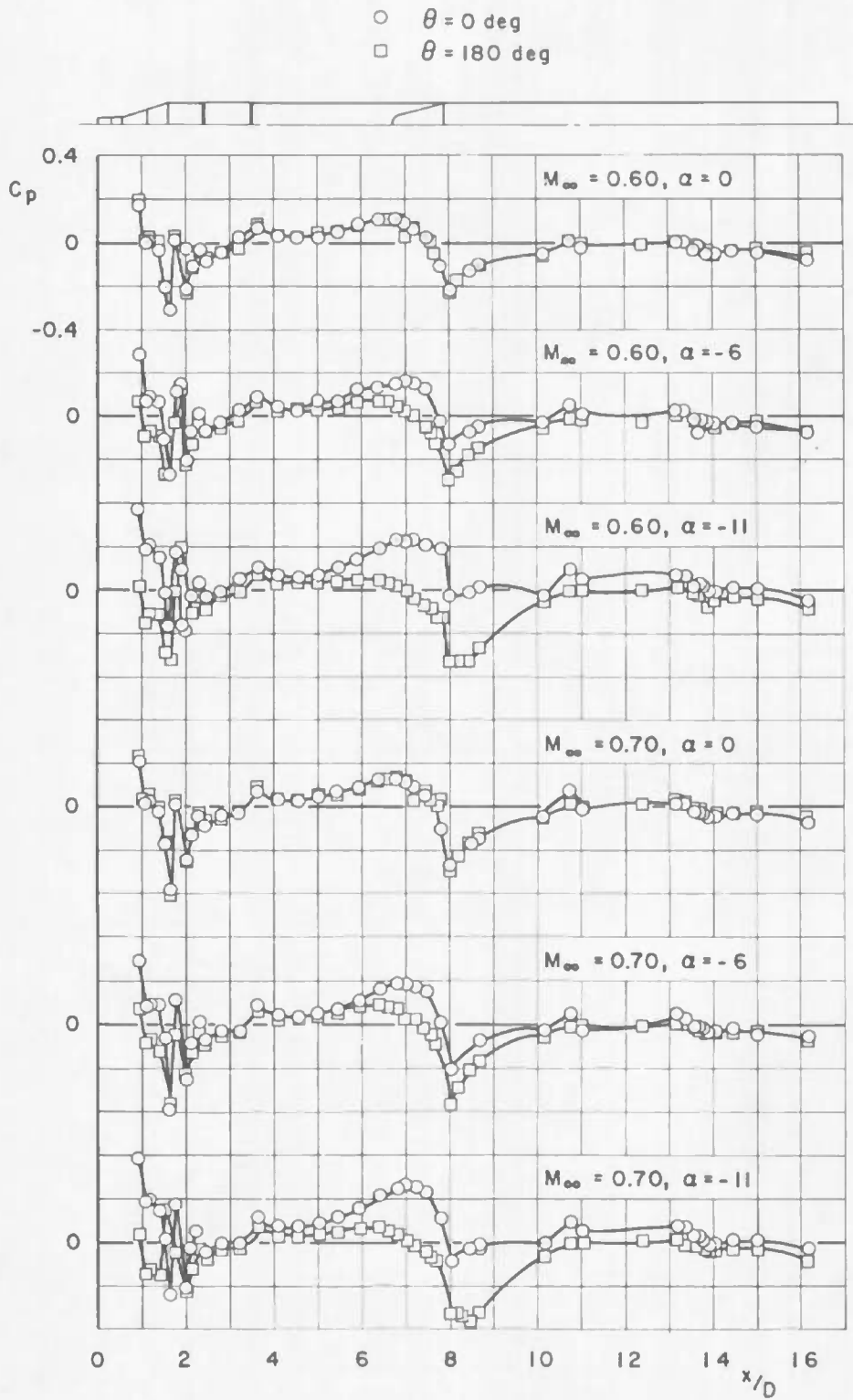
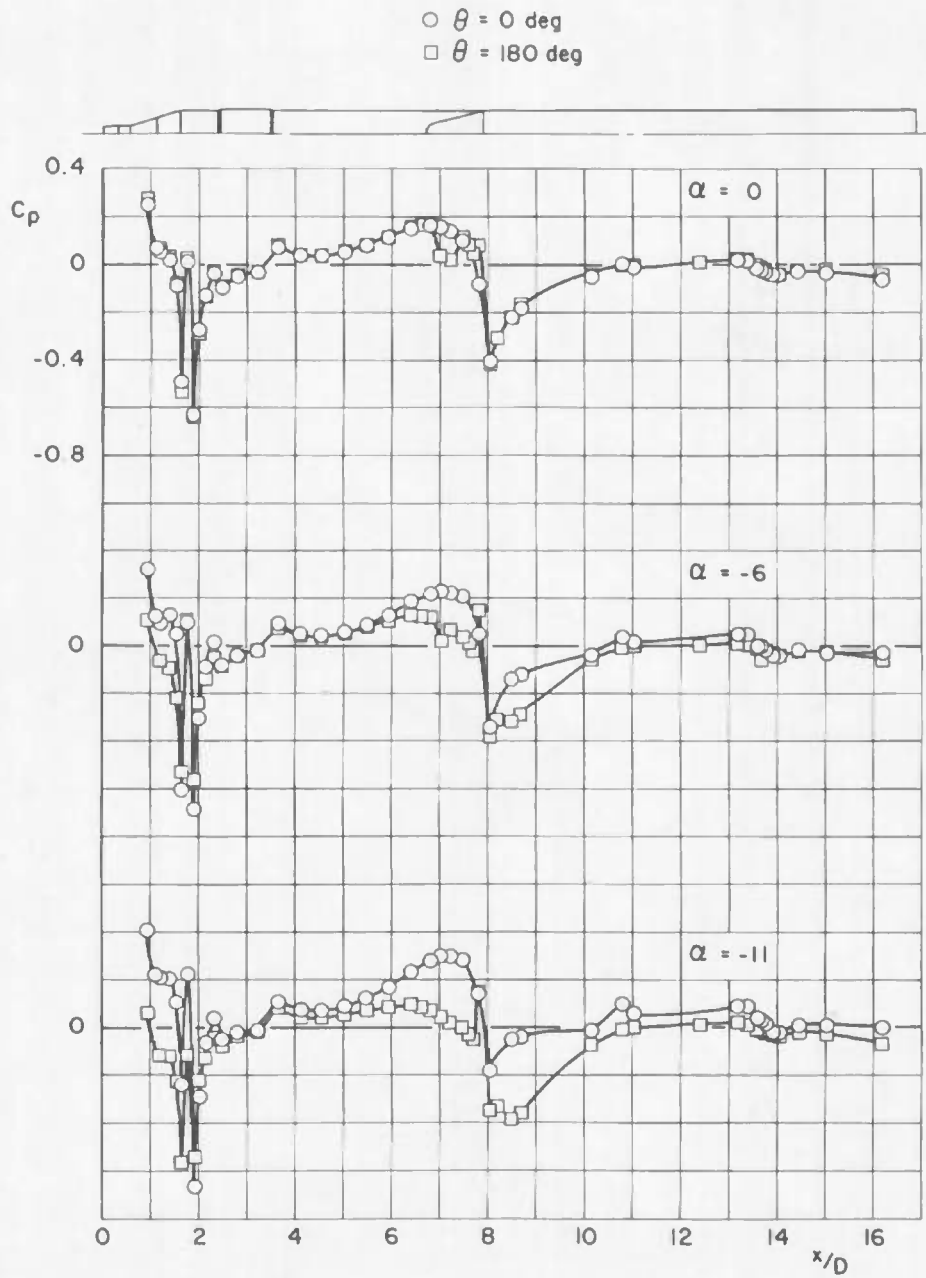


Fig. 47 Variation of SRM Base Axial-Force Coefficient with Mach Number for Configurations 1 and 2



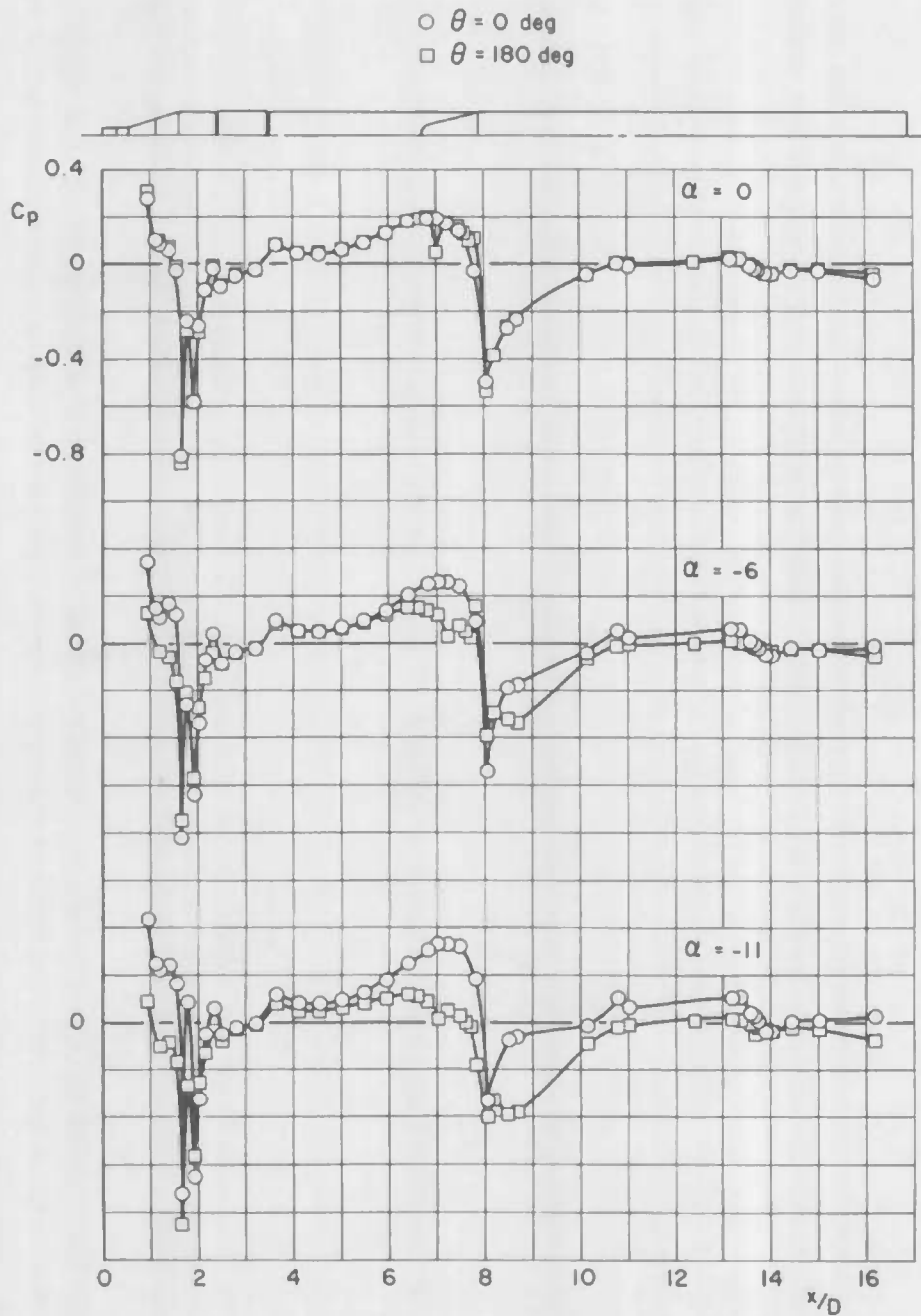
a. Mach Numbers 0.60 and 0.70

Fig. 48 Variation of Centerbody Surface Pressure Coefficient with Model Station for Orifices Oriented at 0 and 180 deg for Configuration 1, $\beta = 0$

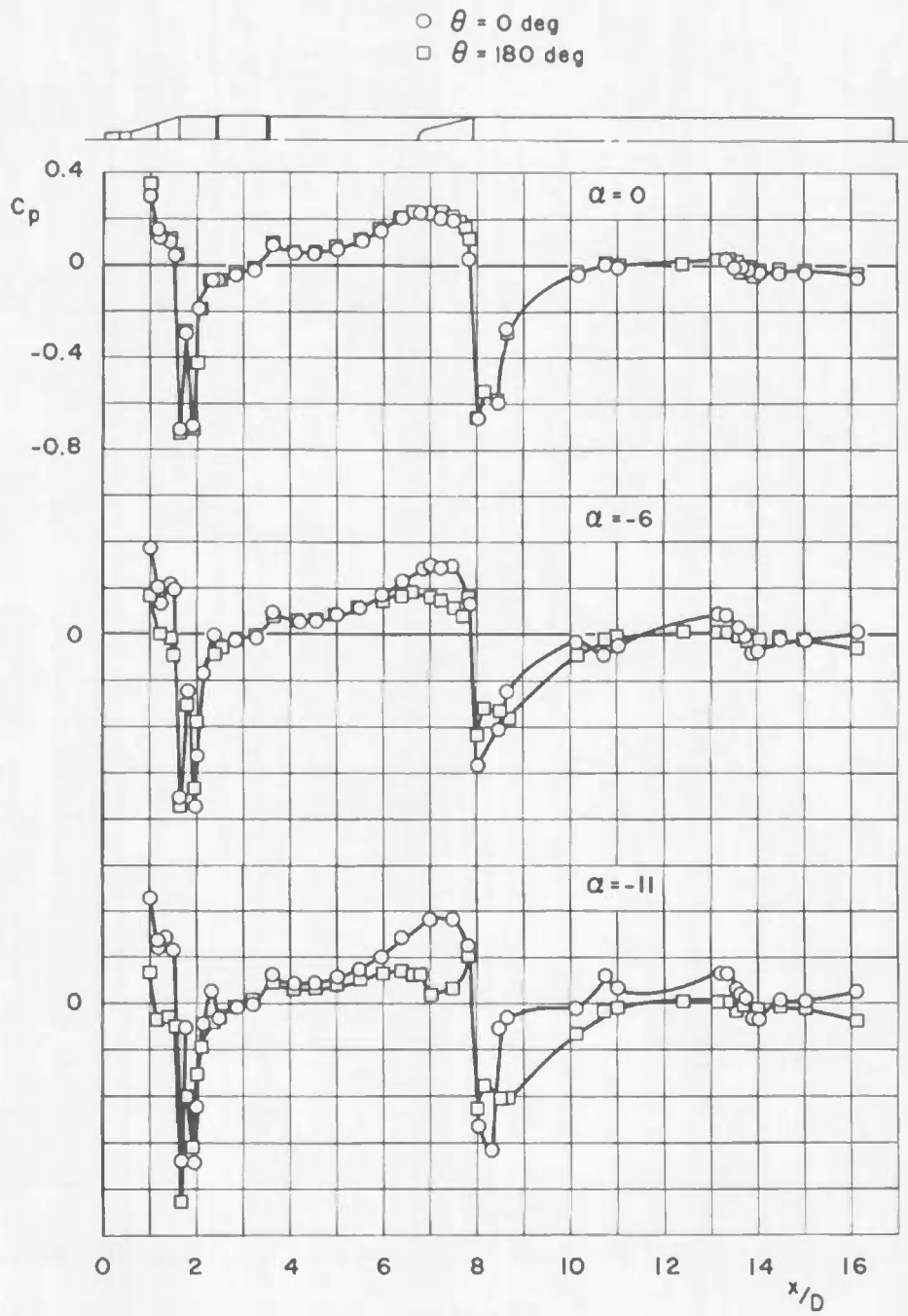


b. Mach Number 0.80

Fig. 48 Continued

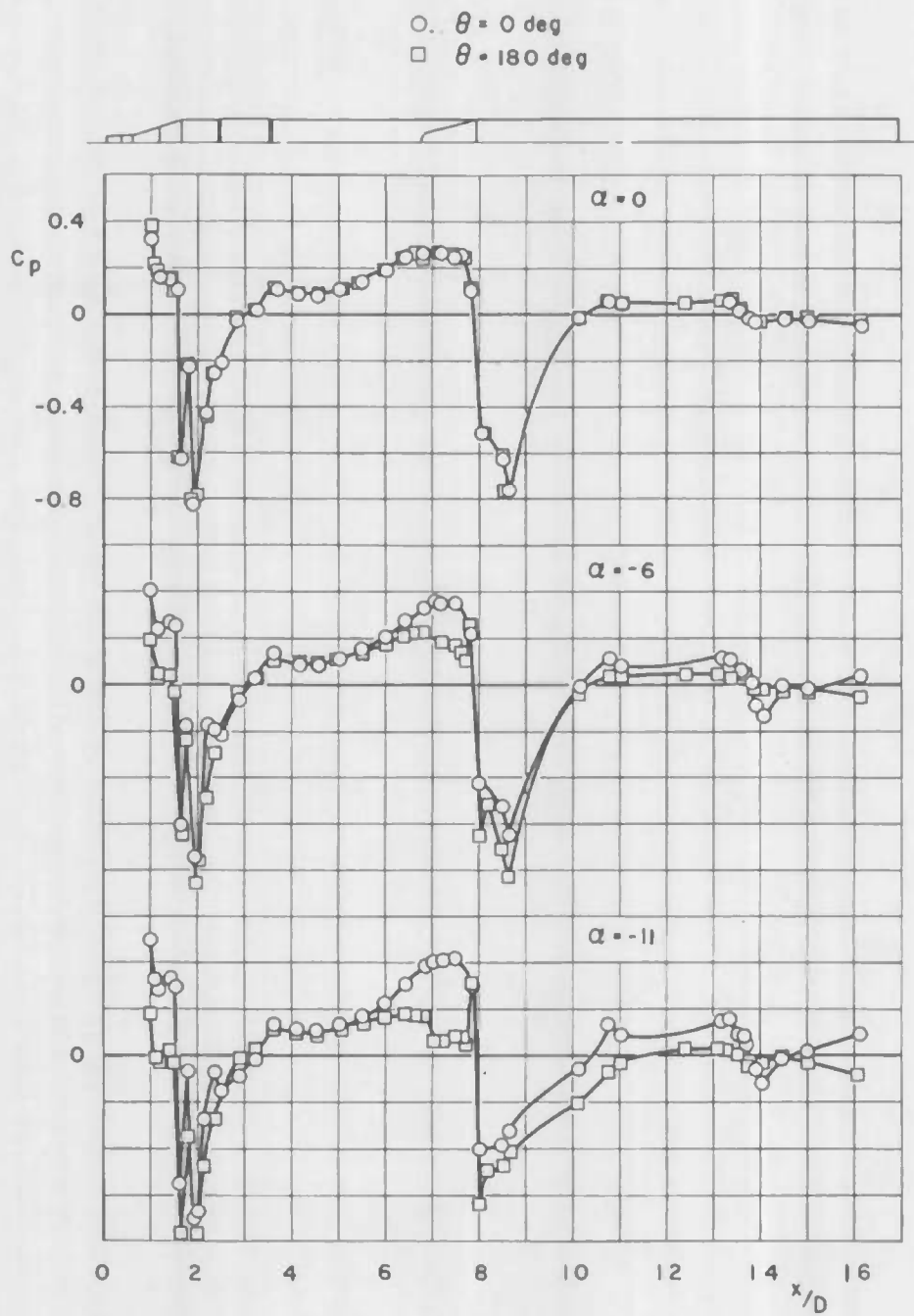


c. Mach Number 0.85
Fig. 48 Continued



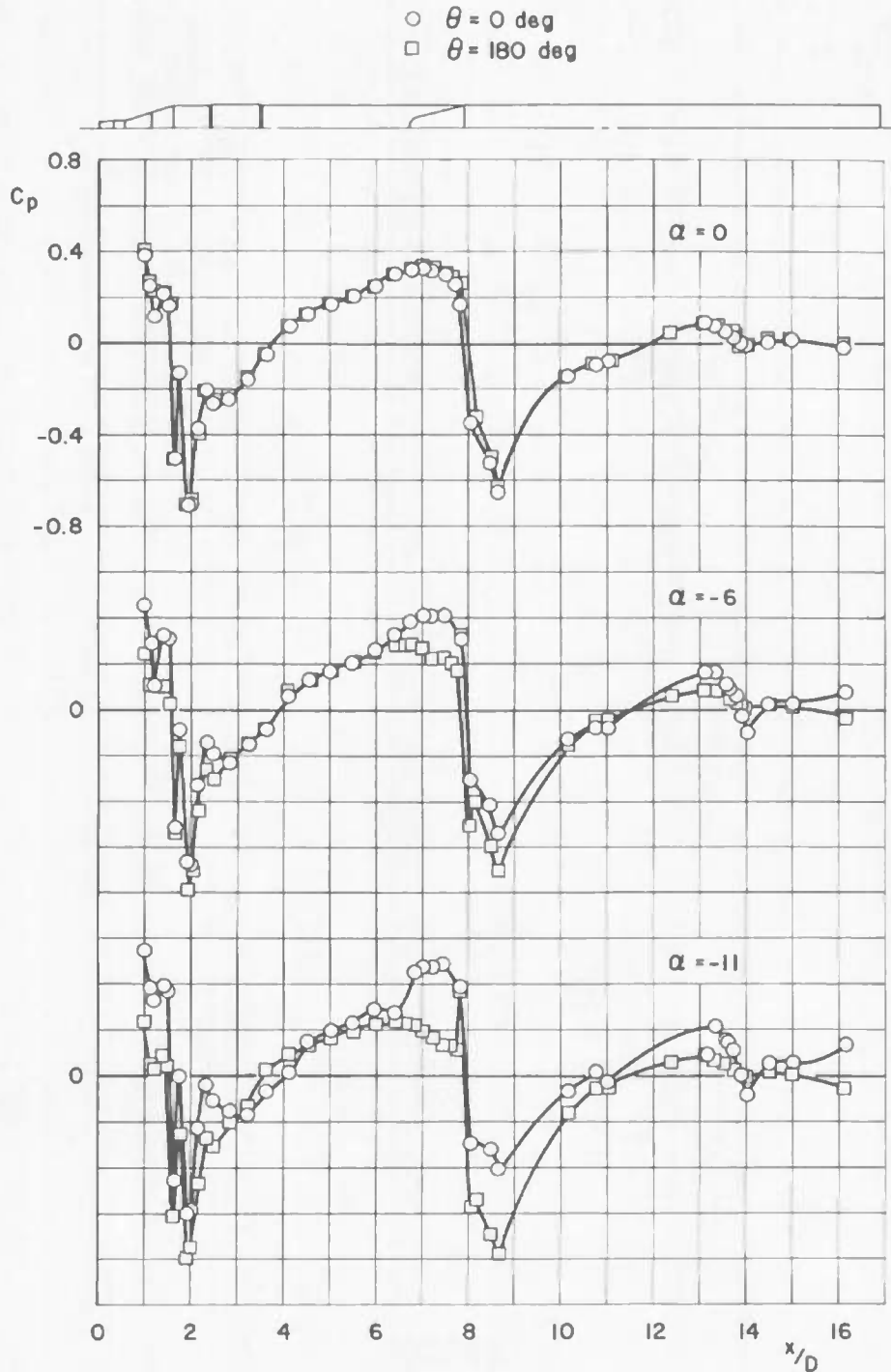
d. Mach Number 0.90

Fig. 48 Continued



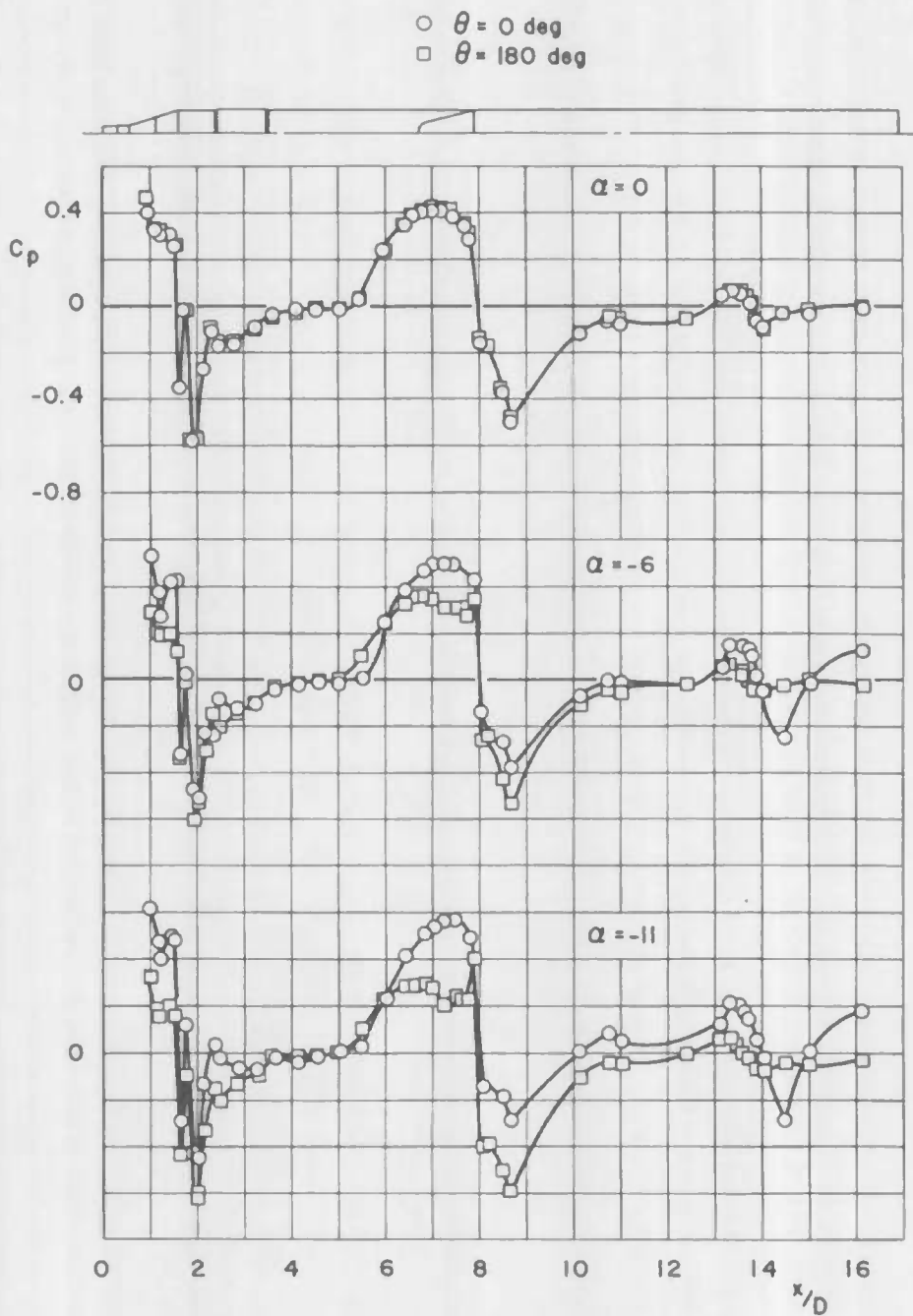
e. Mach Number 0.95

Fig. 48 Continued

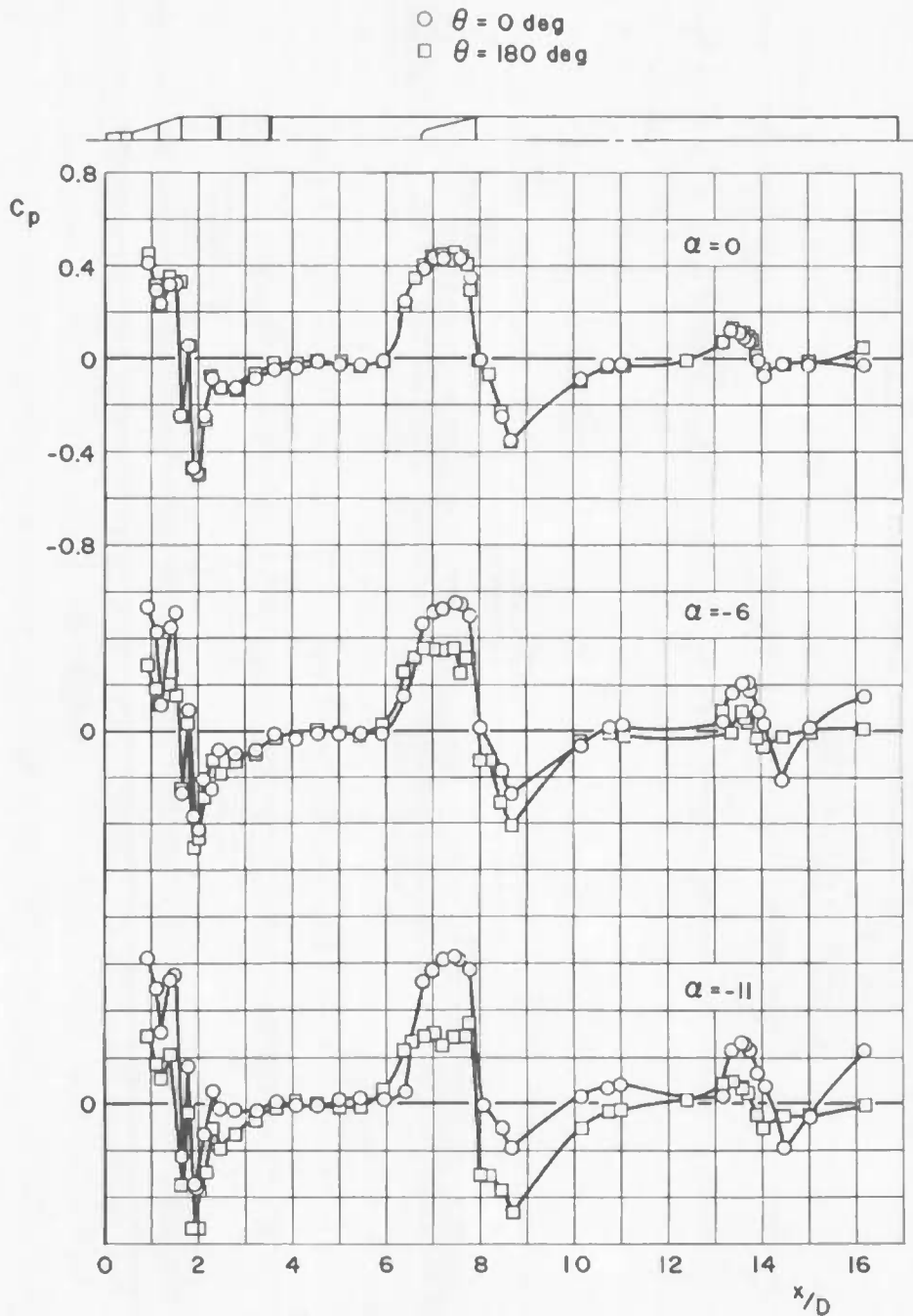


f. Mach Number 1.00

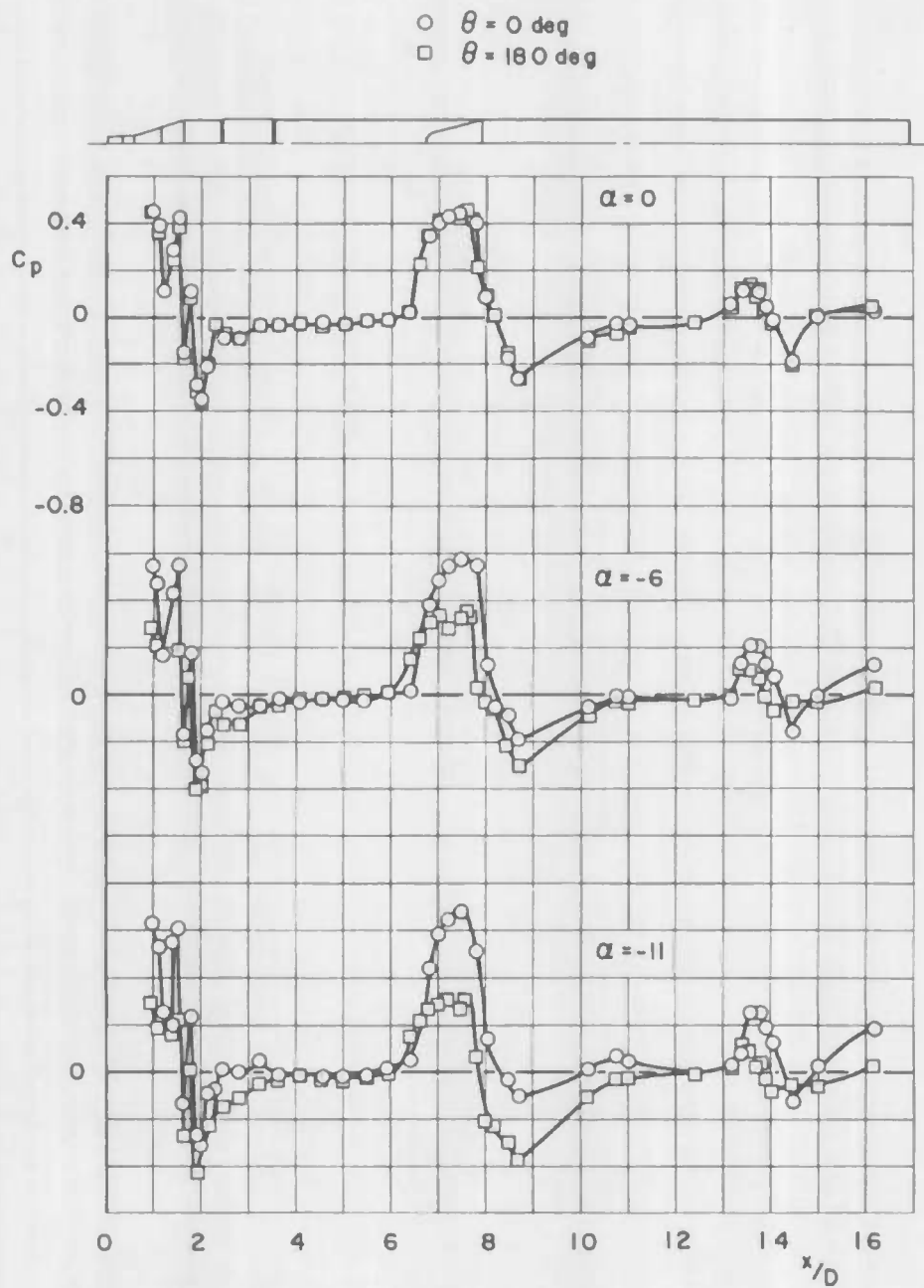
Fig. 48 Continued



g. Mach Number 1.10
 Fig. 48 Continued

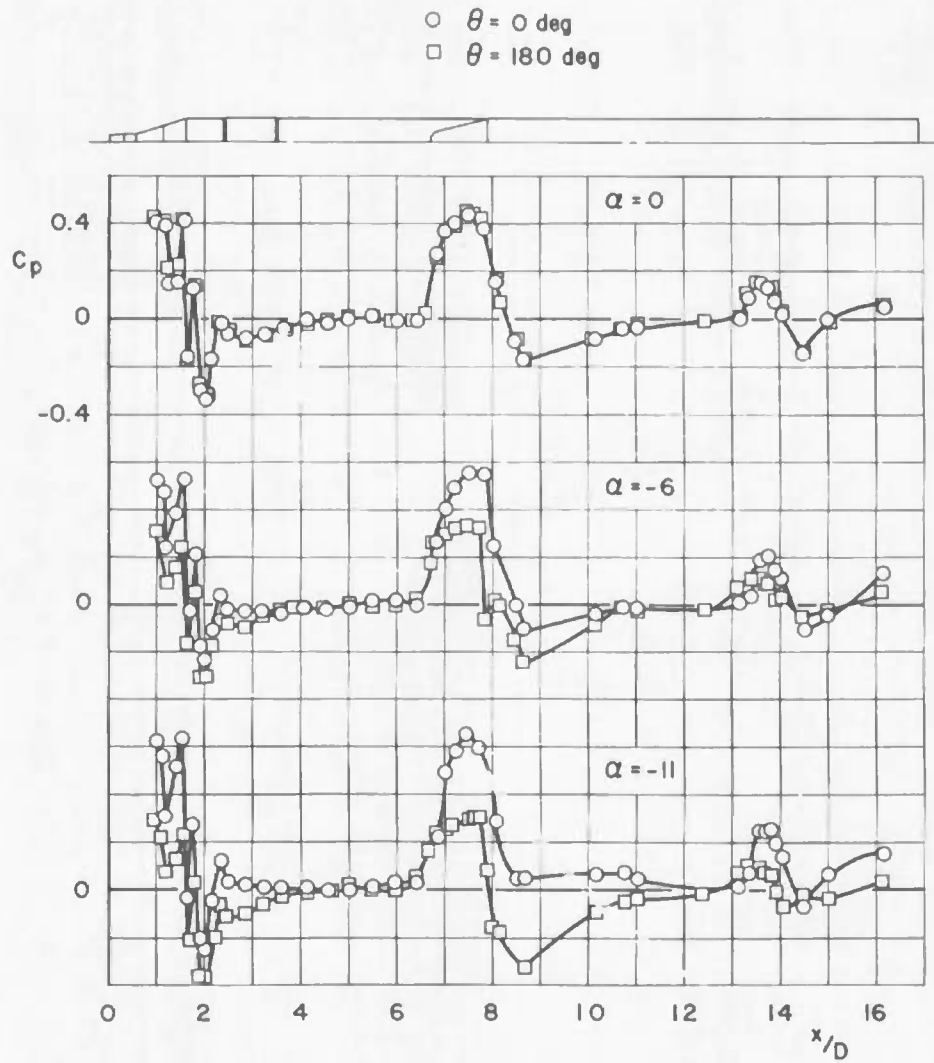


h. Mach Number 1.20
Fig. 48 Continued

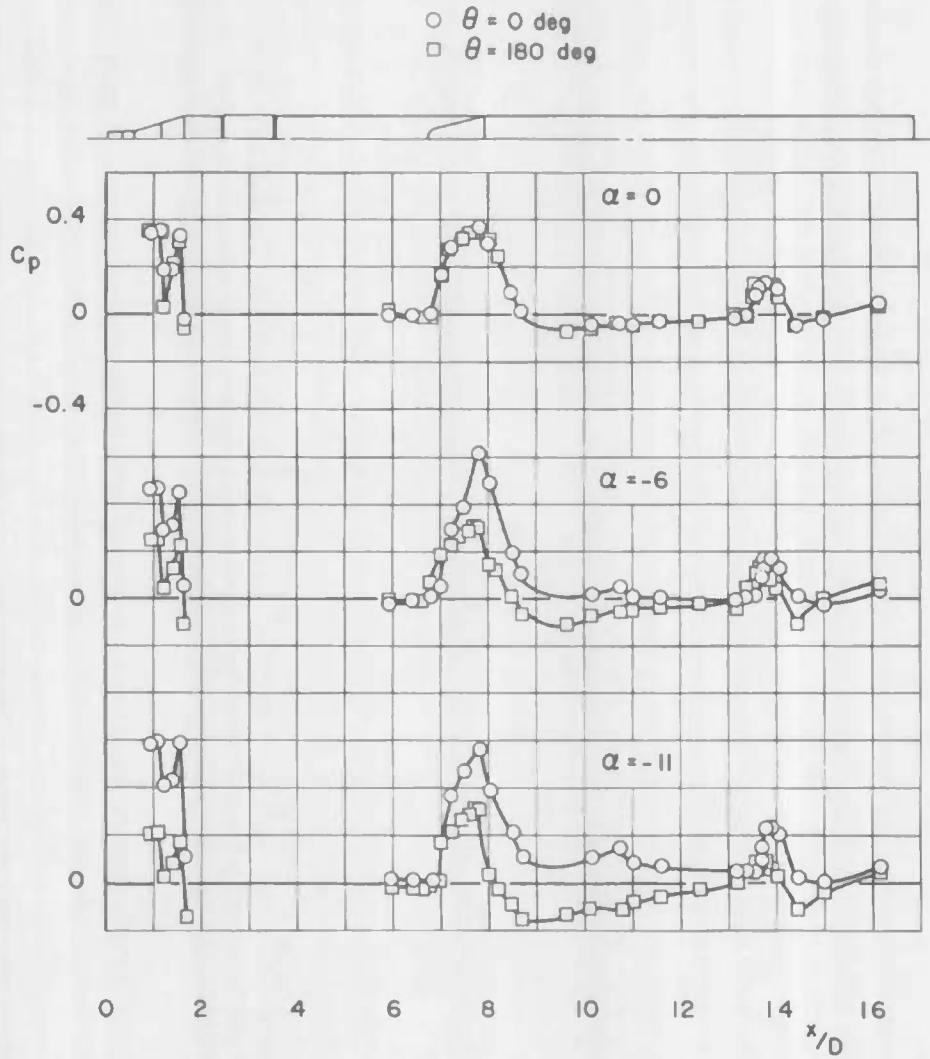


i. Mach Number 1.30

Fig. 48 Continued

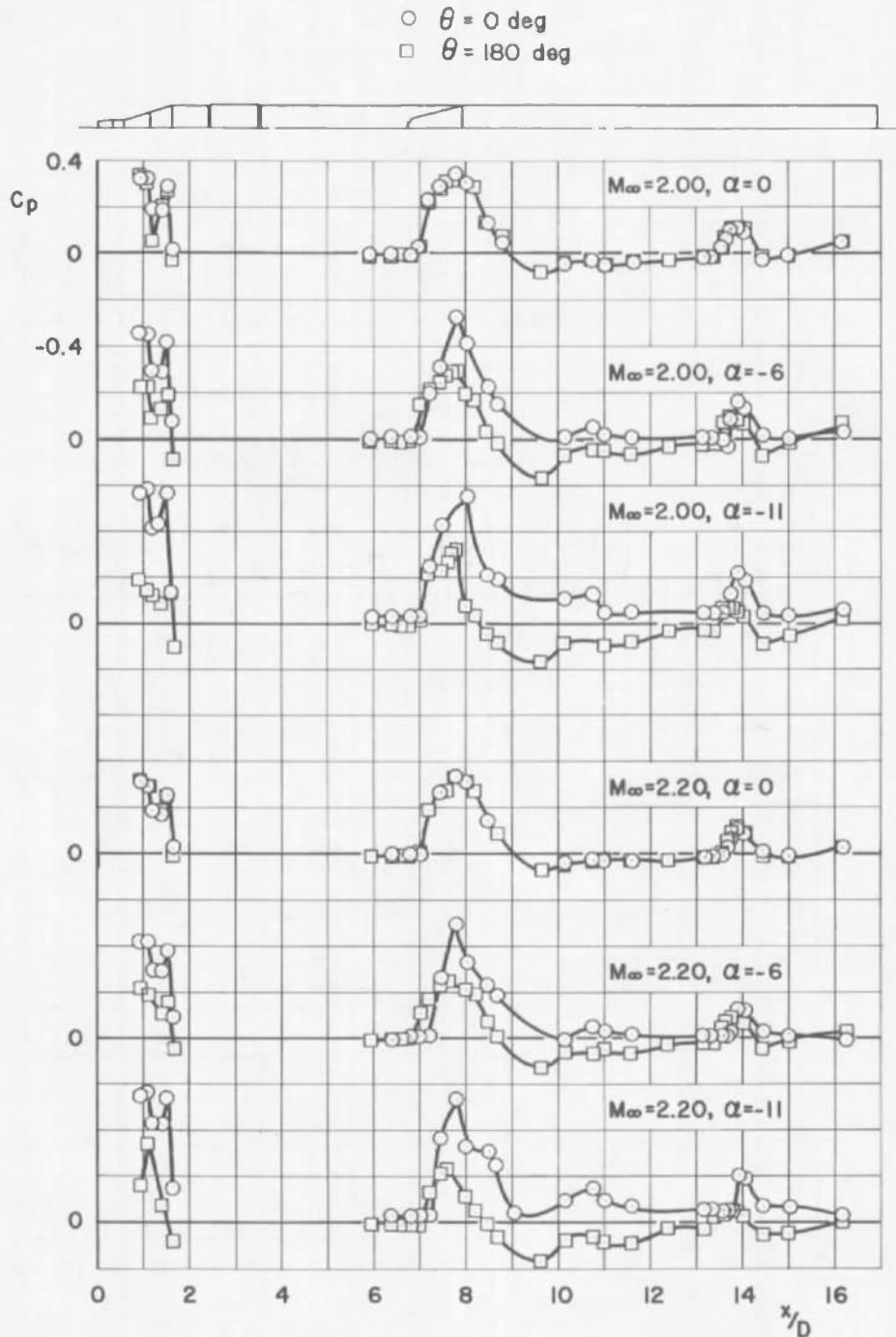


j. Mach Number 1.40
 Fig. 48 Continued

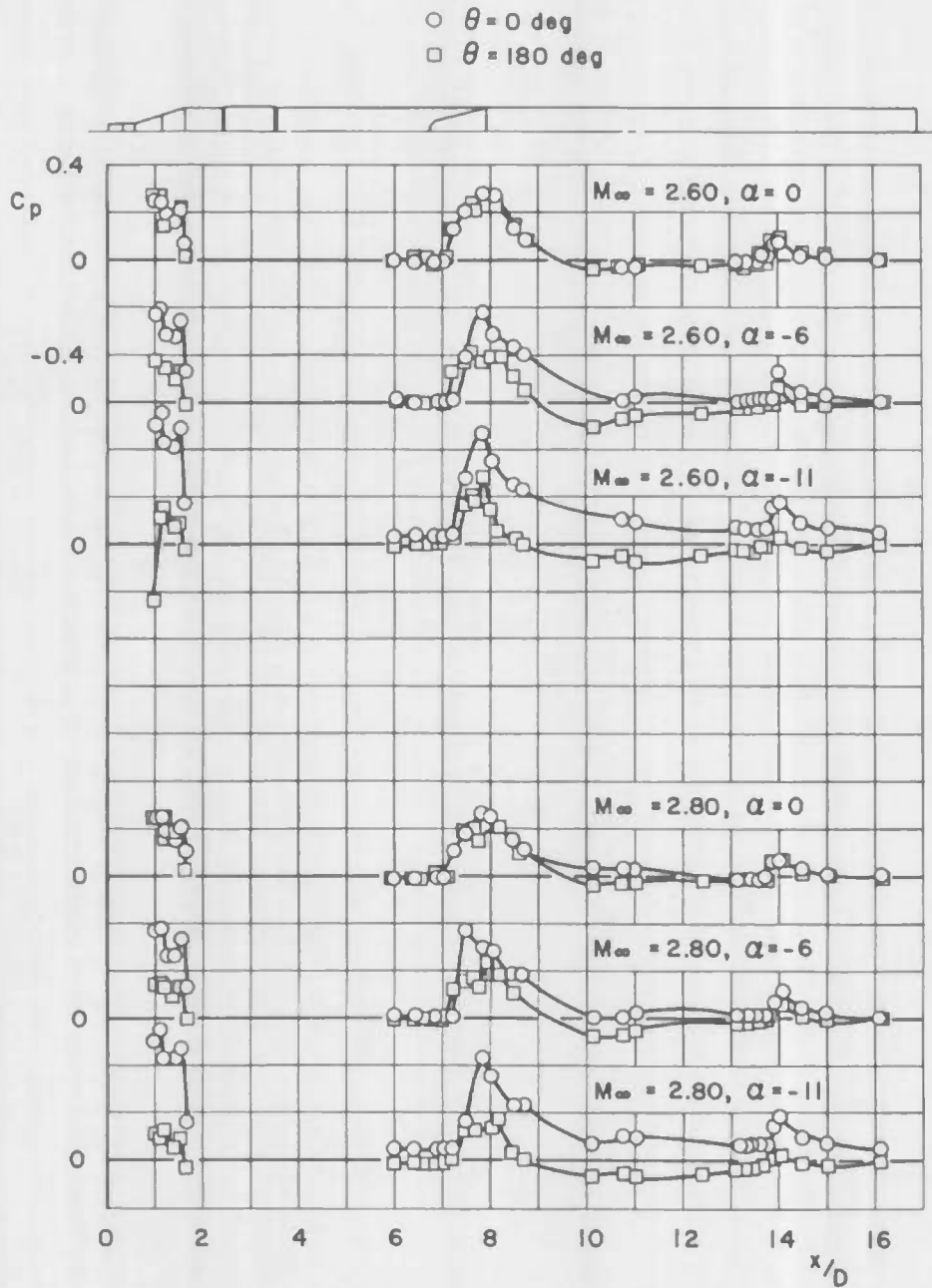


k. Mach Number 1.80

Fig. 48 Continued

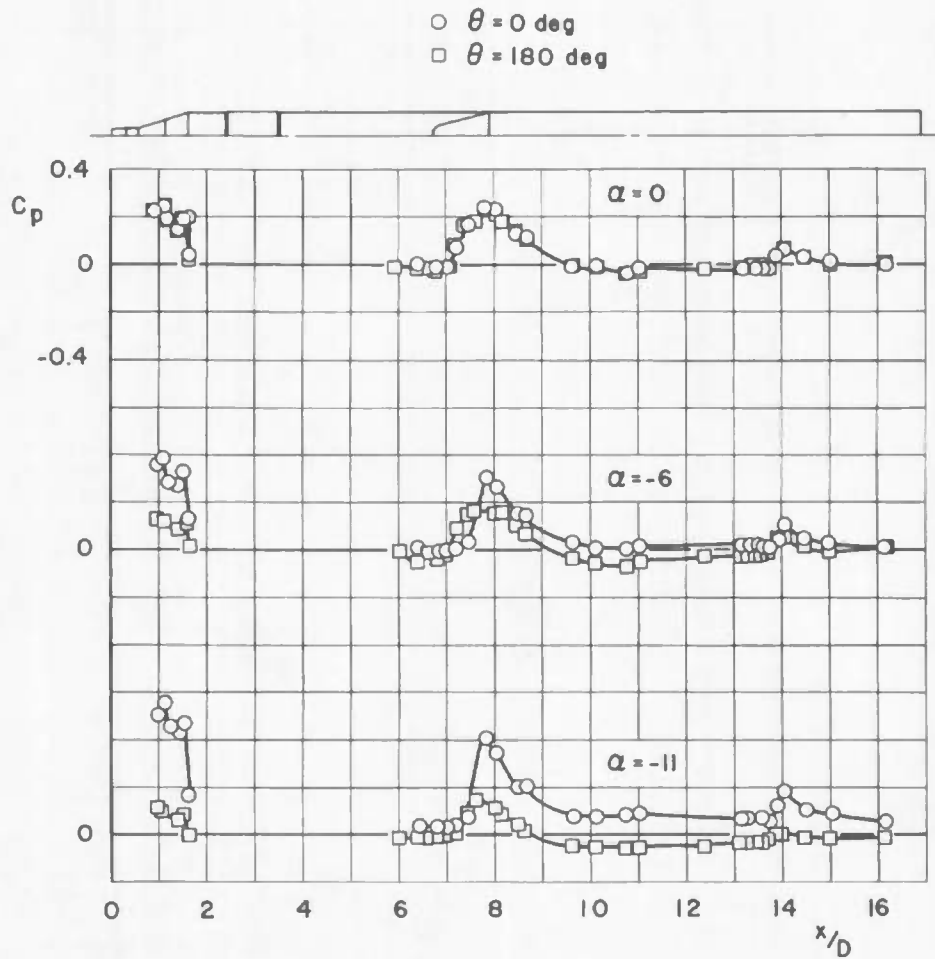


1. Mach Numbers 2.00 and 2.20
 Fig. 48 Continued



m. Mach Numbers 2.60 and 2.80

Fig. 48 Continued



n. Mach Number 3.00

Fig. 48 Concluded

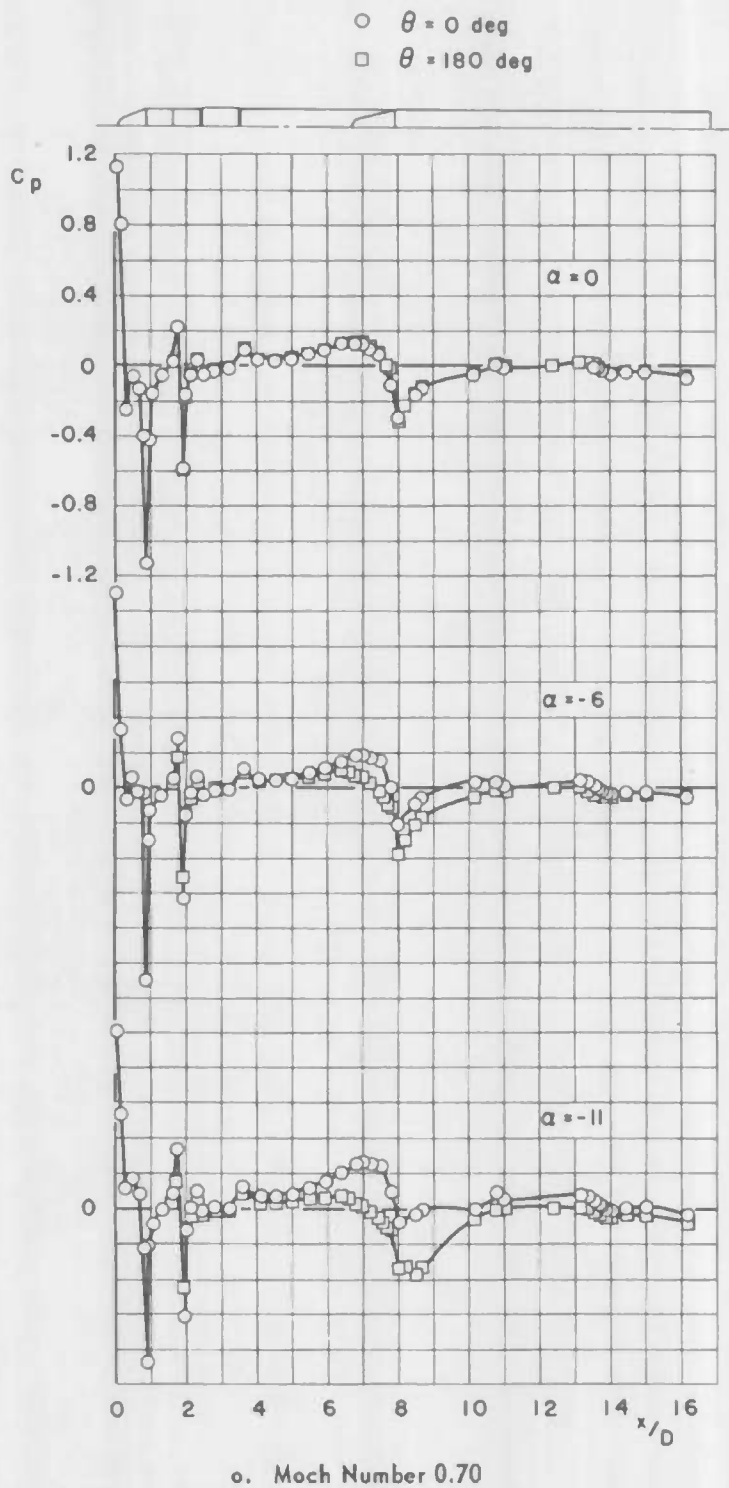
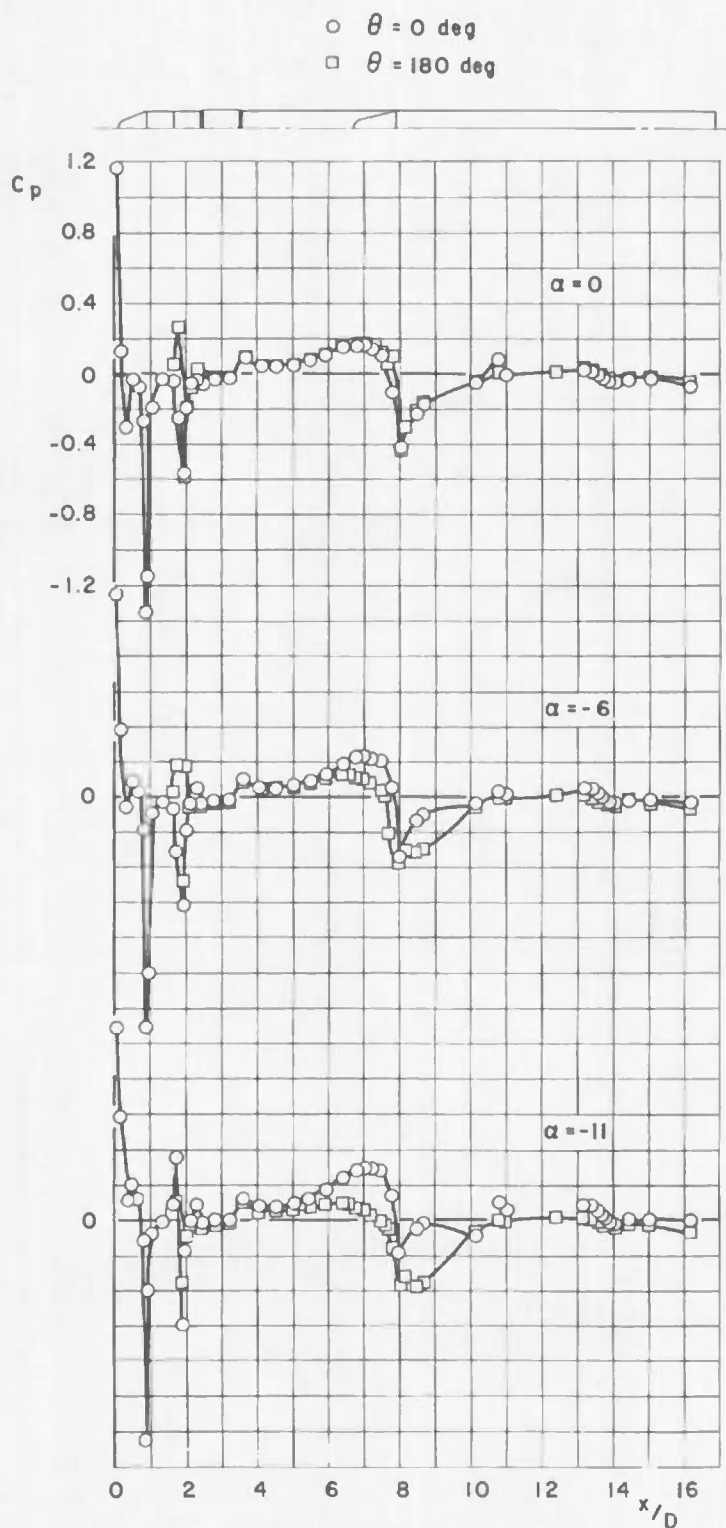
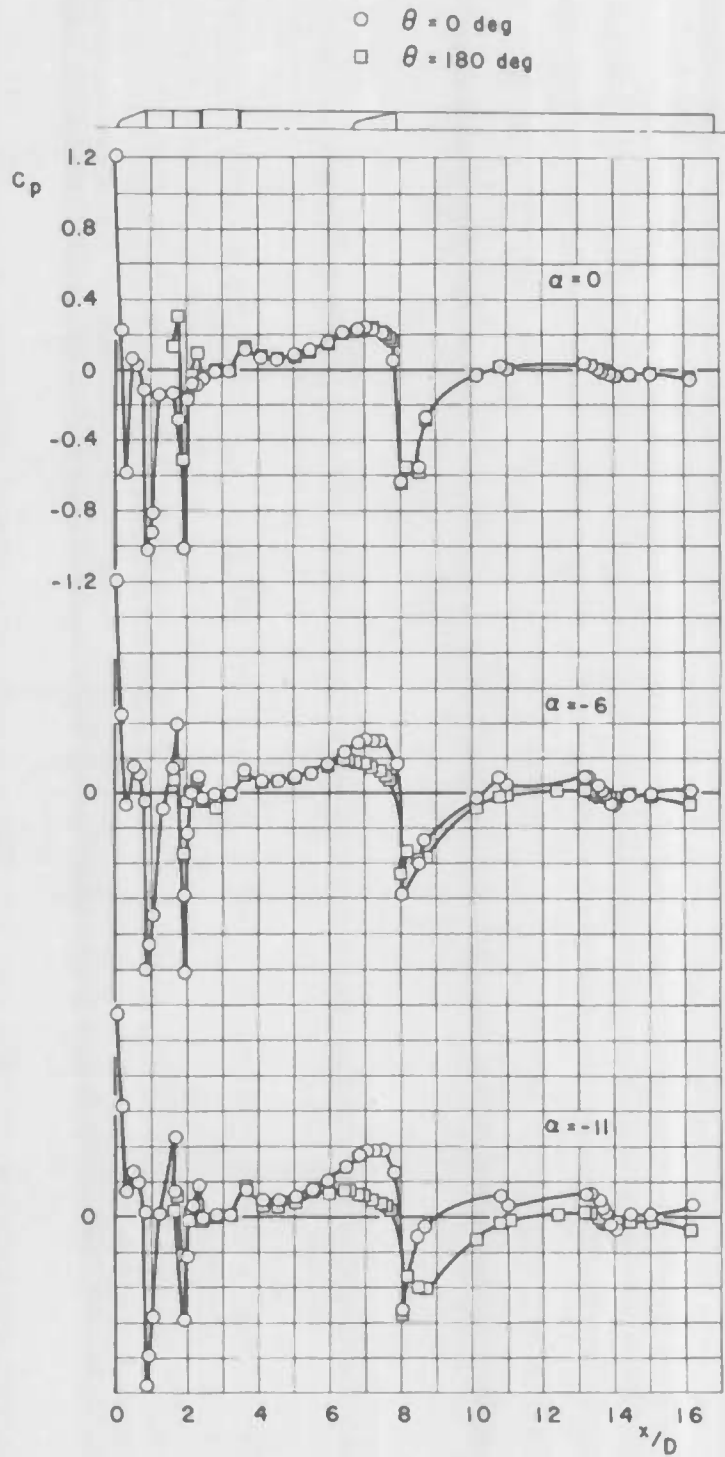


Fig. 49 Variation of Centerbody Surface Pressure Coefficient with Model Station for Orifices Oriented at 0 and 180 deg for Configuration 3, $\beta = 0$

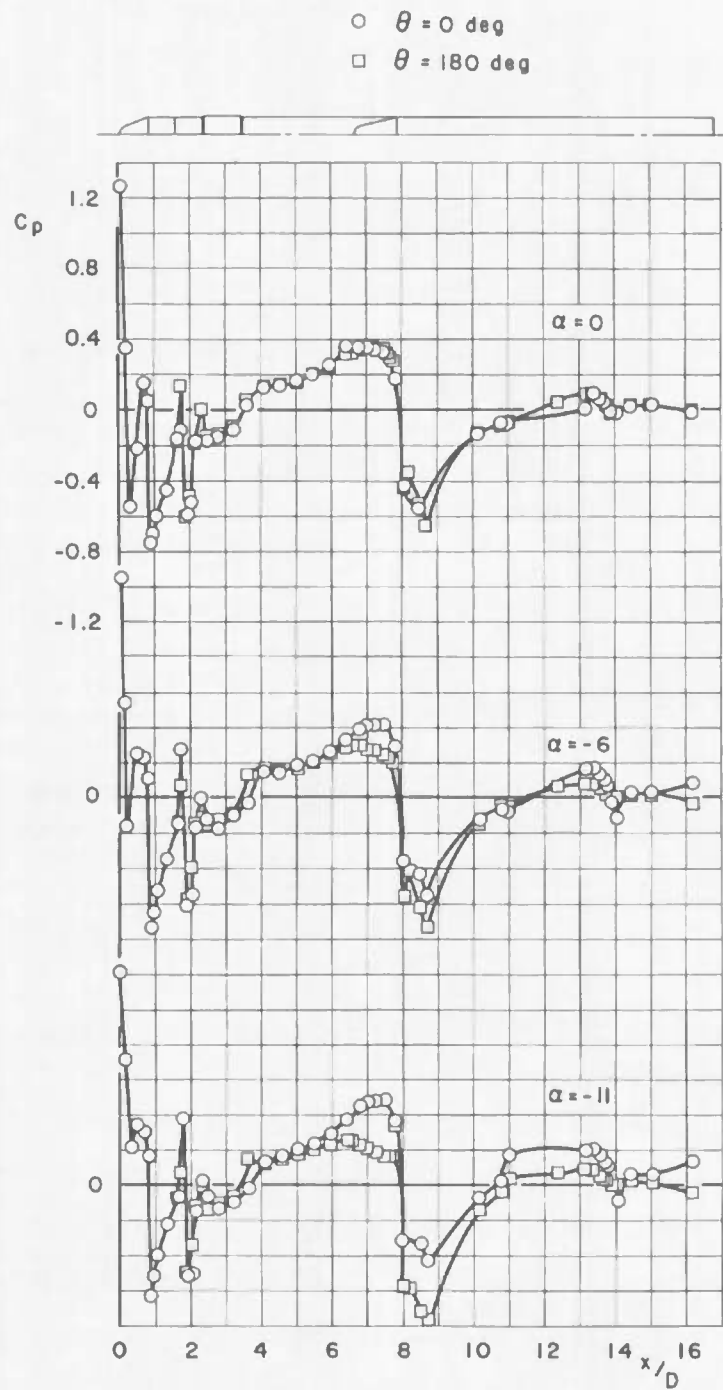


b. Mach Number 0.80

Fig. 49 Continued

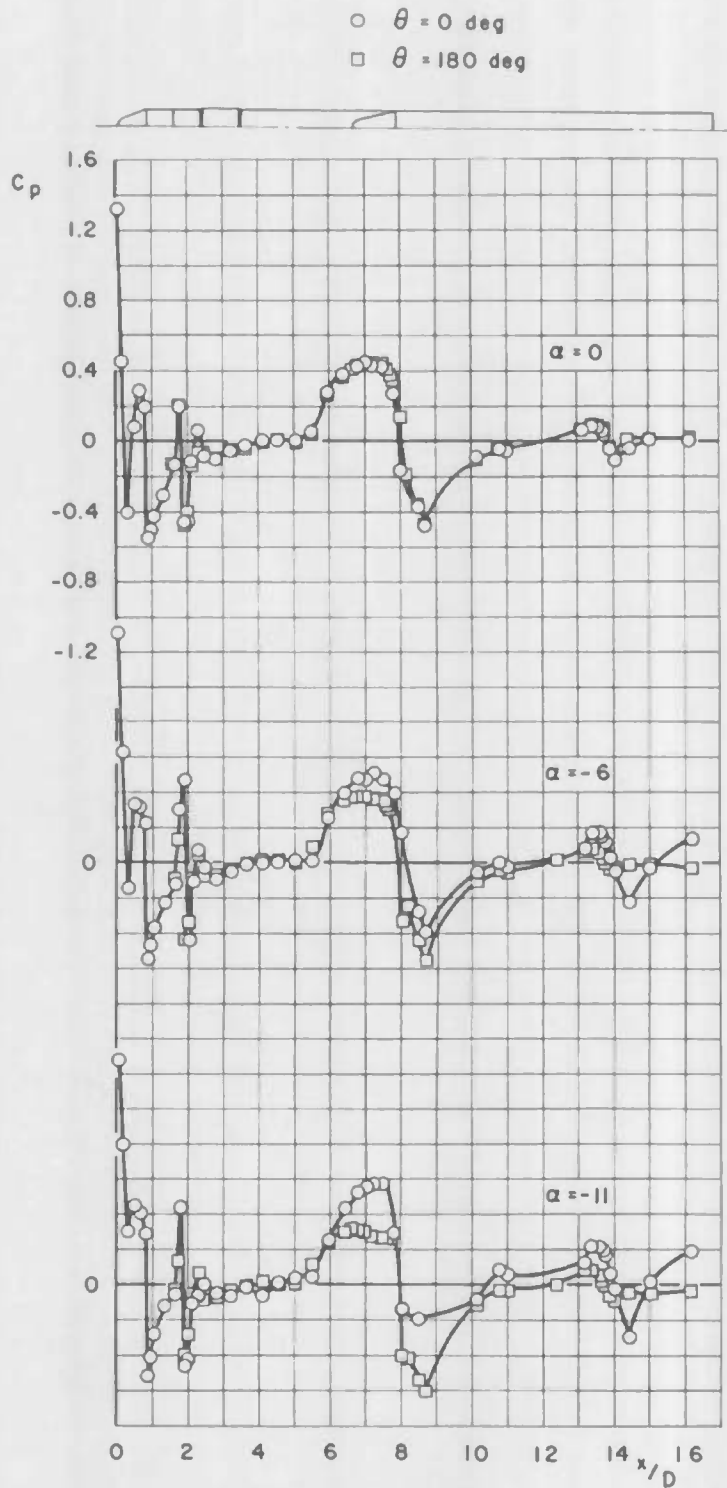


c. Mach Number 0.90
 Fig. 49 Continued



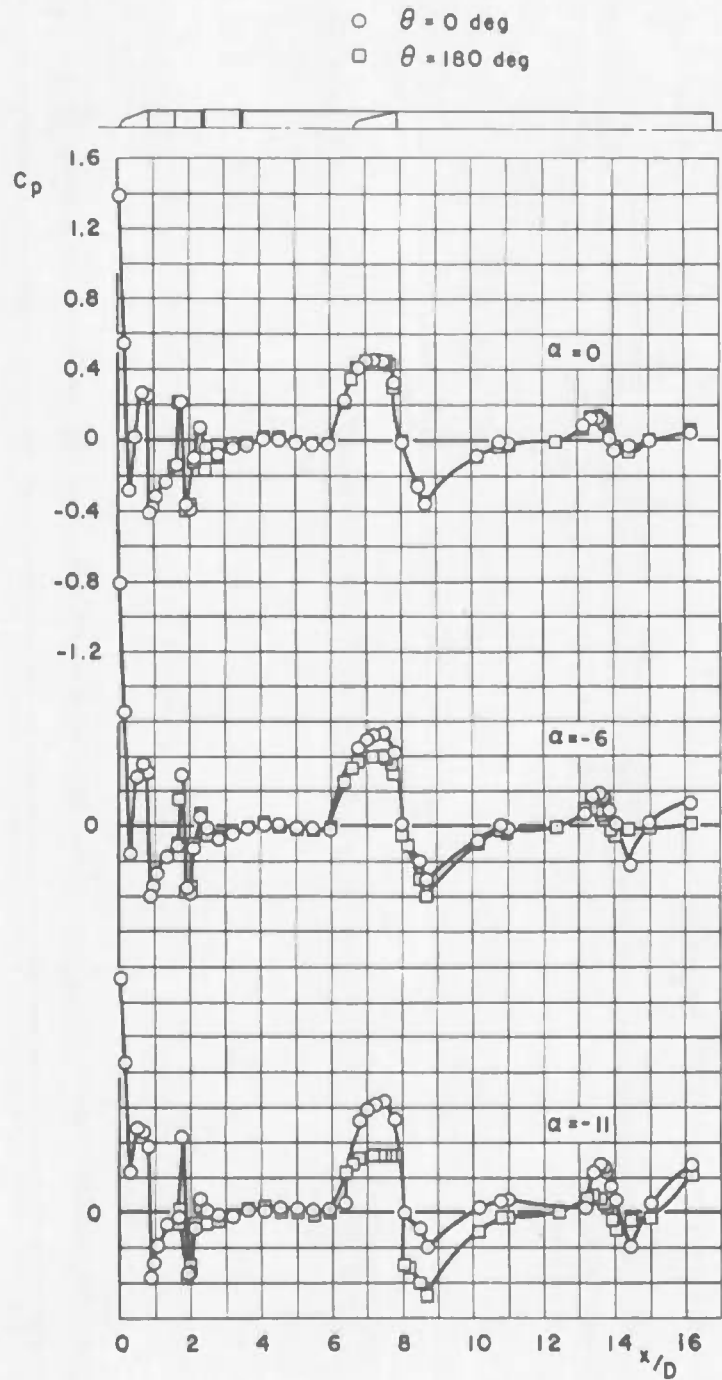
d. Mach Number 1.00

Fig. 49 Continued

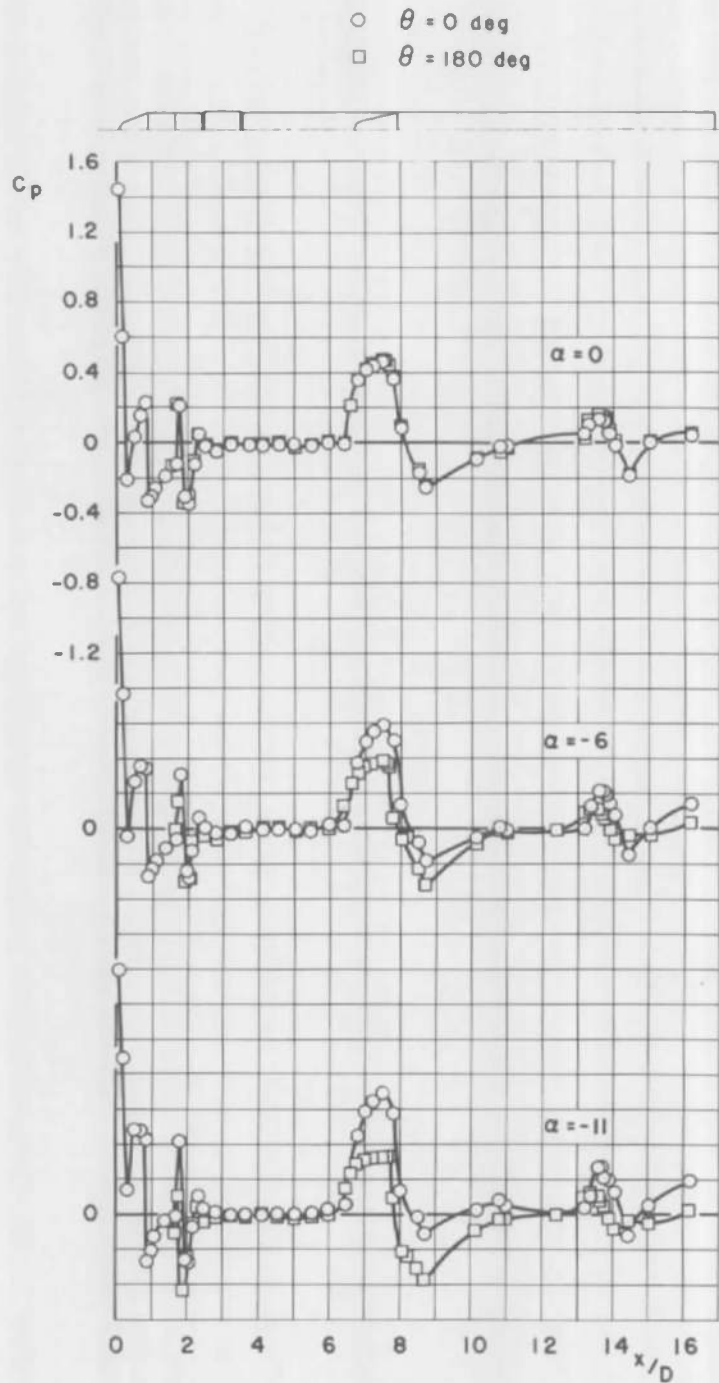


e. Mach Number 1.10

Fig. 49 Continued



f. Mach Number 1.20
 Fig. 49 Continued



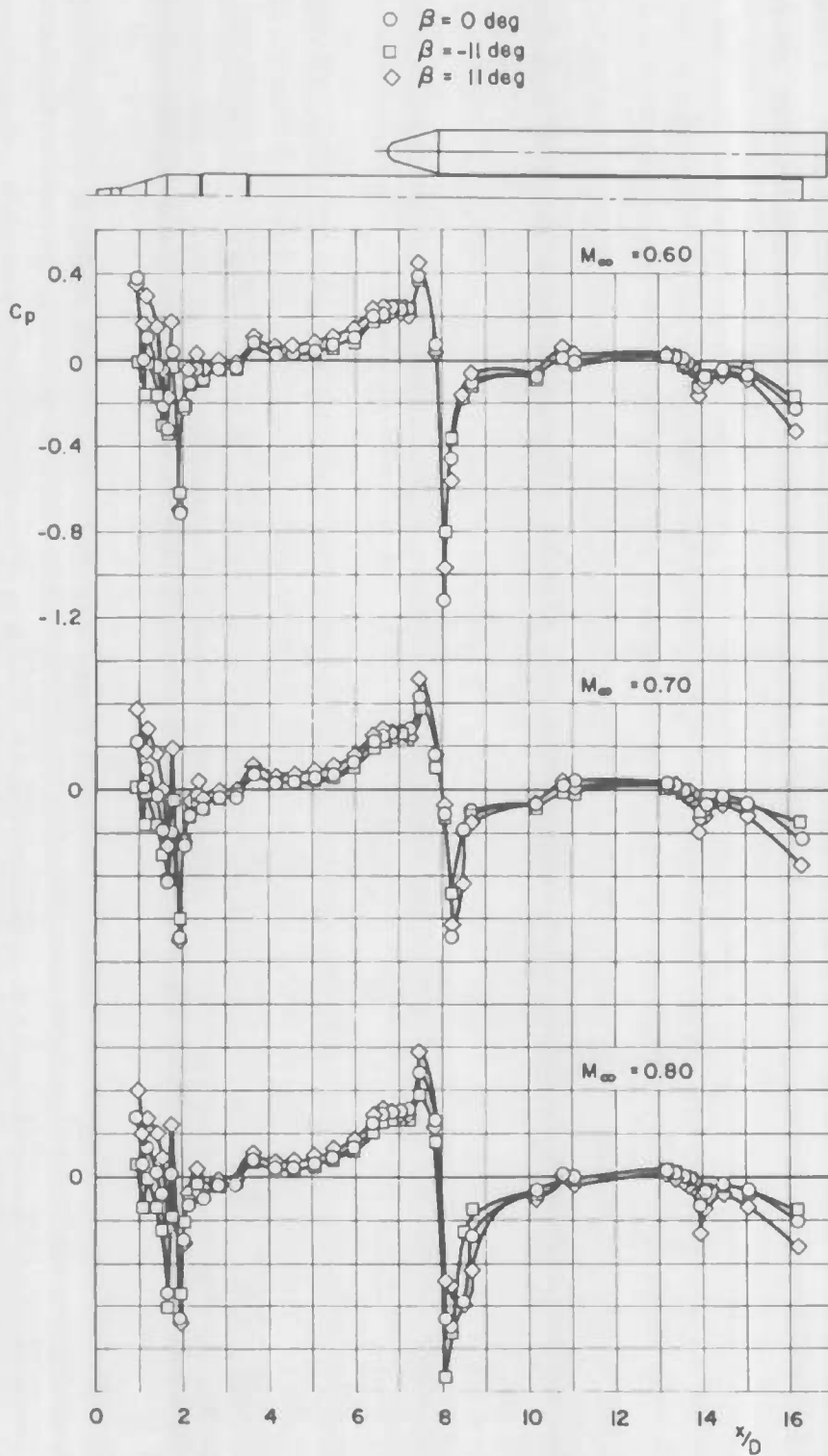
g. Mach Number 1.30

Fig. 49 Continued



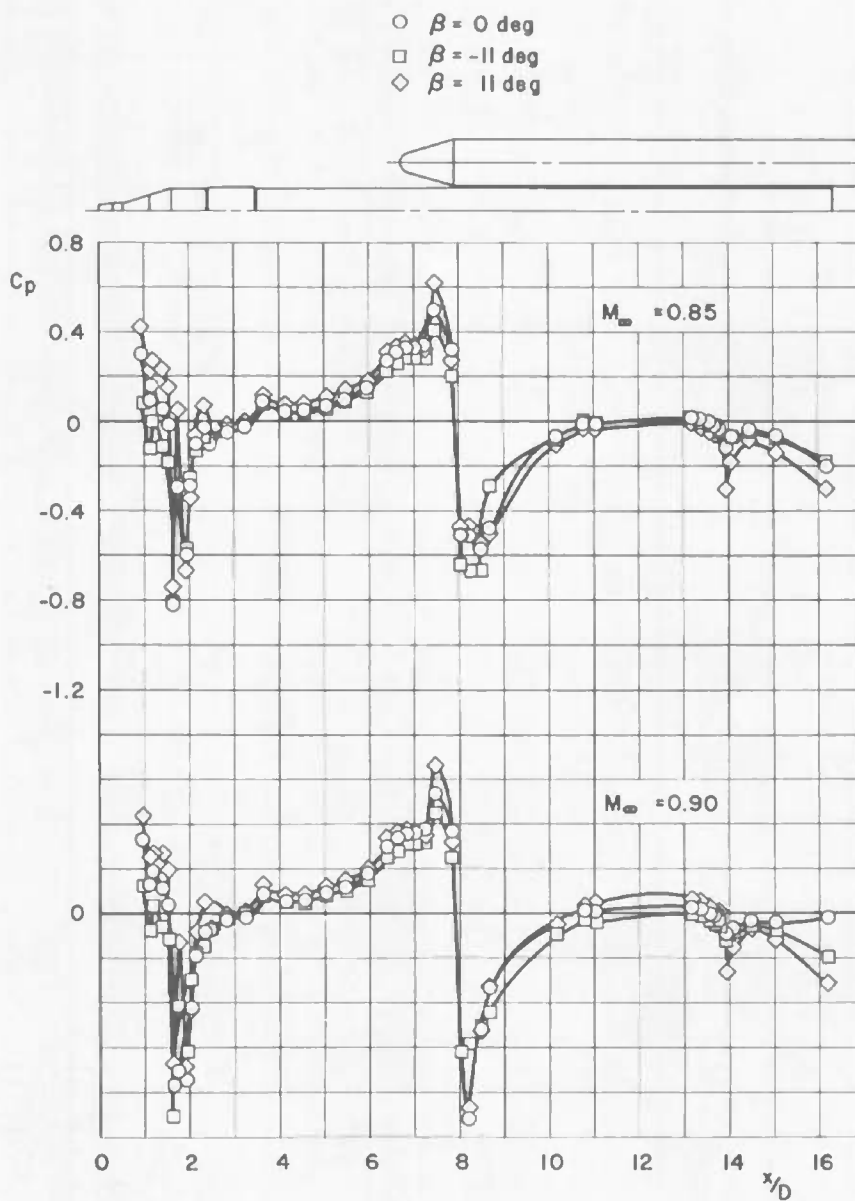
h. Mach Number 1.40

Fig. 49 Concluded



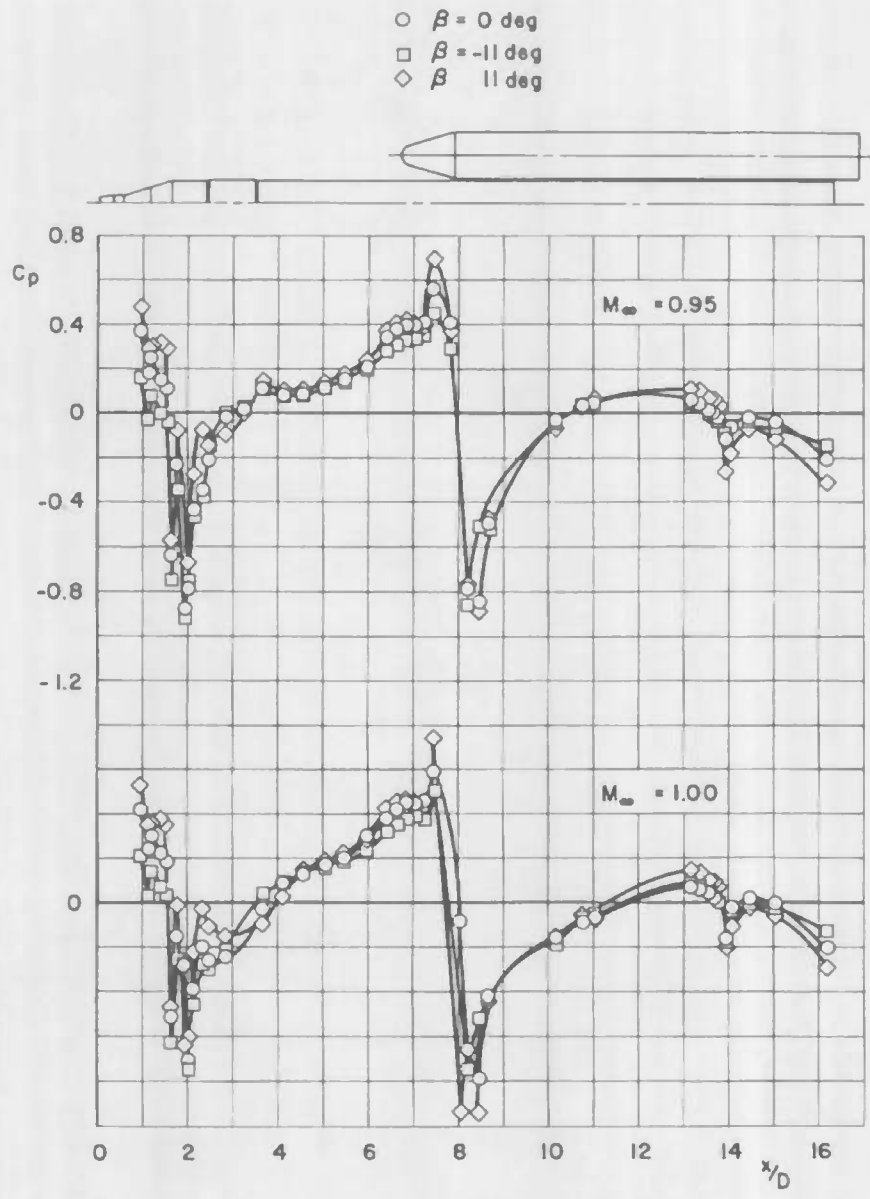
a. Mach Numbers 0.60 through 0.80

Fig. 50 Variation of Surface Pressure Coefficient with Model Station for Orifices Oriented at 90 deg for Configuration 1, $\alpha = 0$

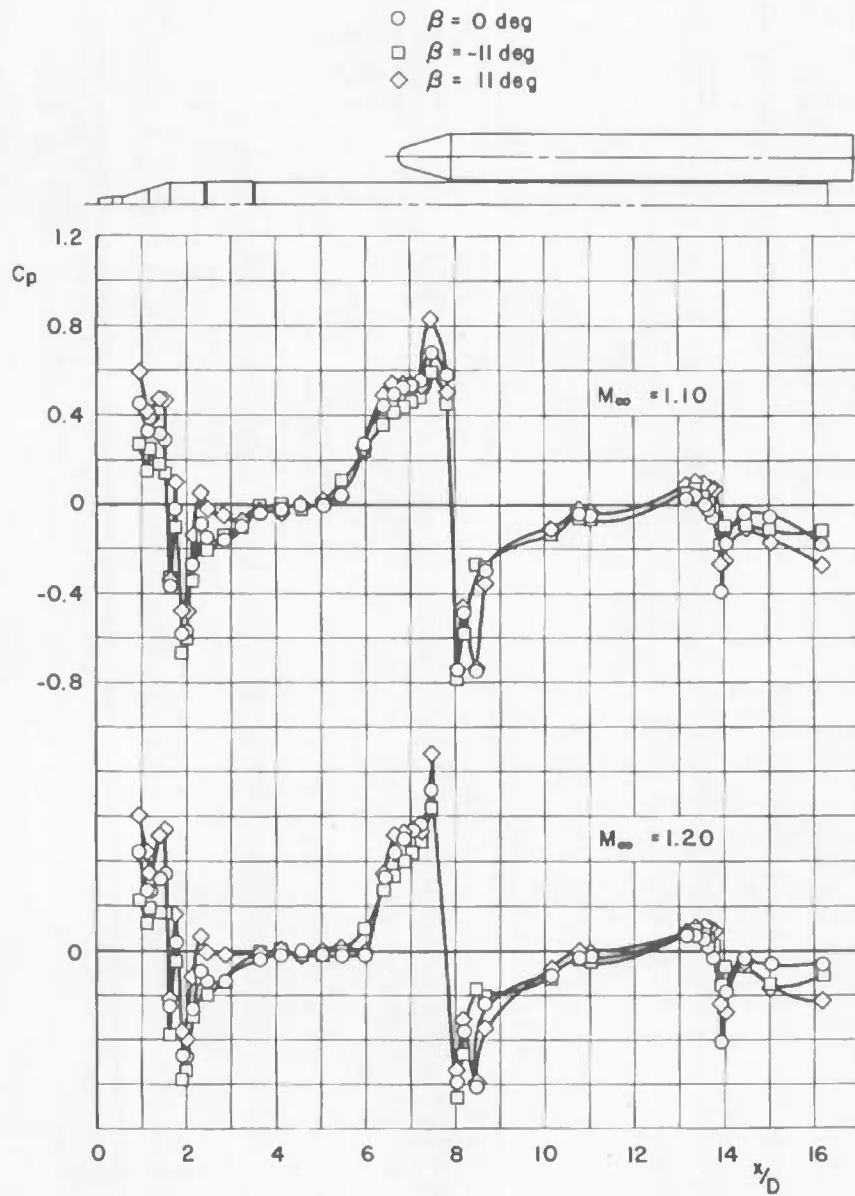


b. Mach Numbers 0.85 and 0.90

Fig. 50 Continued

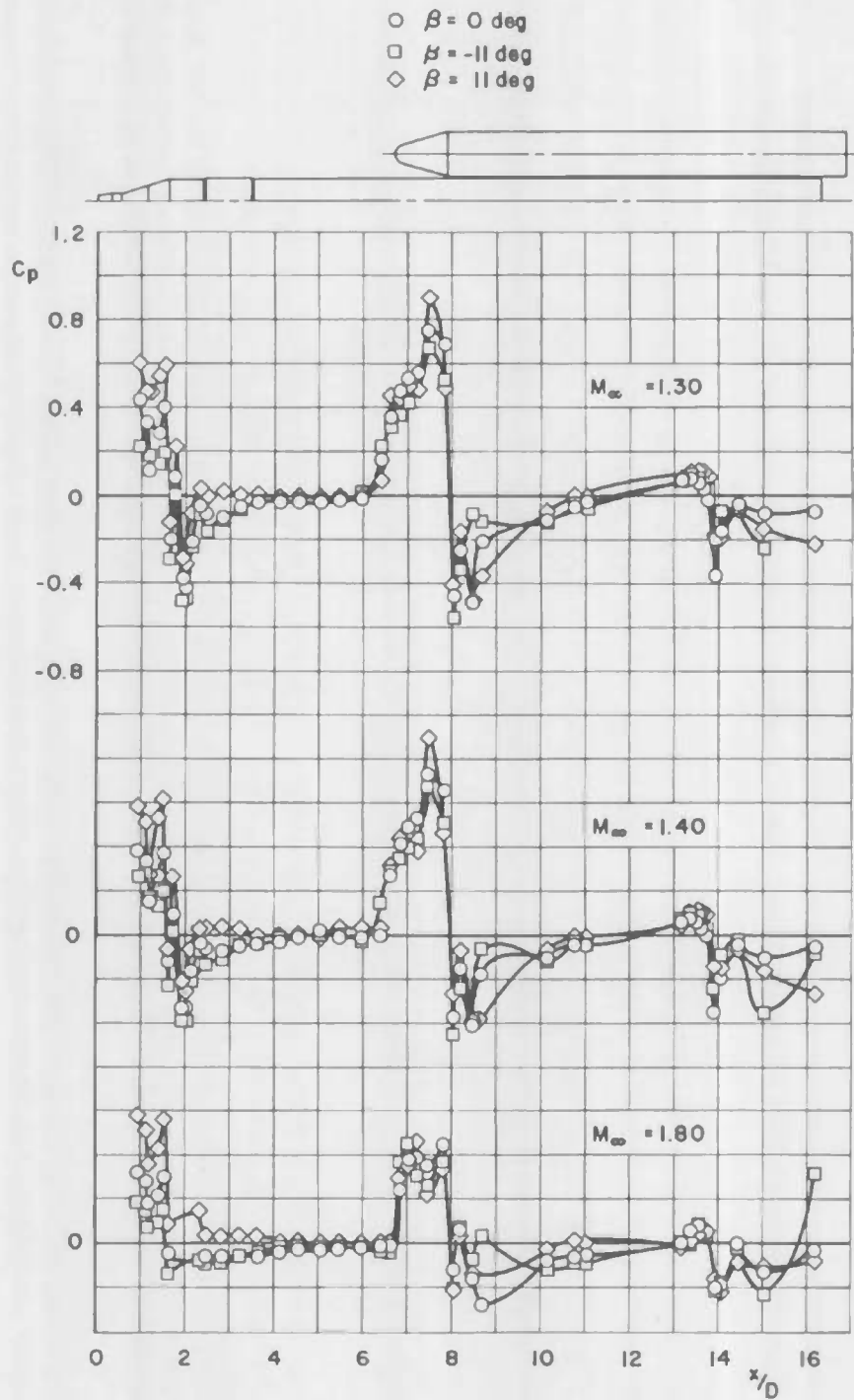


c. Mach Numbers 0.95 and 1.00
 Fig. 50 Continued

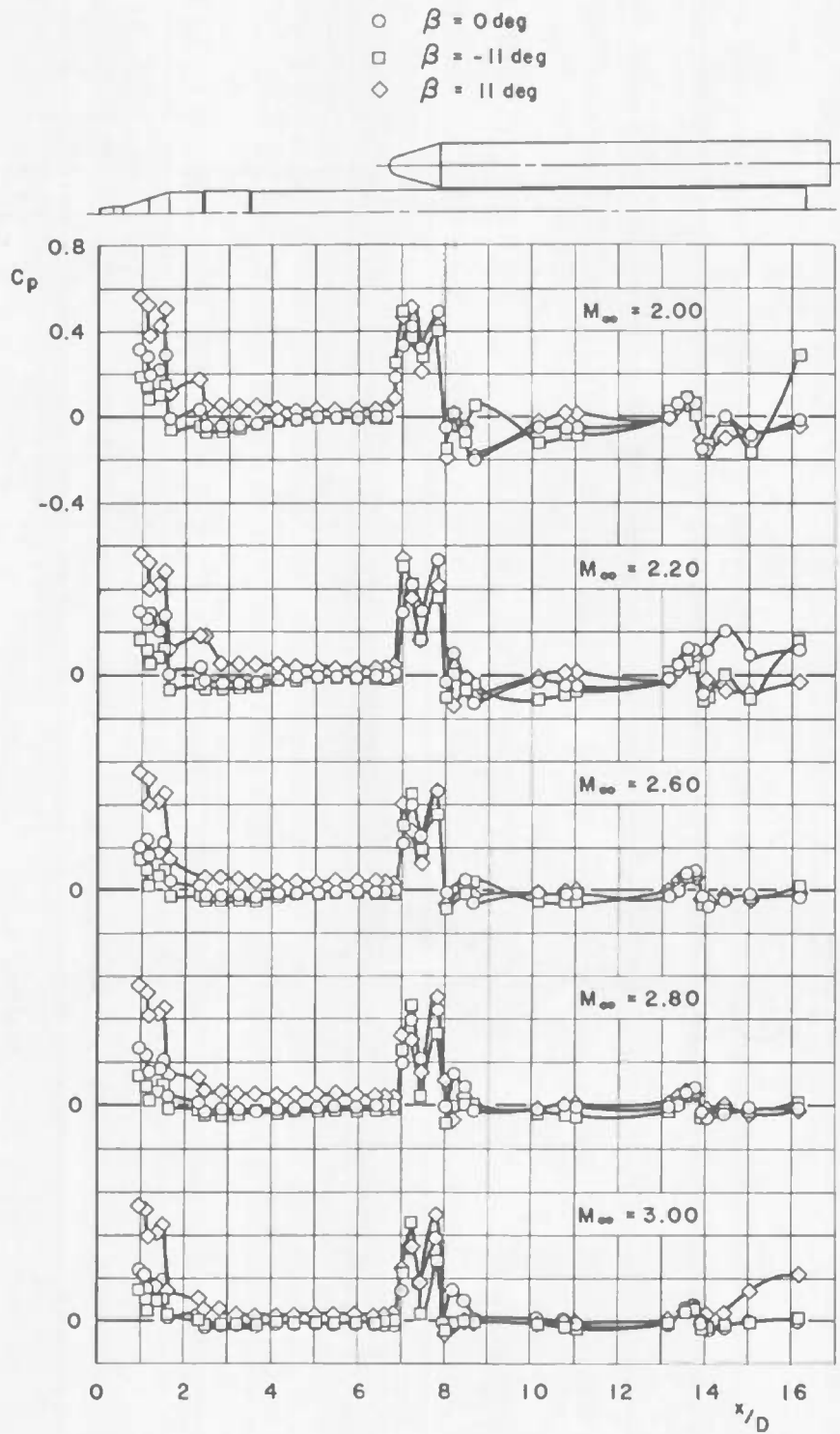


d. Mach Numbers 1.10 and 1.20

Fig. 50 Continued



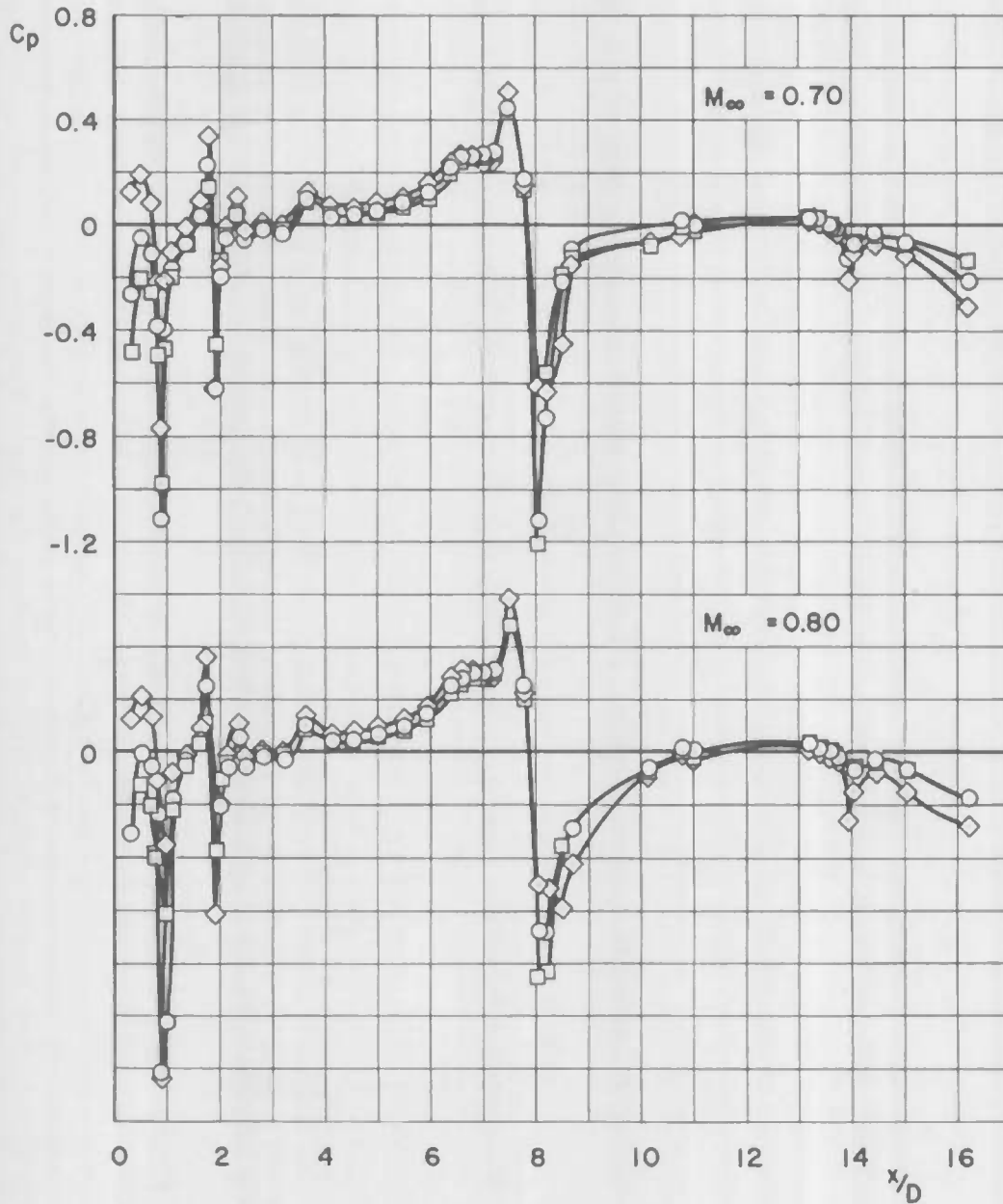
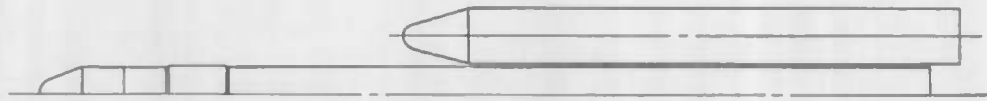
e. Mach Numbers 1.30 through 1.80
 Fig. 50 Continued



f. Mach Numbers 2.00 through 3.00

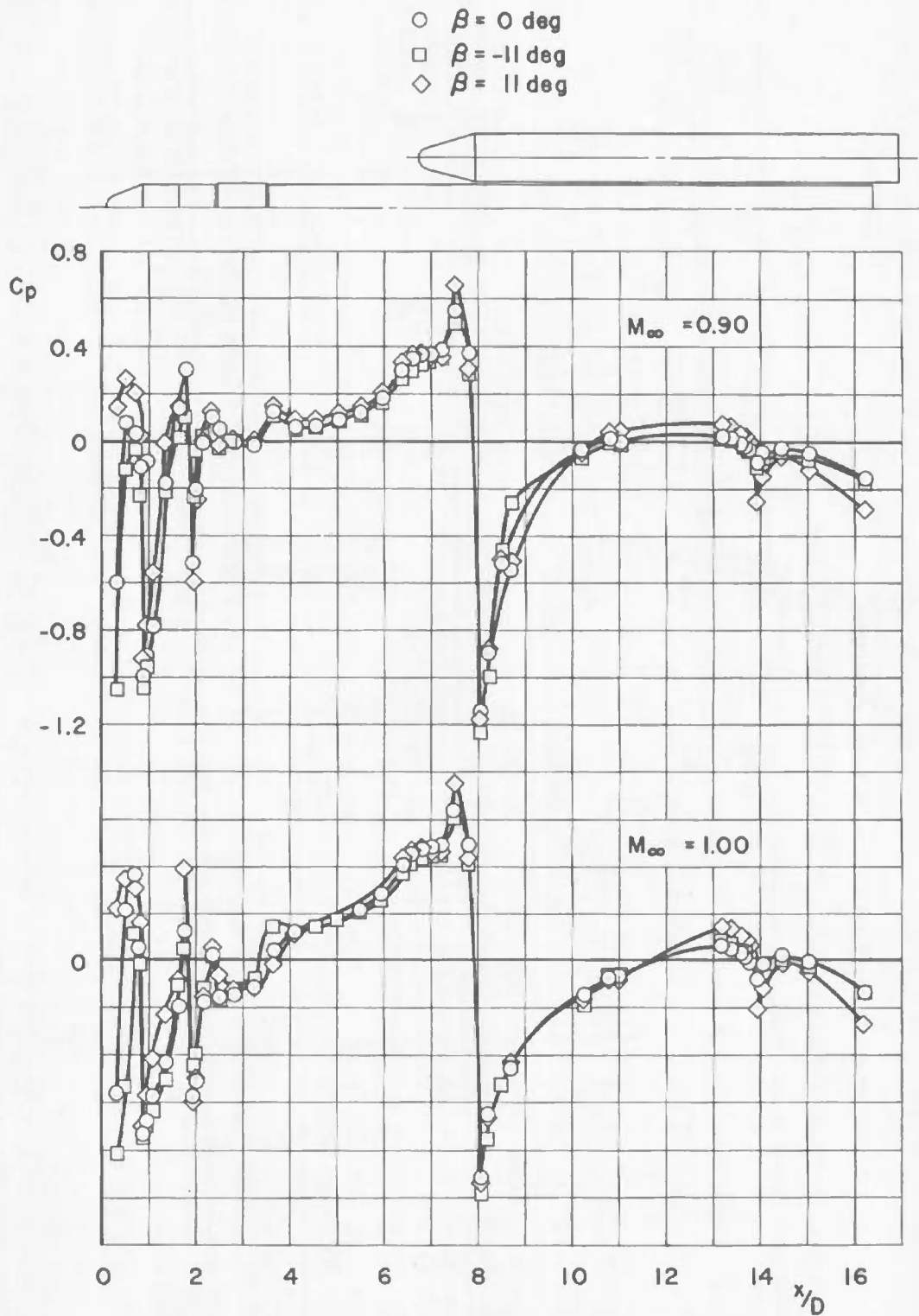
Fig. 50 Concluded

- $\beta = 0$ deg
- $\beta = -11$ deg
- ◇ $\beta = 11$ deg



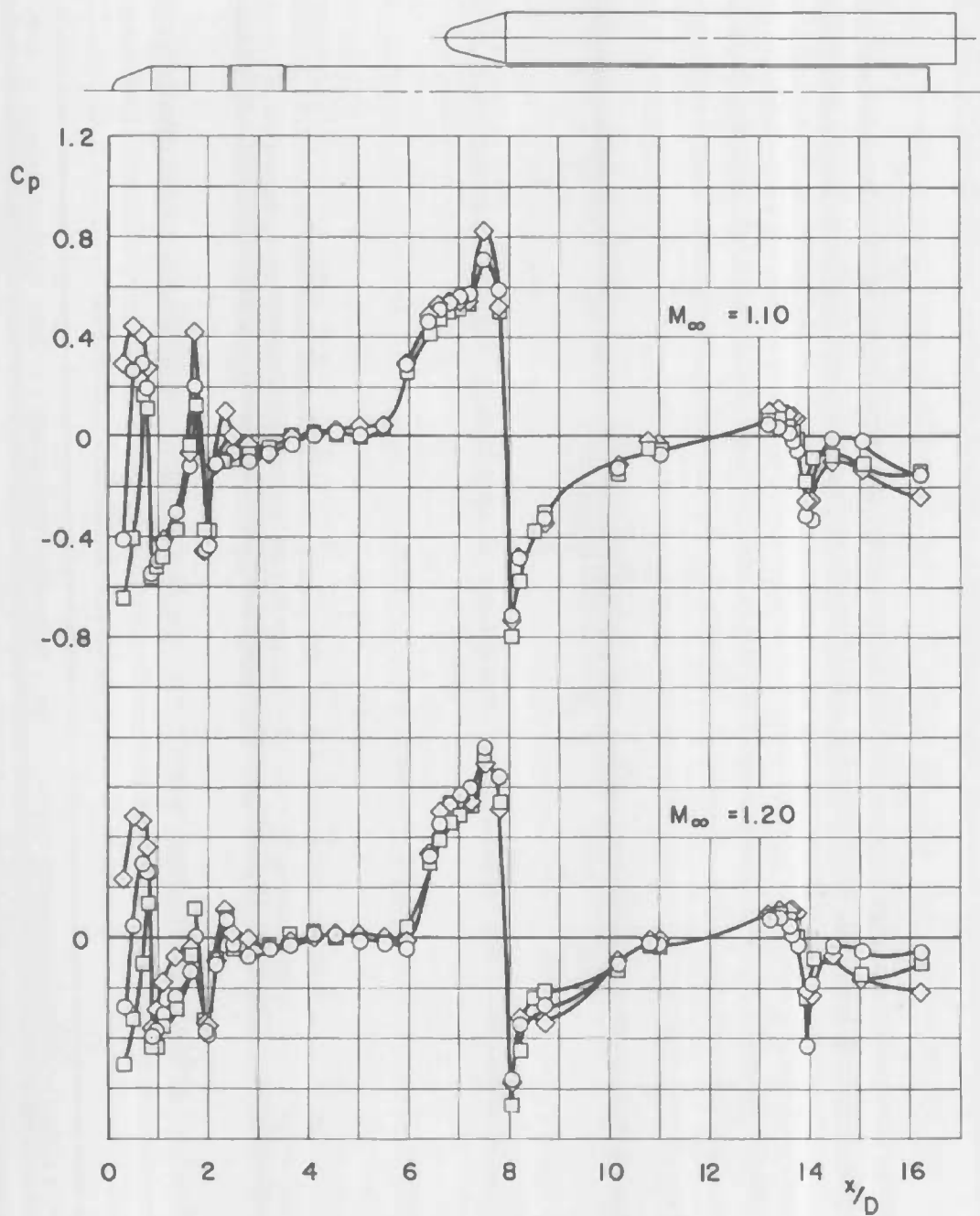
a. Mach Numbers 0.70 and 0.80

Fig. 51 Variation of Surface Pressure Coefficient with Model Station for Orifices Oriented at 90 deg for Configuration 3, $\alpha = 0$



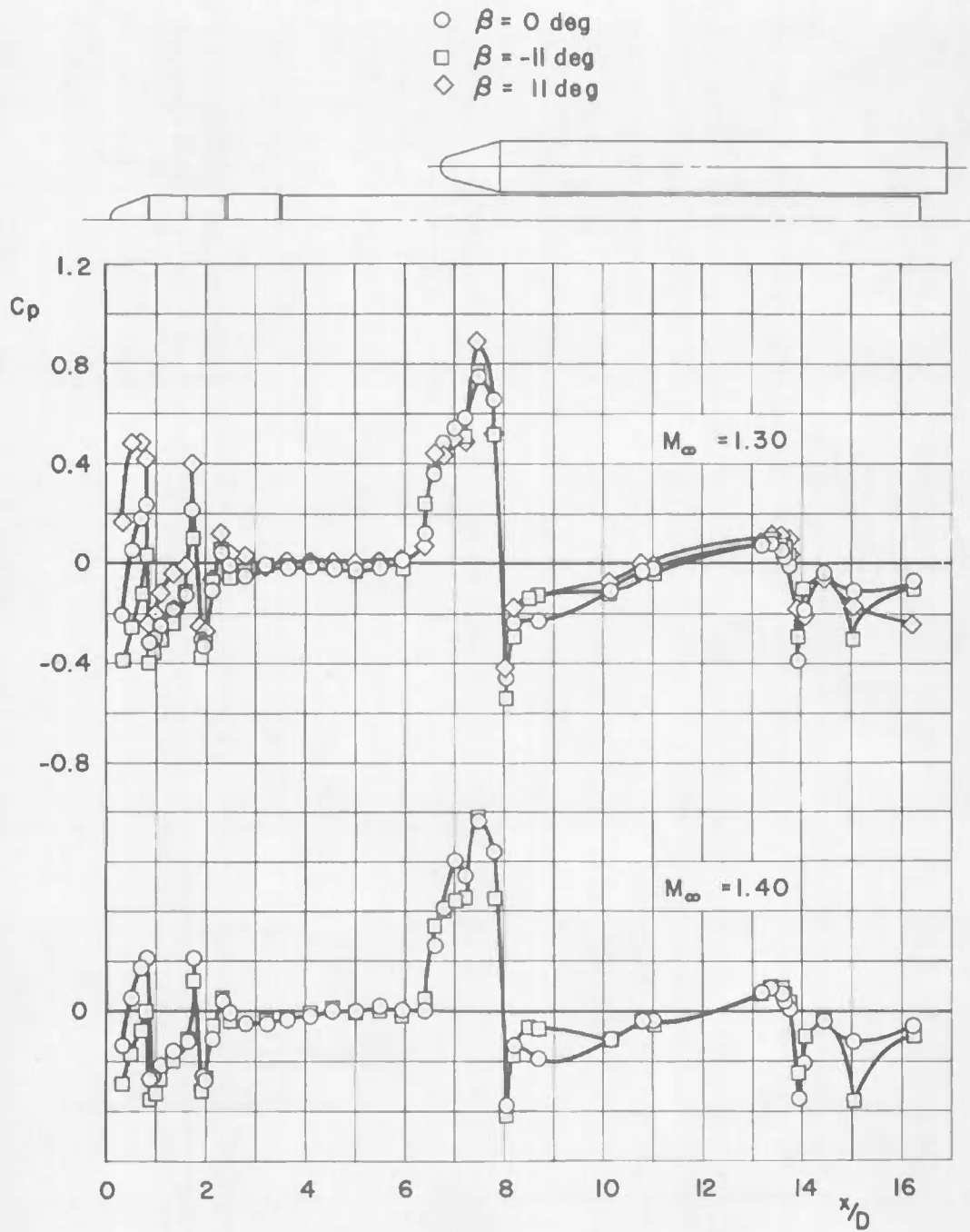
b. Mach Numbers 0.90 and 1.00
 Fig. 51 Continued

- $\beta = 0$ deg
- $\beta = -11$ deg
- ◇ $\beta = 11$ deg



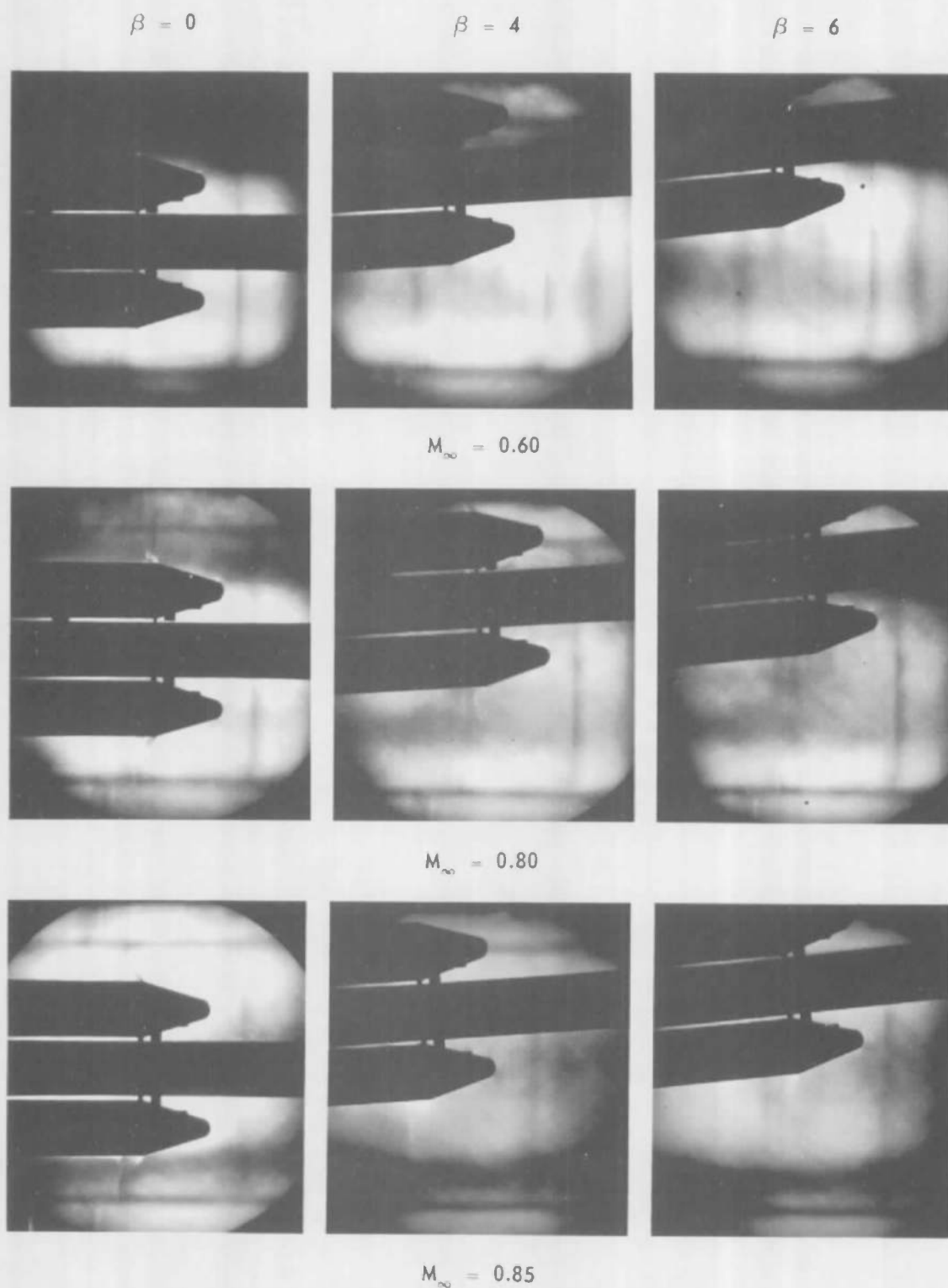
c. Mach Numbers 1.10 and 1.20

Fig. 51 Continued



d. Mach Numbers 1.30 and 1.40

Fig. 51 Concluded



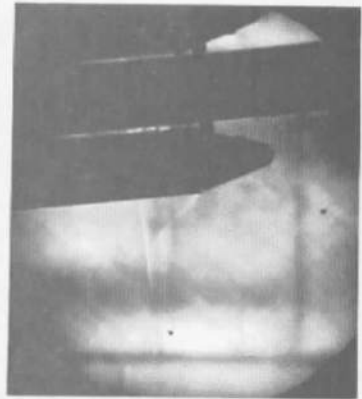
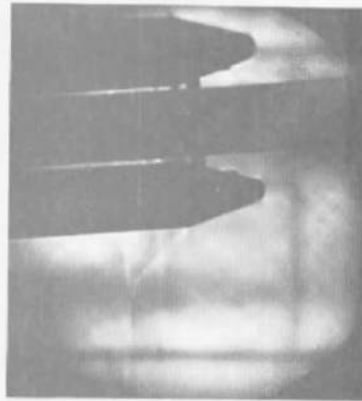
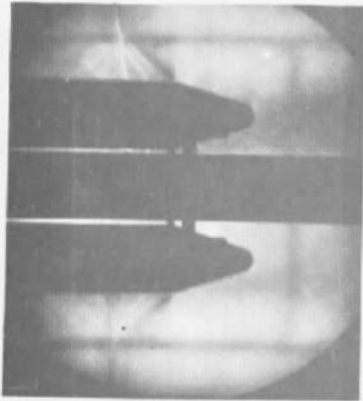
a. Mach Numbers 0.60 through 0.85

Fig. 52 Schlieren Photographs of the SRM Noses for Configuration 1 at $\alpha = 0$ deg

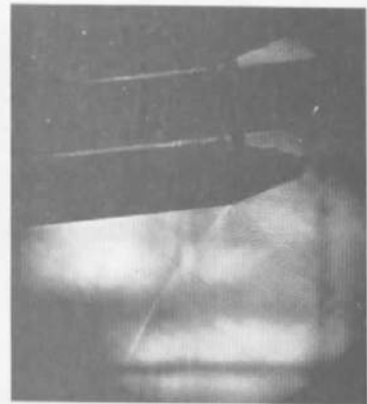
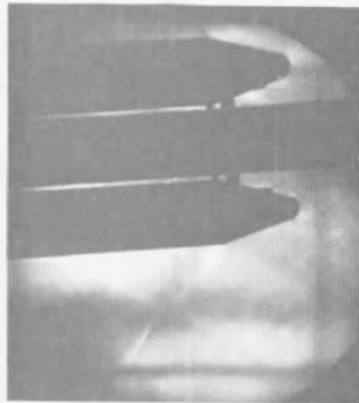
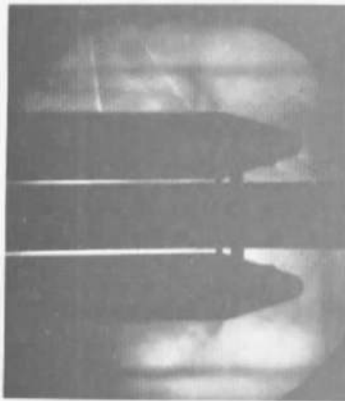
$\beta = 0$

$\beta = 4$

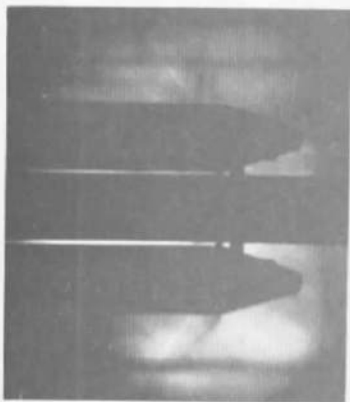
$\beta = 6$



$M_\infty = 0.90$



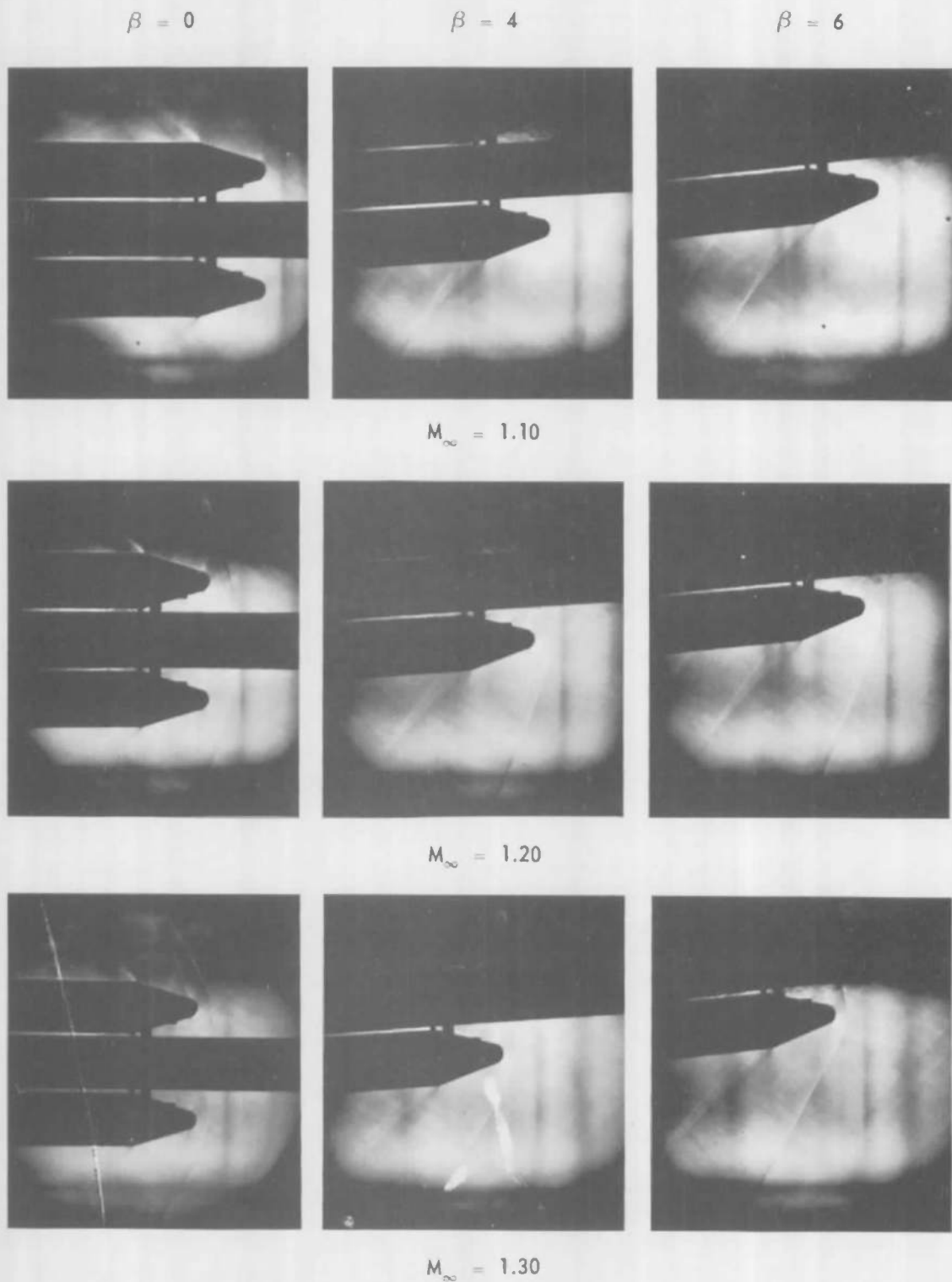
$M_\infty = 0.95$



$M_\infty = 1.00$

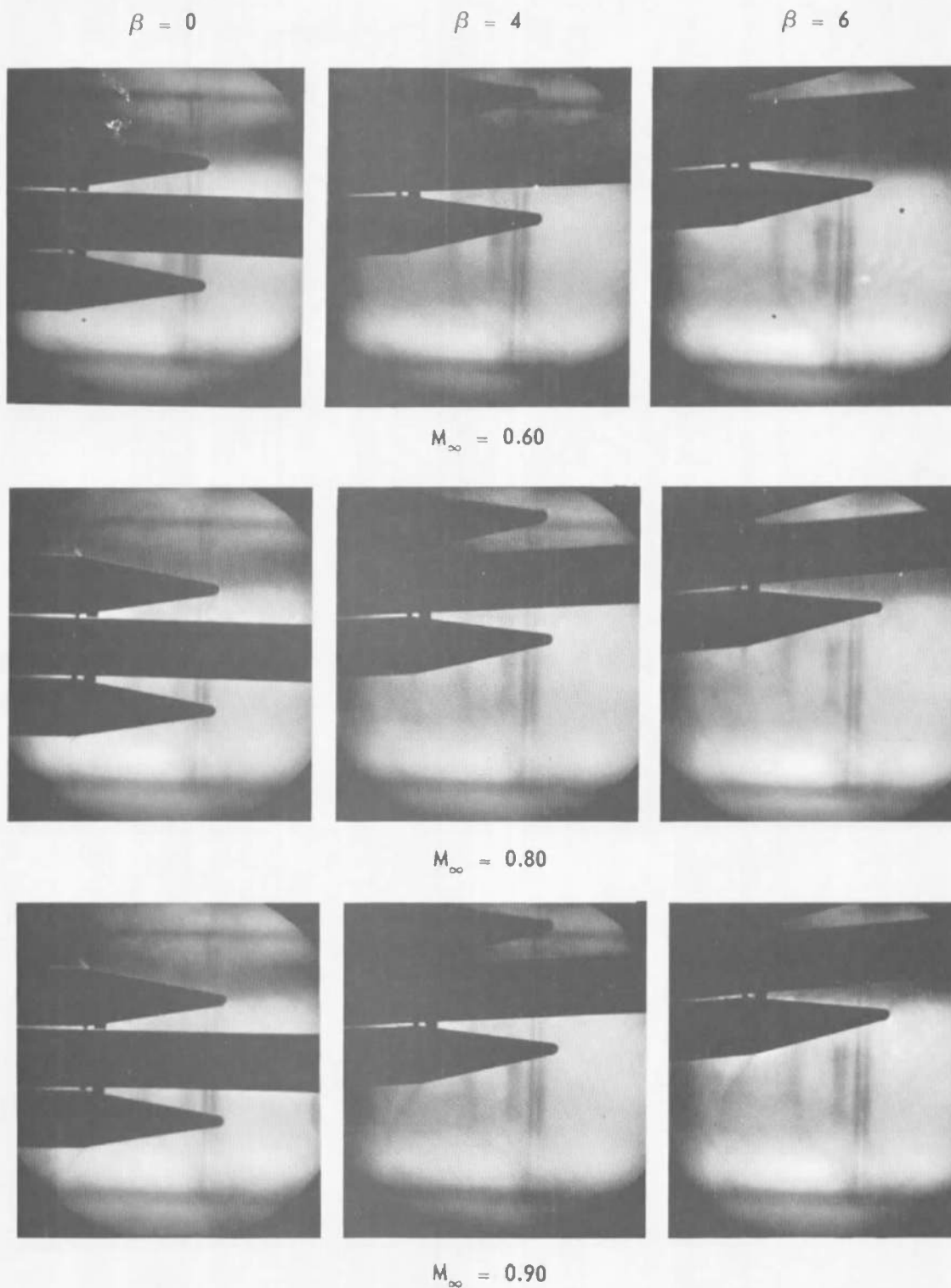
b. Mach Numbers 0.90 through 1.00

Fig. 52 Continued



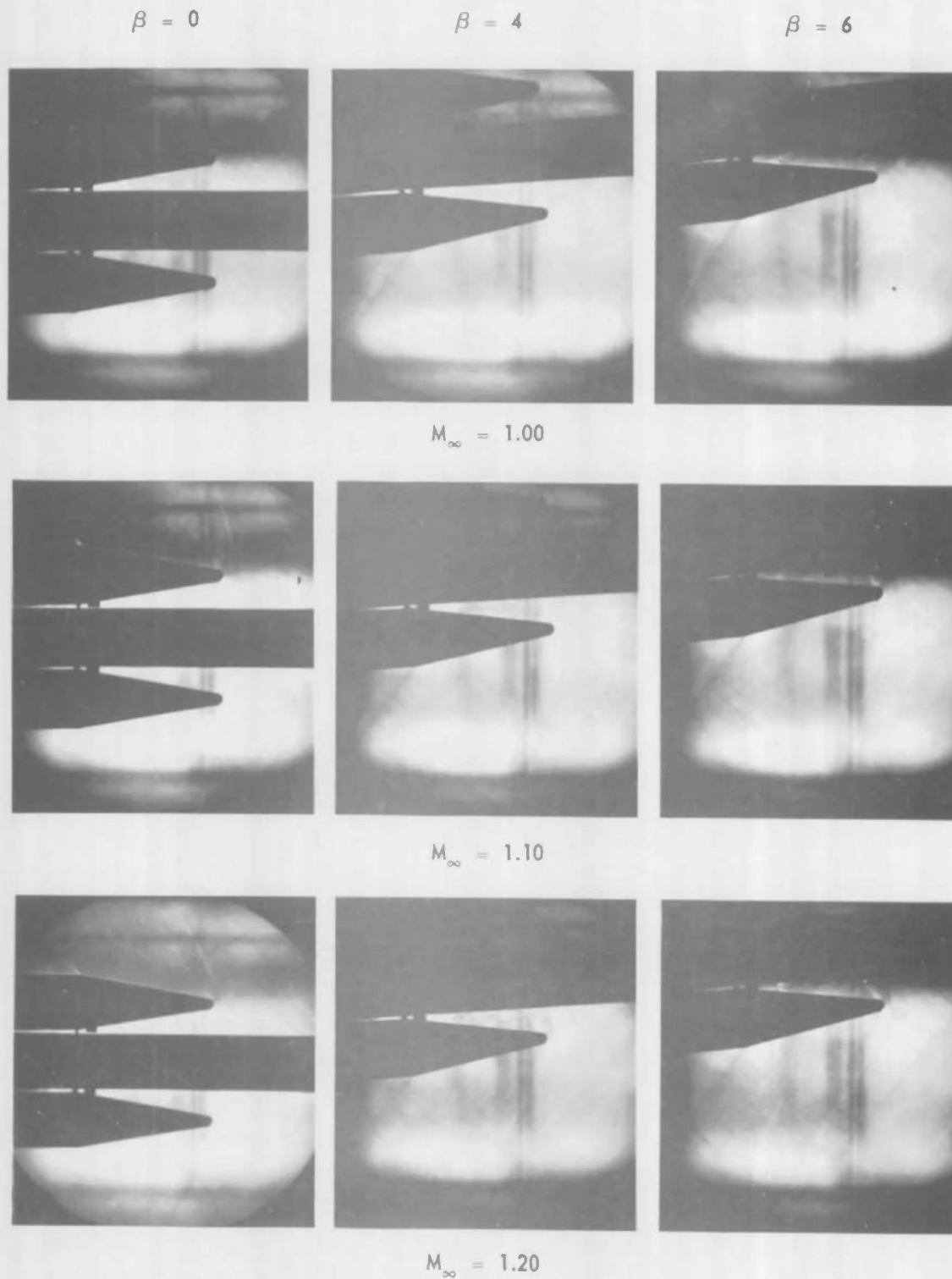
c. Mach Numbers 1.10 through 1.30

Fig. 52 Concluded



a. Mach Numbers 0.60 through 0.90

Fig. 53 Schlieren Photographs of the SRM Noses for Configuration 2 at $\alpha = 0$ deg



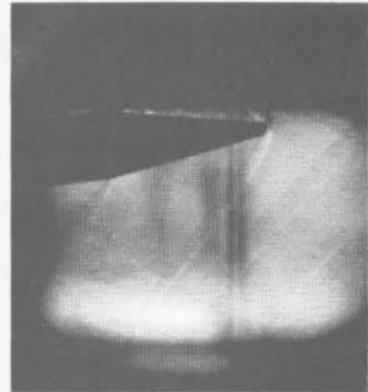
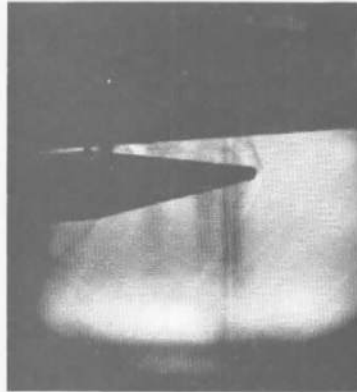
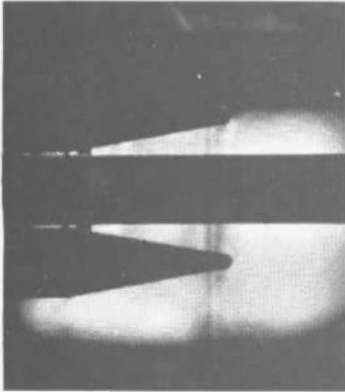
b. Mach Numbers 1.00 through 1.20

Fig. 53 Continued

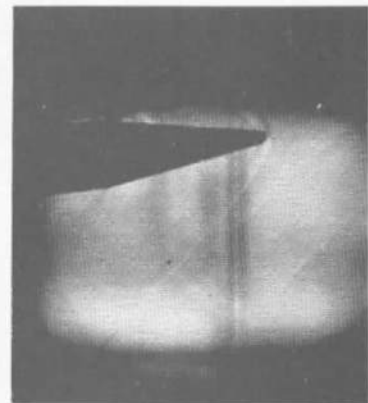
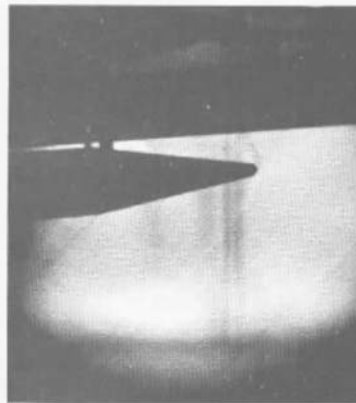
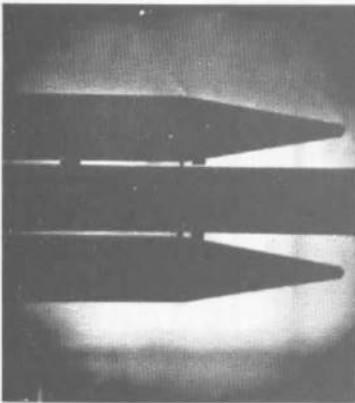
$\beta = 0$

$\beta = 4$

$\beta = 6$



$M_\infty = 1.30$



$M_\infty = 1.40$

c. Mach Numbers 1.30 and 1.40

Fig. 53 Concluded

TABLE I
COEFFICIENT UNCERTAINTIES

Mach No.	Component	$\pm\delta C_m$	$\pm\delta C_N$	$\pm\delta C_n$	$\pm\delta C_Y$	$\pm C_p$	$\pm\delta C_A$	$\pm\delta C_{A,b}$
0.80	Gemini (Balance Number 1) ↓	0.004	0.006	0.002	0.006	0.015	0.015	0.015
1.10		0.003	0.005	0.001	0.005	0.008	0.010	0.011
2.20		0.006	0.009	0.003	0.009	0.002	0.005	0.012
2.80		0.006	0.010	0.003	0.010	0.025	0.003	0.019
0.80	MOL- Gemini (Balance Number 2) ↓	0.033	0.037	0.033	0.037		0.009	0.015
1.10		0.018	0.031	0.018	0.031		0.008	0.011
2.20		0.052	0.060	0.052	0.060		0.015	0.012
2.80		0.055	0.063	0.055	0.063		0.016	0.019
0.80	Composite (Balance Number 3) ↓	0.112	0.064	0.110	0.049		0.030	0.015
1.10		0.090	0.041	0.090	0.040		0.019	0.011
2.20		0.300	0.102	0.143	0.079		0.040	0.012
2.80		0.325	0.103	0.146	0.083		0.042	0.019
0.80	SRM (Balance Number 4) ↓	0.058	0.048	0.093	0.030		0.024	0.015
1.10		0.037	0.039	0.088	0.026		0.020	0.011
2.20		0.115	0.077	0.107	0.047		0.039	0.012
2.80		0.112	0.081	0.107	0.049		0.040	0.019

UNCLASSIFIED

Security Classification

DOCUMENT CONTROL DATA - R&D

(Security classification of title, body of abstract and indexing annotation must be entered when the overall report is classified)

1 ORIGINATING ACTIVITY (Corporate author) Arnold Engineering Development Center ARO, Inc., Operating Contractor Arnold AF Station, Tennessee		2a. REPORT SECURITY CLASSIFICATION UNCLASSIFIED	
		2b. GROUP N/A	
3 REPORT TITLE WIND TUNNEL INVESTIGATION TO DETERMINE STATIC STABILITY AND PRESSURE DISTRIBUTION CHARACTERISTICS OF SMALL-SCALE MODELS OF THE TITAN III/MOL LAUNCH CONFIGURATION AT MACH NUMBERS FROM 0.60 TO 3.10			
4 DESCRIPTIVE NOTES (Type of report and inclusive dates) N/A			
5 AUTHOR(S) (Last name, first name, initial) Riddle, C. D., Shadow, T. O., and Black, J.A., ARO, Inc.			
6 REPORT DATE November 1966	7a. TOTAL NO. OF PAGES 120	7b. NO. OF REFS 1	
8a. CONTRACT OR GRANT NO. AF 40(600)-1200 b. Systems 624A and 632A c. d.		9a. ORIGINATOR'S REPORT NUMBER(S) AEDC-TR-66-202	
		9b. OTHER REPORT NO(S) (Any other numbers that may be assigned this report) N/A	
10. AVAILABILITY/LIMITATION NOTICES This document is subject to special export controls and each transmittal to foreign governments or foreign nationals may be made only with prior approval of SSD (SSBDD).			
11 SUPPLEMENTARY NOTES Available in DDC.		12. SPONSORING MILITARY ACTIVITY Space Systems Division Air Force Systems Command Los Angeles AFS, California	
13 ABSTRACT Models of the Titan III/Manned Orbiting Laboratory (MOL) launch vehicle were tested in Tunnels 16T and 16S of the Propulsion Wind Tunnel Facility at Mach numbers from 0.60 to 3.10 to determine pressure and acoustical characteristics for structural design confirmation and to obtain force balance data for flight control and trajectory analysis. A calibration cone was also tested to evaluate tunnel background noise in the Titan III/MOL acoustical data. Force data were obtained by using four internal balances to sense separate aerodynamic loads on the composite model and on the MOL, MOL-Gemini, and solid rocket motors (SRM) sections. Modification of the SRM noses to a less blunt configuration resulted in a reduction of composite and SRM axial load and tended to position the composite longitudinal neutral point at a more forward location. Lateral neutral point for the composite model exhibited a maximum travel of 2.6 core diameters for the 0.60 and 3.10 Mach number range whereas the longitudinal neutral-point travel was 1.0 diameters. The acoustical results are not presented in this report.			

14

KEY WORDS

LINK A		LINK B		LINK C	
ROLE	WT	ROLE	WT	ROLE	WT

Titan III
 MOL
 surface pressure measurements
 flight control
 trajectory analysis
 supersonic flow

19-4

2. Manned orbiting Sat.
 3. Space Stations - Stability
 4. Missiles
 5. Space vehicles - Stability

INSTRUCTIONS

- 1. ORIGINATING ACTIVITY:** Enter the name and address of the contractor, subcontractor, grantee, Department of Defense activity or other organization (*corporate author*) issuing the report.
- 2a. REPORT SECURITY CLASSIFICATION:** Enter the overall security classification of the report. Indicate whether "Restricted Data" is included. Marking is to be in accordance with appropriate security regulations.
- 2b. GROUP:** Automatic downgrading is specified in DoD Directive 5200.10 and Armed Forces Industrial Manual. Enter the group number. Also, when applicable, show that optional markings have been used for Group 3 and Group 4 as authorized.
- 3. REPORT TITLE:** Enter the complete report title in all capital letters. Titles in all cases should be unclassified. If a meaningful title cannot be selected without classification, show title classification in all capitals in parenthesis immediately following the title.
- 4. DESCRIPTIVE NOTES:** If appropriate, enter the type of report, e.g., interim, progress, summary, annual, or final. Give the inclusive dates when a specific reporting period is covered.
- 5. AUTHOR(S):** Enter the name(s) of author(s) as shown on or in the report. Enter last name, first name, middle initial. If military, show rank and branch of service. The name of the principal author is an absolute minimum requirement.
- 6. REPORT DATE:** Enter the date of the report as day, month, year; or month, year. If more than one date appears on the report, use date of publication.
- 7a. TOTAL NUMBER OF PAGES:** The total page count should follow normal pagination procedures, i.e., enter the number of pages containing information.
- 7b. NUMBER OF REFERENCES:** Enter the total number of references cited in the report.
- 8a. CONTRACT OR GRANT NUMBER:** If appropriate, enter the applicable number of the contract or grant under which the report was written.
- 8b, 8c, & 8d. PROJECT NUMBER:** Enter the appropriate military department identification, such as project number, subproject number, system numbers, task number, etc.
- 9a. ORIGINATOR'S REPORT NUMBER(S):** Enter the official report number by which the document will be identified and controlled by the originating activity. This number must be unique to this report.
- 9b. OTHER REPORT NUMBER(S):** If the report has been assigned any other report numbers (*either by the originator or by the sponsor*), also enter this number(s).
- 10. AVAILABILITY/LIMITATION NOTICES:** Enter any limitations on further dissemination of the report, other than those

imposed by security classification, using standard statements such as:

- "Qualified requesters may obtain copies of this report from DDC."
- "Foreign announcement and dissemination of this report by DDC is not authorized."
- "U. S. Government agencies may obtain copies of this report directly from DDC. Other qualified DDC users shall request through _____."
- "U. S. military agencies may obtain copies of this report directly from DDC. Other qualified users shall request through _____."
- "All distribution of this report is controlled. Qualified DDC users shall request through _____."

If the report has been furnished to the Office of Technical Services, Department of Commerce, for sale to the public, indicate this fact and enter the price, if known.

- 11. SUPPLEMENTARY NOTES:** Use for additional explanatory notes.
- 12. SPONSORING MILITARY ACTIVITY:** Enter the name of the departmental project office or laboratory sponsoring (*paying for*) the research and development. Include address.
- 13. ABSTRACT:** Enter an abstract giving a brief and factual summary of the document indicative of the report, even though it may also appear elsewhere in the body of the technical report. If additional space is required, a continuation sheet shall be attached.

It is highly desirable that the abstract of classified reports be unclassified. Each paragraph of the abstract shall end with an indication of the military security classification of the information in the paragraph, represented as (TS), (S), (C), or (U)

There is no limitation on the length of the abstract. However, the suggested length is from 150 to 225 words.

- 14. KEY WORDS:** Key words are technically meaningful terms or short phrases that characterize a report and may be used as index entries for cataloging the report. Key words must be selected so that no security classification is required. Identifiers, such as equipment model designation, trade name, military project code name, geographic location, may be used as key words but will be followed by an indication of technical context. The assignment of links, rules, and weights is optional.